Estimation of aquifer parameters from available log data and well reports in the Northeast fields of the Great Man-Made River Project (GMRP), East Fezzan (Libya)

Masterarbeit

zur Erlangung des akademischen Grades eines Diplomingenieurs der Studienrichtung Angewandte Geowissenschaften an der Montanuniversität Leoben

Johannes Amtmann B. Sc.

Ich erkläre an Eides statt, dass ich die Masterarbeit selbstständig verfasst, andere als die angegebenen Quellen und Hilfsmittel nicht benutzt und mich auch sonst keiner unerlaubten Hilfsmittel bedient habe.

Leoben, März 2009

Die vorliegende Masterarbeit wurde am Department Angewandte Geowissenschaften und Geophysik am Lehrstuhl für Geophysik der Montanuniversität Leoben eingereicht.

Herr Hon. Prof. Dr. rer. nat. habil. Jürgen Schön betreute diese Arbeit.

Dankesworte

An erster Stelle möchte ich mich bei meinem Betreuer Herrn Hon. Prof. Dr. rer. nat. habil. Jürgen Schön bedanken, der trotz vieler Verpflichtungen immer Zeit für mich gefunden hat und mir mit Rat und Tat zur Seite stand.

Mein weiterer Dank gilt besonders dem Institutsleiter des Instituts für WasserRessourcenManagement, Hydrogeologie und Geophysik, der Joanneum Research Forschungsgesellschaft mbH Herrn Hon. Prof. Dipl.-Ing. Dr. mont. Christian Schmid, der die Daten für die Masterarbeit organisiert hat und der die Benützung der Einrichtungen in Leoben im Zuge der Masterarbeit ermöglicht hat.

Für fachliche Diskussionen und Hilfestellungen im Bereich der Geologie und der Angewandten Geophysik bedanke ich mich bei meinen Arbeitskollegen Dipl.-Ing. Dr. mont. Marcellus Schreilechner sowie bei Dipl.-Ing. Christoph Eichkitz.

Weiterer Dank gilt Ass. Prof. Dipl.-Ing. Dr. mont. Heinrich Mali und Herrn Ass. Prof. Dr. phil. Reinhard Gratzer, die mir Unterstützung bei der Auswahl der Proben und bei den Dünnschlifffotos gaben.

Mein größter Dank gilt meiner Familie und meinen Freunden, die mich in jeglicher Form auf meinen Lebens- und Ausbildungsweg unterstützt und motiviert haben. Ohne sie wäre ich nicht so weit gekommen. Danke!

Abstract

On the basis of 12 wells, which are a part of the Northeast Jabal al Hassouna Wellfield (East Fezzan, Libya) of the Great Man Made River Project phase 2, a preliminary geophysical investigation of the aquifer in a certain area was done. The aim of the investigation was to get information about porosity and permeability from all wells from the available well log data and well reports. Well log data are very limited (resistivity, gamma, caliper). Based on a corrected Archie algorithm, it was possible to estimate the porosity. Permeability was estimated by a combination of poro-perm- correlation and pumping test results. Furthermore, logplots were used for correlation between the wells and for the characterisation of the aquifer along two profiles. The result of the profile interpretation has lead to discussions about the type of porosity in the aquifer.

Zusammenfassung

Es wurde eine geophysikalische Voruntersuchung auf der Basis von 12 Bohrungen in einem Gebiet im Nordost- Bohrungsfeld von Jabal al Hassouna (Fezzan, Libya) des Great Man Made River Projekts Phase 2 durchgeführt. Das Ziel der Untersuchung war es, Porosität und Permeabilität aus den vorhandenen Bohrlochmessungen und Reports für den gesamten Aquiferbereich abzuschätzen. Aufgebaut auf einen Algorithmus nach Archie konnte die Porosität abgeschätzt werden, und in weiterer Folge konnte die Permeabilität mit Hilfe der Poro-Perm- Korrelation und der Ergebnissen der Pumptests abgeschätzt werden. Darauf folgend wurden eine Korrelation und eine Interpretation zwischen den einzelnen Logplots anhand von zwei Profilen durchgeführt. Die Interpretation der Profile hat zu Diskussionen über die Art der Porosität im Aquifer geführt.

Index of contents

1. Introduction

The area of interest is at the border between the district of Al Jufrah and Ash Shati, close to the road between Birak and Tripoli in Libya (Figure 1.1).

Fig. 1.1. Map of the surrounding of the area of interest (http://www.lib.utexas.edu/maps/libya.html)

It is situated in the wellfields of the Great Man Made River Project (GMRP). In the course of the GMRP project of phase 2, about 400 production wells were drilled in the late nineteenth century. The wells are subdivided into different wellfields: the Northeast Wellfield, the East Wellfield and the South Wellfield. The area of interest is situated in the Northeast Wellfield. In this area, water is produced from a Cambro-Ordovician aquifer and is transported through pipelines to the coast where the water is consumed. The produced water has a high-quality standard. The high standard can only be achieved by an intelligent pump steering. But if the production of a well reaches a certain amount, geogen nitrates decrease the water quality. That means that there is a higher amount of water which can be produced if the origin of the nitrate can be located. For this reason, the Ground Water Authority is eager to find a solution to solve the problem.

A possible method of resolution is to understand the geological situation of the aquifer by getting aquifer parameters like porosity and permeability from the available data.

The aim of the work is to find solutions to get the aquifer parameters from the available log data and reports. If the preliminary investigation achieves good results, the investigation can be done for all 400 wells, and finally, a 3D-model of the aquifer can be made. Hence, the problem of the nitrate contamination could be solved, because the origin of the geogen nitrate sources can be located by using the geological model and by using geochemical data from a geochemical investigation.

For this reason, there are a few questions that should be answered by the following investigation:

Is there a possibility to get aquifer parameters like porosity or permeability from the available data?

Is the determination automated?

Is there a possibility to correlate the specific wells?

Are the data sufficient to build a 3D-model of the aquifer in the future?

If not, which log data are necessary?

Which samples are necessary?

The following investigation tries to give the answers.

2. Geological Overview

2.1. Introduction

The following map (Figure 2.1) displays the current geological situation in Libya. The map should only give an overview of the geological situation in Libya. The geological situation of the area of interest will be discussed in detail in chapter 2.2.

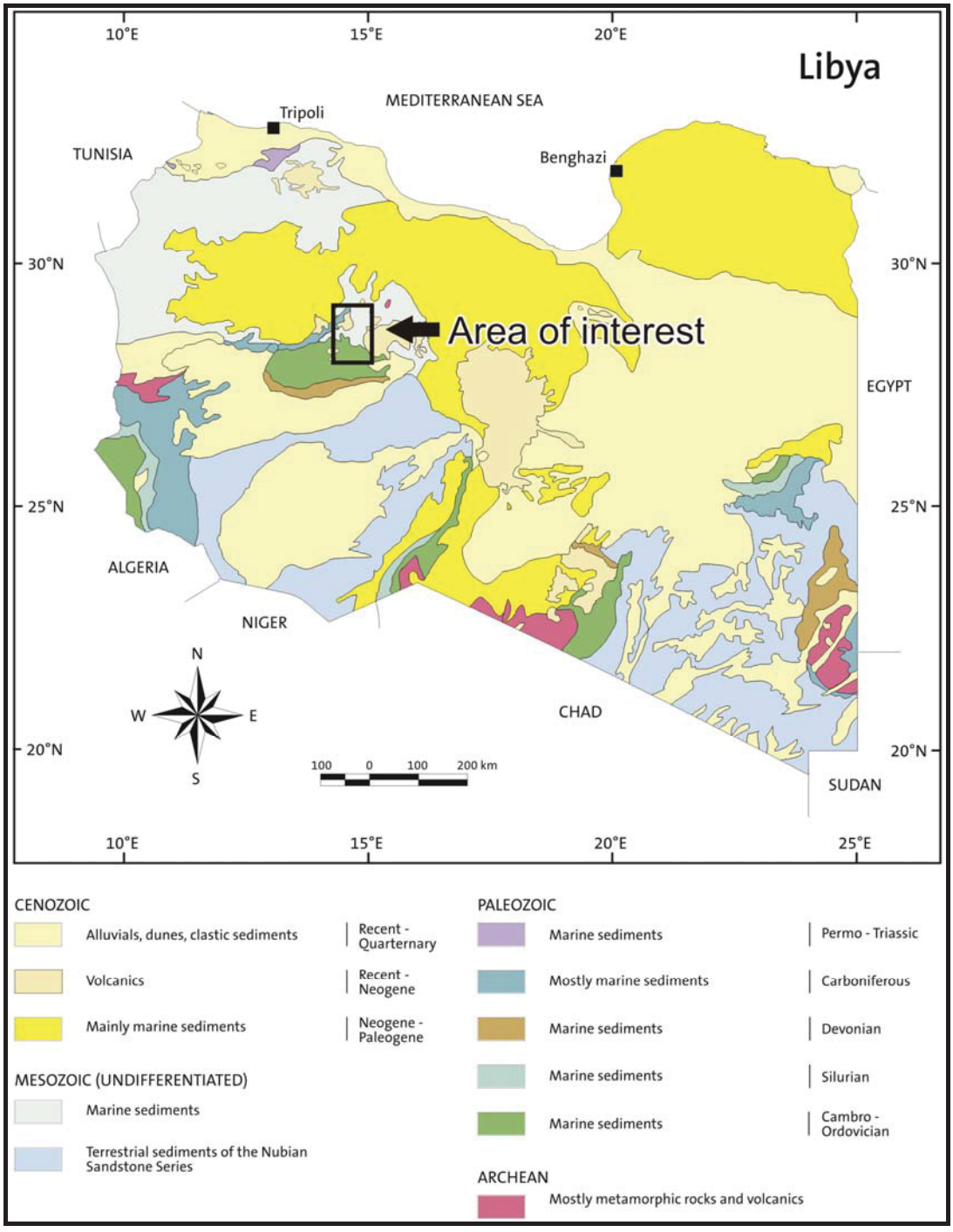

Fig. 2.1. Geological map of Libya (Schluter, 2008)

In Libya, there are areas where sediments stem from Precambrian, Palaeozoic, Mesozoic and Cainozoic age.

There are three areas where the Precambrian crops out. That is in south-west Libya the Ghat area, in south Libya the Tibisti area and in south-east Libya the Al Awaynat area. Palaeozoic sediments are mainly marin sediments, and these sediments are distributed in south and central Libya. Mesozoic sediments can be found in the north-west of Libya as marine sediments and in south Libya as terrestrial sediments. Cainozoic rocks crop up in north and south Libya as marine sediments and in central Libya as volcanic rocks.

Since the Precambrian, several tectonic events took place where plates and micro-plates were assembled and disassembled. The following list after Don Hallet (2005) demonstrates the main plate tectonic events together with the sedimentological history of Libya and its adjacent areas:

ERA	AGE (Ma)	PLATE TECTONIC EVENTS	LIBYA AND ADJACENT AREAS
CAINOZOIC	6.7 - 5.2	Messinian salinity crisis. Sea level in Mediterranean lowered by 500m. Evaporites formed in deep Mediterranean basins.	Messinian evaporites present in Sahabi Fm. onshore and Marsa Zouaghah Fm. offshore. Sahabi Channel cut to 500m below present sea level. Volcanics, Tibisti Mountains.
	15 - 6	Thrusting in Rif and Betic areas. Calabrian and Kabylie terranes emplaced in present location.	Eruption of Al Haruj al Aswad volcanics. Regression in Ajdabiya Trough and Cyrenaica.
	30 - 15	Main Alpine Orogeny. Thrusting in Alps and western Mediterranean. Subduction of ocean floor beneath Alboran, Kabylie and Calabrian terranes.	Continental, littoral and shallow marine facies in Sirt Basin. Volcanic eruptions in Jabal Sawda and Gharyan.
	50 - 30	Beginning of Alpine Orogeny. Closure between Iberia and north Africa marks end of Tethys.	Ring intrusions in Jabal Awaynat. Shallow water carbonates in Sirt Basin. Inversion in Atlas Mountains.
	65 - 50	Progressive closure of Tethys Ocean due to northeast movement of African plate.	Uplift in west Libya. Subsidence in Sirt Basin. Carbonate platforms and reefs in Sirt Basin.
MESOZOIC	80 - 65	Relative movement of African plate changed from eastwards to northeastwards. End of seafloor spreading in Mediterranean	Infill of grabens with marine shales and micrites. Shallow marine carbonates and clastics on horsts. Deposition of organic rich shales in Sirt Basin.
	125 - 80	Seafloor spreading axis switched to southern axis (south of Turkish, Balkan and Lombard terranes).	Major flooding episode in Sirt Basin. End of rift phase. Subsidence in Sirt Basin. Formation of horsts and grabens.
	165 - 125	Seafloor spreading in Tethys Ocean along northern axis (north of Sila, Lombard and Austrian terranes).	Progressive collapse of Sirt Arch. Deposition of Nubian sands.
	165 - 155	Establishment of Tethys seaway from Asia to the Pacific	Tensional regime in Libya. Continued rifting and deposition of continental clastics.
	240 - 155	Break up of Pangaea along Caribbean - North Atlantic - Mediterranean axis.	Beginning of rift phase. Triassic continental clastics found in rift grabens in Libya.
PALAEOZOIC	290 - 260	Calving of terranes from West Gondwana and translation northwards on transit plate.	Major regression. Establishment of continental conditions over much of Libya. Dextral wrenching in north Africa.
	330 - 290	Hercynian Orogeny. Culmination of collision between Gondwana and Laurasia to produce Pangaea	Uplift and deformation. Formation of E-W/NE-SW tectonic elements. Carboniferous deltaic deposition.
	380 - 360	Initial collision of Gondwana with Laurasia.	Deposition of stacked, deltaic and littoral, clastic sequences. Major transgression, organic rich shales over much of north Africa.
	435 - 380	Northward drift of Gondwana.	
	440	West Gondwana located close to South Pole	Brief glacial episode over large part of north Africa.
	500 - 440	Detachment of Avalonian and Cadomian terranes from passive margin of West Gondwana.	North Africa formed passive margin of West Gondwana. Deposition of three transgressive clastic cycles.
	550 - 450	Separation of Laurentia from Pannotia to produce Gondwana.	Late Pan African activity produced broad north to south troughs and swells in Libya and eastern Algeria.
PRE CAMBRIAN	600 - 550	Pan African Orogeny brought together the dis-assembled plates of Rodinia into the new supercontinent of Pannotia.	Evidence of Pan African remobilised belt in Tibisti Mountains, on Al Qarqaf Arch and in wells in southern Libya. Period of major tectonism and metamorphism.
	700 - 600	Rodinia dis-assembled, rotated and turned inside out.	
	880 - 550	Pharusian microplates formed as island arcs in Pharusian Ocean.	Evidence of Pharusian accreted terranes in wells in northern Libya and on Touareg Shield of Algeria and Mali.
	1000 - 800	East Sahara craton formed on periphery of Rodinia.	Evidence of east Saharan craton in Hoggar Mountains of Algeria and at Adrar in Yahia near Ghat.
	1600 - 1000 2900 - 2600	Assembly of Rodinia from cratonic nuclei. Formation of cratonic blocks including West African, Nile and Congo-Kalahari.	Evidence of Nile craton at Jabal Awaynat and eastern Tibisti massif, West African craton in Eglab massif, Algeria.

Fig. 2.2. Tectonic and stratigraphic overview of Libya (Hallet, 2002)

2.2. Tectonics and stratigraphy

The geological situation of the area of interest is as follows: There are two formations which outcrop in the area of interest. The Cambrian Hassouna Formation, which is displayed in green in the map, and the Late Cretaceous Al Gharbiyah formation, which is displayed in yellow (Figure 2.3). Additionally, volcanic rocks of the Cainozoic age crop up, which are displayed in pink (Figure 2.3) north-west and south-east of the area of interest.

From the tectonic point of view, two main phases of orogeny, the Pan-African Orogeny between Pre-cambrian and Cambrian and the Hercynian Orogeny, which took place in the Late Palaeozoic, embossed the area of interest. (Don Hallet, 2005)

After the Pan-African Orogeny, the Precambrian basement was formed, and during the Cambrian, the Hassouna Formation was deposited in the area of interest.

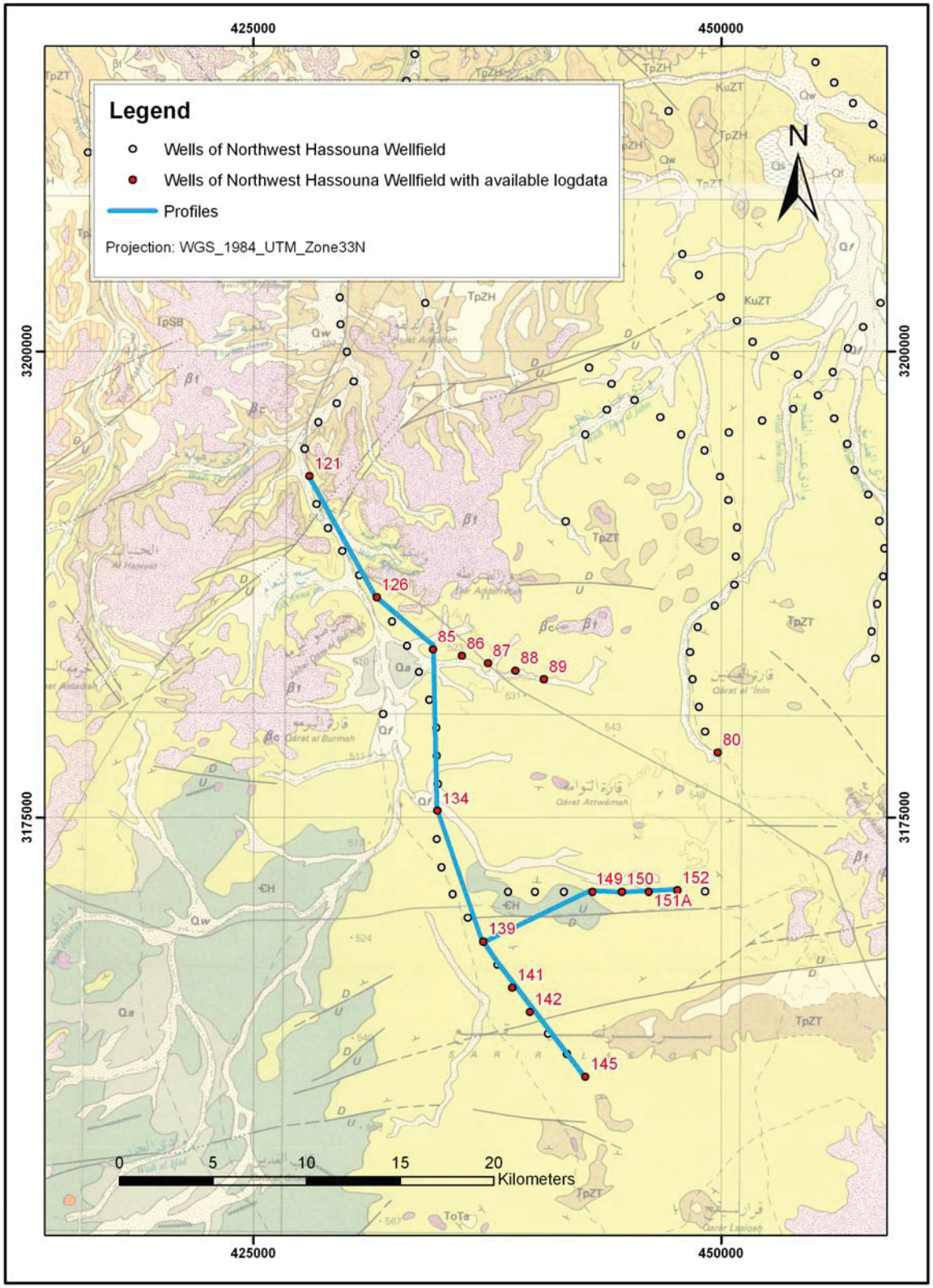

Fig. 2.3. Geological map in the area of interest (green: Hassouna Formation; yellow: Al Gharbiyah Formation; pink: Miocene volcanic areas) (Background map: Jurak, 1978)

2.2.1. Hassouna Formation

The Hassouna Formation is extremely widespread and lithologically uniformly deposited, extending over large areas of Libya and is overlying the eroded and folded Precambrian basement. The area was embossed by a shallow marine environment.
Because no fossils, apart from the trace fossils, were found, the age attribution is based on its stratigraphic position between Pan-African basement and the overlying rocks, which means that the Hassouna Formation has to be of Cambrian age. After Cepek (1980), the Hassouna Formation can be subdivided into three parts because of its accommodation conditions:

The lower part, which overlies the Precambrian granites, consists of conglomeratic quartzitic pebbles. This unit is about 2 m to 13 m thick and is overlain by massive banks of cross-bedded sandstones. Each of the banks has a thickness up to 10 m and the matrix of the unit comprises silt and clay. The accommodation area is fluviatile and deltaic and becomes intertidal towards the top.
The middle unit is more fine-grained and silty. The accommodation area is intertidal and becomes sub-tidal towards top.

The upper part is composed of cross-bedded sandstones where Tigillites can be observed. The accommodation area is subtidal.

Because of the Hercynian Orogeny, the Hassouna Formation is the only formation of the Paleozoic in the area of interest.
During the Hercynian Orogeny, the area of interest was uplifted at the Al Qarqaf Arch, which can be observed in figure 2.4. During Triassic, Jurassic and almost the whole Cretaceous, the deposited sediments of the Palaeozoic were eroded. The formation above the Hassouna Formation is finally the Al Gharbiyah Formation, which has Cretaceous age.

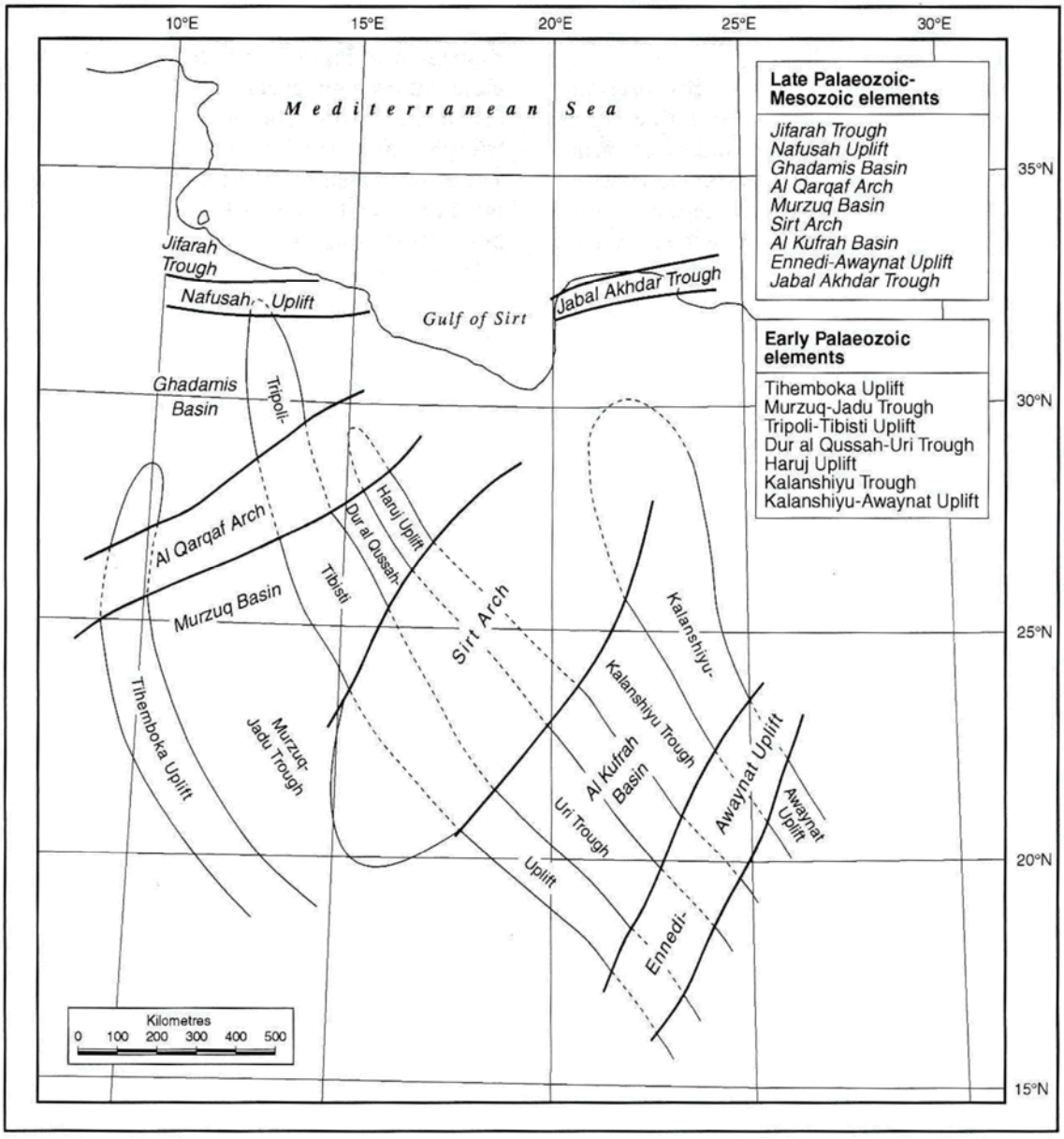

Fig. 2.4. Elements of the Pan-African (early Palaeozoic elements) and Herzynian Orogenies (late Palaeozoic elements)

2.2.2. Al Gharbiyah Formation

The Al Gharbiyah Formation overlies the Hassouna Formation. The Al Gharbiyah Formation is divided into three members in the area of interest: the Bi'r al Ghurab Member, the Lawdh Allaq Member and the Lower Tar Member. But in the area of interest, only the Lower Tar Member is present. The lithology consists of conglomerates at the base, further interbedded marlstones and sandy limestones. Also Lumachelles of pelecypod shells are often found. The layer is about 50 m thick and the lithology varies rapidly (Don Hallet, 2005).

3. Data Conditions, selection of study area

3.1. Introduction

The starting point of the investigation displays the position of all available data in GIS software together with different maps. With the aid of the maps, the location of the area of interest can be understood and important information can be ordered quickly. Because the geophysical data, which are obtained, are not digital, the data have to be digitized (explained in chapter 4.1).

Well log data from 19 wells on paper format from the Northeast Wellfield (Figure 3.1) plus further information from "Drilling, testing and completion reports" are obtained. Several specific measurements are made by logging runs, which is documented in the following points. The contractor of the drilling, testing and completion services is the Dong Ah Consortium, which has its headquarter in Seoul, South Korea.

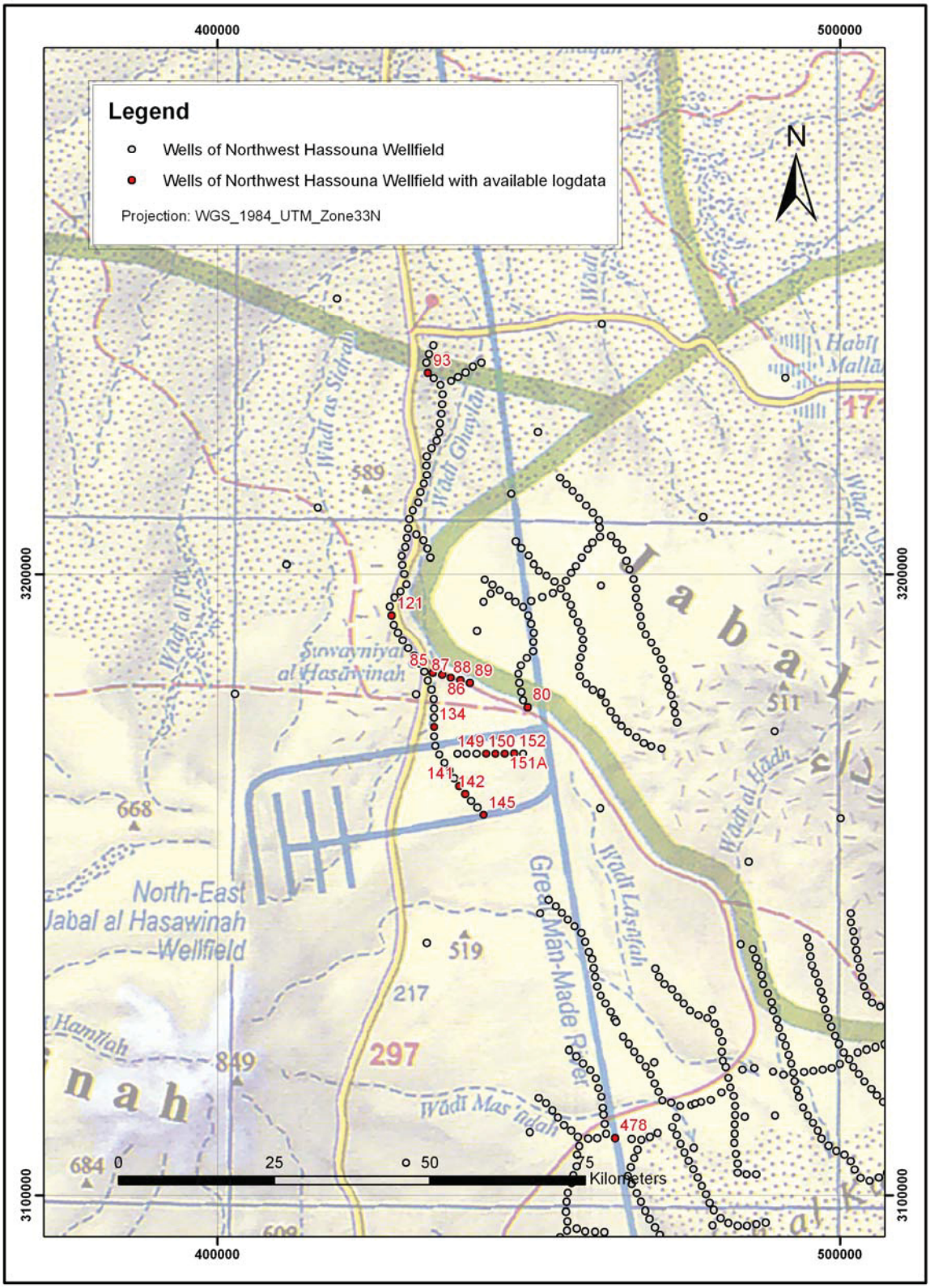

Fig. 3.1. Location of wells

3.2. Logs

From the following wells (Table 3.1), log data are available. The logging tool and the logging probes, which where used, are explained in point 3.2.1., and the several logging runs are explained in point 3.2.2.

Well Nr.	Easting	Northing	Elevation
80	449817.843	3178495.247	532.68
149	443134.862	3171019.680	528.96
150	444685.953	3171020.613	532.5
152	447659.185	3171097.378	538.14
151A	446143.316	3171021.491	534.2
85	434587.365	3184015.991	515.14
86	436131.978	3183667.733	518.09
87	437532.234	3183267.205	523.1
88	439009.458	3182873.347	524.89
89	440532.664	3182416.546	527.04
93	433850.905	3232372.794	458.26
121	428000.101	3193342.143	513.87
126	431589.784	3186821.815	515.46
134	434819.193	3175353.357	509.87
139	437292.098	3168351.327	520.25
141	438839.957	3165854.861	528.37
142	439781.936	3164563.835	531.88
145	442757.618	3161113.413	543.34
478	463887.838	3109084.900	-

Tab. 3.1. Available wells in utm coordinates (Zone 33)

3.2.1. Logging tools

After the "Drilling, testing and completion report" of Well Nr142, the geophysical logging is realised with a Robertson Geologging unit, which was installed in a Toyota Landcruiser. The surface equipment was a RG-PRO-LOGGER System, which operated a RG 2000 winch unit, equipped with a 1000m 3/16" cable. The Probes which were used are explained in the following points.

3.2.1.1. Electric Logging Probe

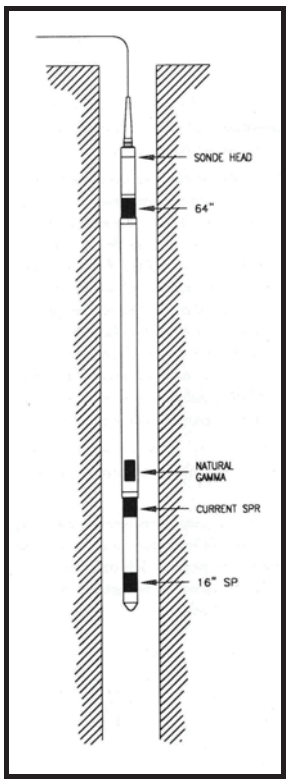

Fig. 3.2. Electric Logging Probe

The electric logging probe (after Robertson Geologging Descriptions) is a classic water-well-combination probe with

16" Normal resistivity measurement,
64" Normal resistivity measurement,
a single-point resistivity measurement,
a self potential measurement,
natural gamma measurement and
a temperature measurement.

Furthermore, the electric logging probe includes downhole electronics and digital signal transmission in order to not have to deal with cable effects in deeper boreholes.

The tool consists of a down-hole probe with electrodes and measurement electronics and an insulated bridle. A low-frequency bi-directional electric current is produced by the probe and is returned by the formation to the armour above the bridle.

The potential differences due to this current flow are measured with sense electrodes with respect to a voltage-reference electrode located at the surface or downhole on the bridle. A downhole micro-processor converts these measurements for transmission to the surface to apparent formation resistivities in a digital format. To enhance the resolution and accuracy over a range of more than four decades of apparent resistivity, the probe electronics include constant power circuitry.

The self potential (SP) is measured using a non-polarising lead electrode on the probe and a surface voltage reference stake. An optional natural gamma detector is available for correlation with other logging runs.

3.2.1.2. Focussed Electric Probe(Guard Log)

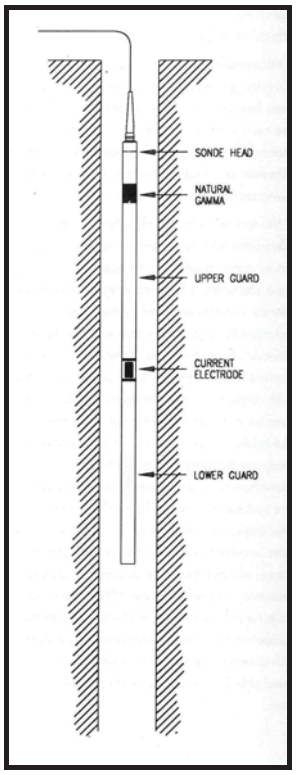

Fig. 3.3. Focused Electric Probe

The guard log probe provides a focussed resistivity measurement with good vertical resolution and depth of investigation. For correlation purposes, a gamma ray detector is also available. The advantages of the guard log is that it can provide measurements under adverse conditions like high borehole fluid salinity and high formation resistance where conventional 16" and 64" Normal resistivity logs provide inaccurate results. The probe consists of a central current source electrode situated between two guard electrodes, maintained at the same potential by internal electronics. By the presence of the guards, current from the central electrode is focused to a thin disk and returns to the cable armour above a 10m insulated section. The potential of the central electrode, determined in cooperation with a surface voltage reference stake, and the measured current are combined by a downhole micro-processor to calculate the apparent formation resistivity. Additionally, an internal resistor, which simulates a formation resistance of 100 ohm-metres, is responsible for the calibration. Close to the top of the probe, there is the

natural gamma measurement, which uses a high sensitivity scintillation detector, and to permit log presentation in standard API units, a held calibrator is available.

3.2.1.3. Three-Arm Caliper Probe

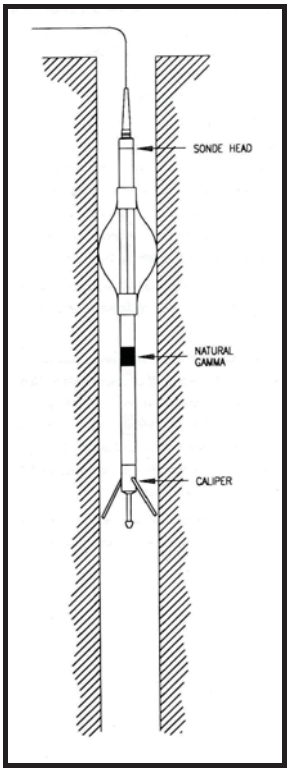

Fig. 3.4. Three-Arm Caliper Probe

The Three-Arm Caliper Probe consists of three mechanically-coupled arms which are in contact with the borehole walls and determine a single continuous log of borehole diameter. Both short and long arm options are available to suit a wide range of well diameters. The caliper log is a helpful first log to determine the borehole condition before running more costly probes or those containing radioactive sources. Allowing the probe to be run into the borehole with the arms retracted, the opening and closing of the motor-driven caliper arms are under surface control. At the start of logging, the arms open and the probe raise up the borehole. The spring-loaded arms finally measure the borehole diameter variations. The coupling between the arms means that the resulting log usually represents the minimum diameter in non-circular boreholes. To allow logs to be displayed directly in linear metric or imperial units, a Held calibrator is provided. An optional natural gamma detector is available for

correlation with other logging runs. Furthermore, a held calibrator is available to permit log presentation in standard API units.

3.2.1.4. Neutron Probe (Single Spacing)

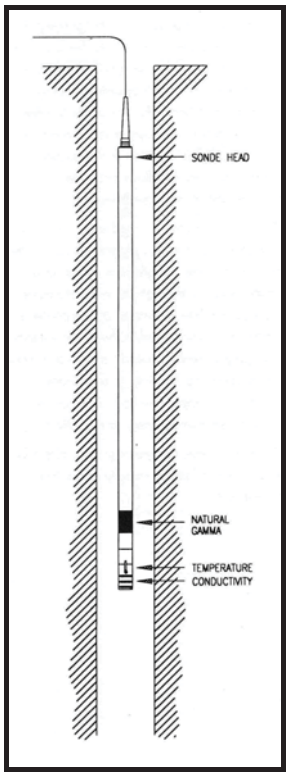

Fig. 3.5. Neutron Probe

The single neutron probe is versatile and capable of quantitative measurements under most borehole conditions including logging through steel or plastic casing and drill pipe. A ^{3}He proportional detector is used as a neutron measurement and is located 45 centimetres from a detachably sealed neutron source. Fast neutrons from the source are scattered and slowed principally by hydrogen in the formation until they reach thermal energy levels and are absorbed. The flux of thermal neutrons reaching the detector is related to the formation hydrogen content and porosity. An optional natural gamma detector is available for correlation with other logging runs. Furthermore, a held calibrator is available to permit log presentation in standard API units.

3.2.1.5. Temperature/Conductivity Probe

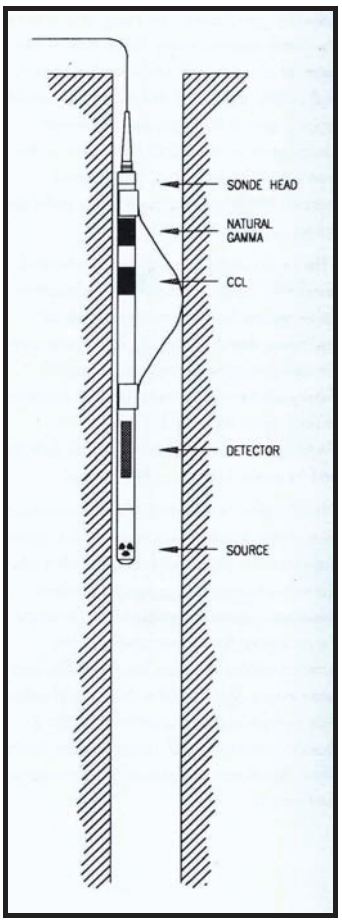

Fig. 3.6. Temperature/Conductivity Probe

This probe combination provides continuous depth-based measurements of temperature and conductivity which can be output in absolute and in differential forms. An optional natural gamma detector is available for correlation with other logging runs. At the base of the probe, there are measurement sensors located in an insulated housing where borehole fluid flows during logging, freely through ports on the side and base of this housing and over the sensors. A high sensitivity semiconductor transducer is used for temperature measurements. The conductivity cell comprises three carbon contact rings driven by a constant voltage source of alternating polarity to avoid cell polarisation effects. To ensure optimal results, the probe should be calibrated periodically at base using a constant temperature bath and standard KCI conductivity solutions. Finally, no held calibration is required for this probe.

3.2.2. Logging runs

After the well construction sketch from the "Drilling, testing and completion report", the wells consist of two different casings on the upper part of the wells and of an uncased part on the lower part of the wells. The first casing is a 26" Carbon steel casing and the second casing is a 16" ID GRP casing. According to the well construction, mostly two geophysical logging runs were realised. The Neutron Probes were only used for the target horizon, which comply the uncased hole.

The SP measurements cannot be used for the interpretation because the borehole fluid was always the same as the formation fluid.

3.2.3. Logging descriptions and reports

From well 142, the "Drilling, testing and completion report" was available. From the other 11 wells, only parts of the "Drilling testing and completion report" were able to be obtained: the Sieve analysis of the cuttings, the multi-stage pumping test and a stratigraphical and lithological description of the cuttings.

3.3. Rocksamples

For calibrating and upgrading the data from the logging tools, rock samples are necessary. The available samples consist of unconsolidated rocks which are not the perfect samples for petrophysical investigation, but some information can be obtained through these samples. For the thin sections, pieces of several centimetres of thickness can be taken (Figure 3.7) out from the samples and the grain composition can be appointed.

Fig. 3.7. Rock samples of the Hassouna Formation

The sampling is done on two spots at the outcrops of the Hassaouna Formation close to the wells were log data are available. The exact sampling locations are illustrated in the figure 6.1 in chapter 6.8.

3.4. Conclusion and summary

For the petrophysical parameter estimation 12 wells, located in two profiles, are selected and prepared for the calculations (Figure 3.8). The selection is based on the geological similarity of the 12 wells, which makes a petrophysical determination more reproducible and more exact.

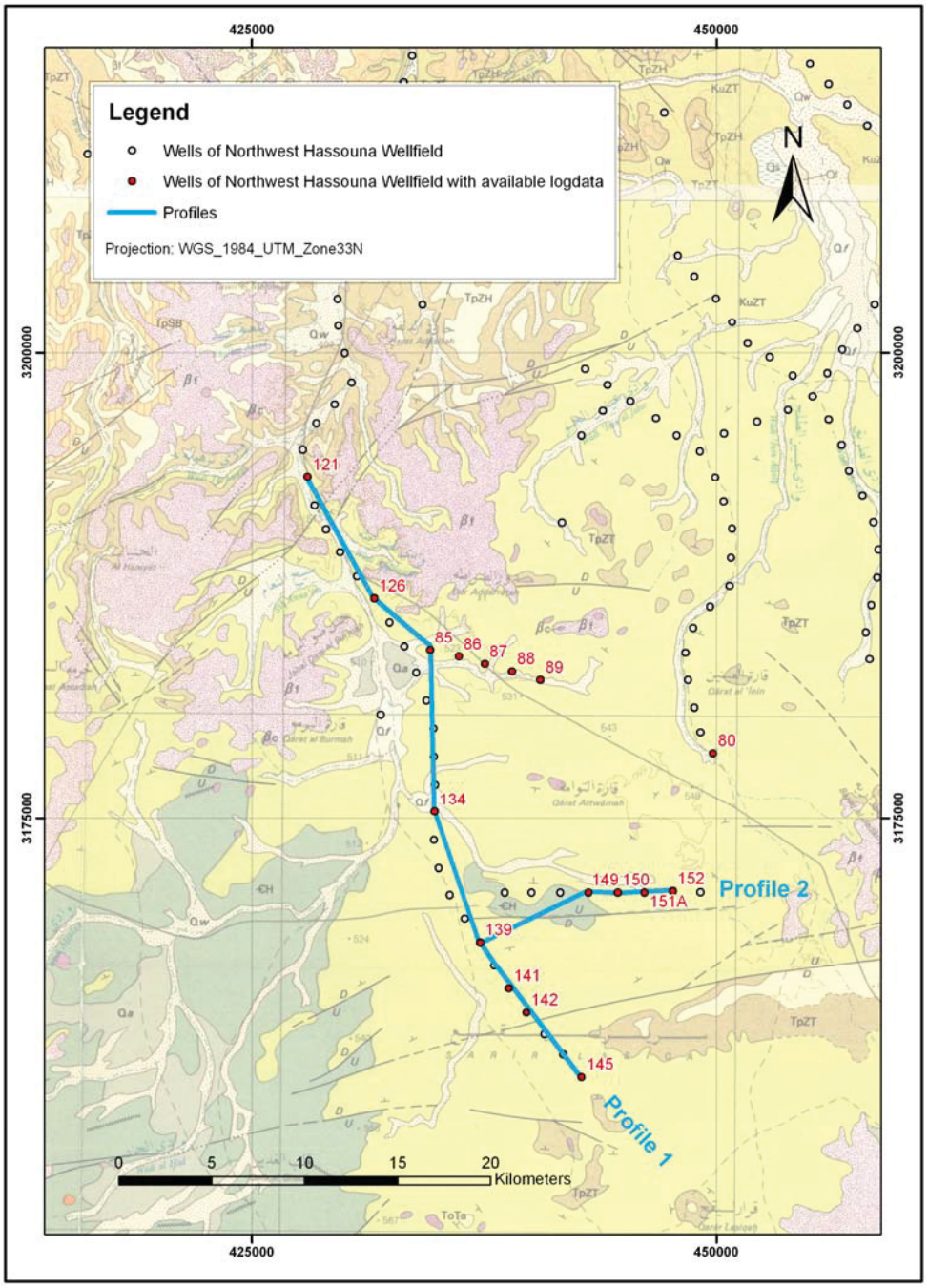

Fig. 3.8. Selected Profiles for petrophysical determinations

4. Data preparation, database:

4.1. Digitalization

The Digitalisation was realized with the program Didger 1.0.37, where points, lines or squares can be digitized. The digitalisation can be done on a digitalisation board or directly on the monitor screen, but the former possibility is more exact. To receive the plotted points or lines, a mouse with cross chairs is used. By pressing the left button of the mouse, the program Didger 1.0.37 saves a point.

The medium which is digitised consists of log plots, which are printed on endless paper. The quality of the paper differs depending on the age of the logs. Also the consistence of the fixation of paper appoints to the accuracy of the digitalisation because of paper shifting.

An important step for digitalization of the data is defining a coordinate system for each log plot by digitizing 3 points on each of the log sheet.

After geo-referencing, the log plot is received by using the mouse with the cross chairs. To get a precise image of the log curve, it is important to digitize as many points as possible. Especially sharp curves have to be digitized carefully, because after resampling, the shape of the log curve should not be different.

The digitized file is saved in a pit-file but can also be exported as a .dat-, .bln-, .ban-, .dxf-, .bmp- or .wmf- file.

4.2. Database

Finally, the digitized data are inserted into an Excel sheet and conjugate logs are copied together to get one file for each measurement and each borehole. The files consist of 2 columns. The first column is the depth column and the second the measurement column. These files are loaded in Petrel 2008 and are displayed in log plots. There, the quality is checked and an adequate digitalisation is controlled. Badly digitized logs are digitized again and obvious faults are eliminated.

After the quality check, the data are resampled by getting an increment rate of 0.5 m, which enables a correlation and data management. After resampling, the data are exported as ascii-files and are opened in Interactive Petrophysics 3.4. (IP). In IP las-files are created for each of the wells and all available log data of each well are

saved in that type of file. Furthermore, additional information is saved in the log header of the las- file.

Finally, the database of the well logs consists of one file for each well and the type of the file is a las- file, which can be easily opened with the interpretation software Petrel 2008 or IP 3.4. Both programs are used for further calculations and interpretations.

5. Technique of Interpretation

5.1. Determination of Formation Factor and Archie Parameter

Archie's equation (Archie, 1942) for water-saturated porous rocks offers a possibility of porosity estimation. As input, the measured formation resistivity (R_t or R_0 if S_W = 1), the water resistivity (R_w) and Archie's exponent m are necessary. Archie's equation is only valid for "clean" rocks.

5.1.1. Determination of the Formation Factor

To determine the Formation Factor, the cell, as it is described in figure 5.1, is filled up with water. Then, in the two outer electrodes, a certain current is applied, and the voltage is measured first in the water-saturated sample zone of position two and then in the fluid zone of position one. The current is in both measurements the same. Because the distance between ring one and ring two of position one and position two is identical, the geometry factor is not important.

Finally, R_t and R_w are obtained, and by using Archie's equation (Equation 5.2), the Formation Factor can be determined:

$$R = \frac{U}{I} \qquad (5.1)$$

$$F = \frac{R_t}{R_w} = \frac{a}{\phi^m} \qquad (5.2)$$

For both measurements, the same current is used:

$$I_1 = I_2 = I_{cons\tan t} \qquad (5.3)$$

After that the equation 5.4 is reached:

$$F = \frac{R_t}{R_w} = \frac{\frac{U_t}{I_1}}{\frac{U_w}{I_2}} = \frac{U_t}{U_w} \qquad (5.4)$$

I… electric current [A]

U… electric voltage [V]

R… resistance [ohm]

R_t… formation resistivity [ohmm]

R_w… resitivity of the fluid [ohmm]

F… Formation Factor

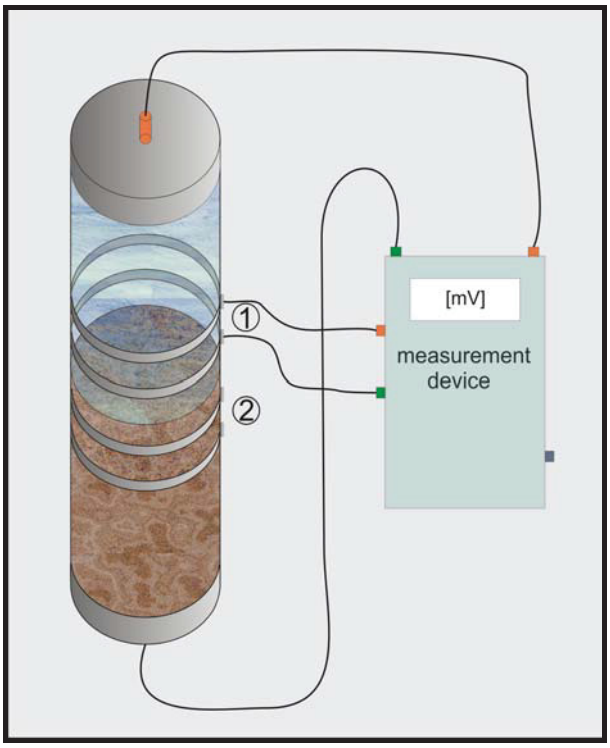

Fig. 5.1. Sample cell for voltage measurement

5.1.2. Investigation of the factor m of Archie's equation

To determine the factor m of Archie's equation (5.2), porosities and Formation Factors are cross-plotted.

The obtained points of the cross-plot should ideally follow a function. To achieve this function, a power law function is overlaid and is adapted to the points. Finally a power law function is obtained, where the power can be picked out. The obtained power describes the factor m.

5.2. Determination of shale content

The typical determination of shale content in water wells is made with the assistance of the gamma-ray measurements. Gamma-radiation from sediment is essentially originated through the potassium, uranium and thorium content of the minerals. Potassium is an element that is often a component of clay minerals, alkali feldspars, mica and others. Uranium and Thorium are elements which are abandoned in very small quantities in materials which have a large internal surface like in sediments with small grain sizes (silt and clay). According to this, clay and silt have a higher gamma-ray response than sands. In any case, the method has to be applied with attention to the case when sand occurs which contain mica or feldspar minerals or other more gamma-ray radiating minerals like glauconite coating. Such particles or zones have to be excluded from calculations, or else, other techniques like density-neutron-combination must be applied.

For using the gamma-ray measurements for further calculations, the gamma-ray probe has to be calibrated in API units.

5.2.1. GRI

The simple determination for the shale content is a linear relation from the gamma-ray measurement, which is called the Gamma Ray Index:

$$GRI = \frac{GR - GR\min}{GR\max - GR\min} \qquad (5.5)$$

GRI ...Gamma Ray Index
GR ...measured gamma radiation
GR_{min} ...GR – measured value of clean rock
GR_{max} ...GR – measured value of clay

To evaluate the GR_{min} and the GR_{max} value, all values of the gamma-ray measurements in API units have to be plotted in a histogram.

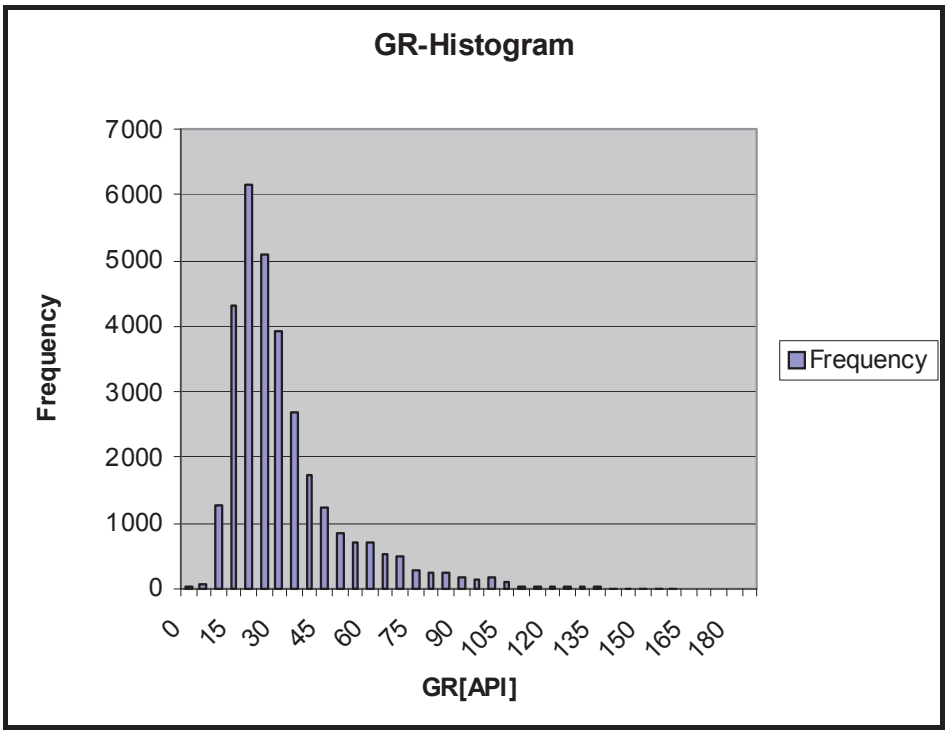

Fig. 5.2. Histogram of all gamma ray measurements of available wells (table 3.1)

Generally, the minima gamma-ray responses refer a clean sandstone with little to no shale content and low content of radioactive elements. To the contrary, the maxima

gamma ray response refers a shale horizon or an accumulation of radioactive minerals. But this interpretation has to be done with care: Not all maxima values represent the shale line. For example, if there is no shale horizon in the measured section, the maxima value does not represent GR_{max}. Then, GR_{max} has to be determined by using different data or through estimation from other wells.

According to the GRI, the shale content can be determined with the linear equation:

V_{sh} = GRI (5.6)…Clay and Silt
(Grainfraction < 0,063mm)

5.2.2. Nonlinear Relationships

Additional to the linear relationship of GRI, further equations enhance the shale content determination, especially through good understanding of the petrology of the target horizon:

$V_{sh} = 0.083 \cdot (2^{3.7 \cdot GRI} - 1)$ (5.7)…LARINOV(1969) – Neogenic and Palaeogenic rocks

$V_{sh} = 0.33 \cdot (2^{2 \cdot GRI} - 1)$ (5.8)…LARINOV(1969) – consolidated old rocks

$V_{sh} = 1.7 - \sqrt{(GRI + 0.7)^2}$ (5.9)…CLAVIER et al. (1971)

5.2.3. Determination of the influence of shale content

The content of shale influences the Formation Factor and finally, it influences all further determinations, which are based on resistivity measurements. To understand the influence of shale, the conductivity of the sample fluid (C_o) and of the sample (C_w) is measured. The procedure of measurement is the same as in chapter 5.1.1.
The following figure, 5.3, demonstrates the influence of shale on the ratio of C_o and C_w, which means the Formation Factor.

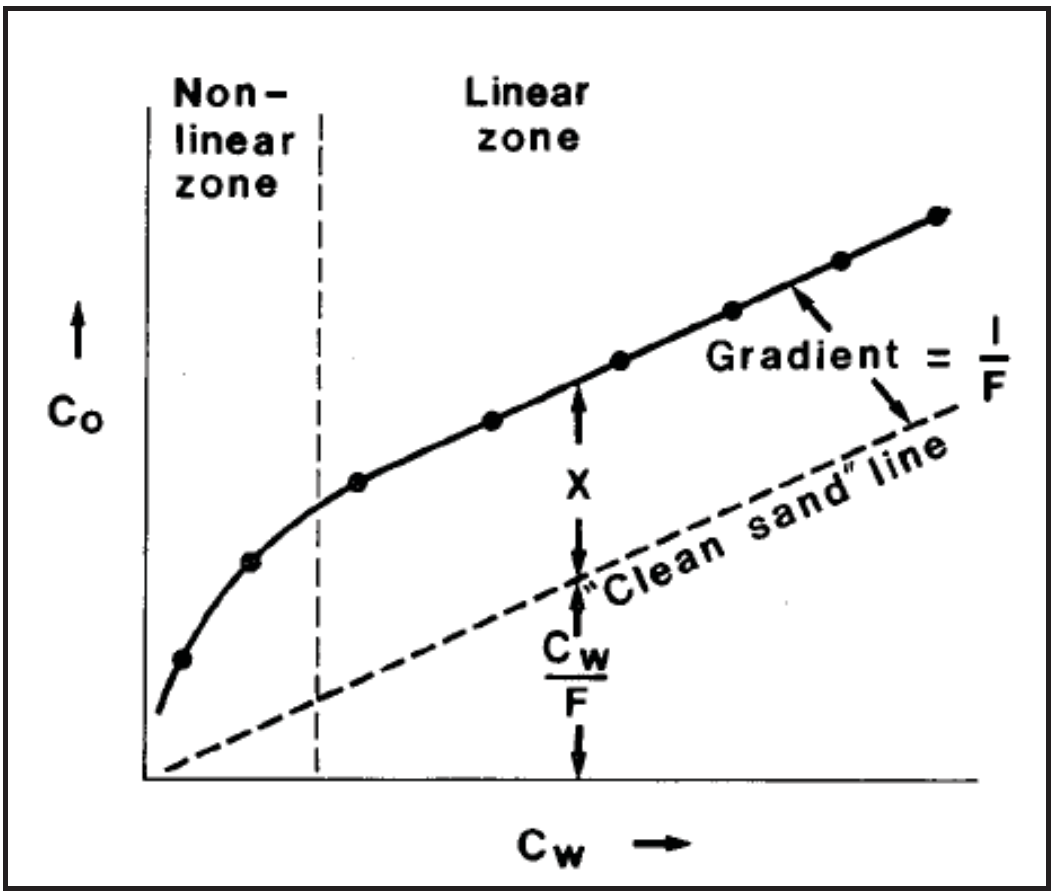

Fig. 5.3. Influence of shale on the Formation Factor after (Patnode and Wyllie, 1950)

The Formation Factor is the Apparent Formation Factor in case of a shaly rock. The conductivity of the shaly water-saturated rock is:

$$C_0 = \frac{C_w}{F} + X \qquad (5.10)$$

Cw …Conductivity of the formation water

F …Apparent Formation Factor

X …Excess conductivity

The corrected resistivity is therefore:

$$R_{0,korr} = \left(\frac{1}{R_{0,measured}} - X \right)^{-1} \qquad (5.11)$$

$R_{0,measured}$... measured resistivity

$R_{0,corr}$... corrected resistivity

5.3. Determination of porosity

5.3.1. Introduction to porosity

Porosity of a porous medium describes the fraction of void space in the material, where the void may contain, for example, air, water or hydrocarbons. The porosity is defined by the ratio:

$$\phi = \frac{V_p}{V} = 1 - \frac{V_m}{V} \qquad (5.12)$$

$V_{...}$ total or bulk volume
$V_{p...}$ volume of pore space
V_m ... volume of solid matrix

The unit of porosity is dimensionless and is expressed either as a decimal fraction or as a percentage (Schön 1996).
For a usable determination of porosity, some important issues have to be known:

Basically, porosity is the result of various geological, physical and chemical processes, and it is distinguished between the porosity generated through the sedimentation process "primary porosity", and the porosity generated through the geologic history of the sediment, called "secondary porosity" (Schopper, 1982).

Because of various processes of porosity building, the porosity has different petrography fabrics, which is important to know for porosity determination.

5.3.2. Possibilities of porosity determination

The précised way to determine the porosity of a formation in a borehole is combining petrologic and petrophysical investigations of cores or samples of the formation and logging tools.

5.3.2.1. Measurement by using samples

For porosity determination, two methods are used: The first method uses the raw density and the grain density for the determination of the porosity, and the second method uses the volume of the pore fluid and the volume of the matrix to reach the porosity.

5.3.2.2. Porosity determination by using densities

To investigate the porosity a cell is used (Figure 5.4), where for which the volume is easily determined. Then, an amount of sample material is weighted and is put into the cell. Next, the volume of the sample material is measured and the density can be determined. After equation 5.15, the porosity of the sample material can be calculated.

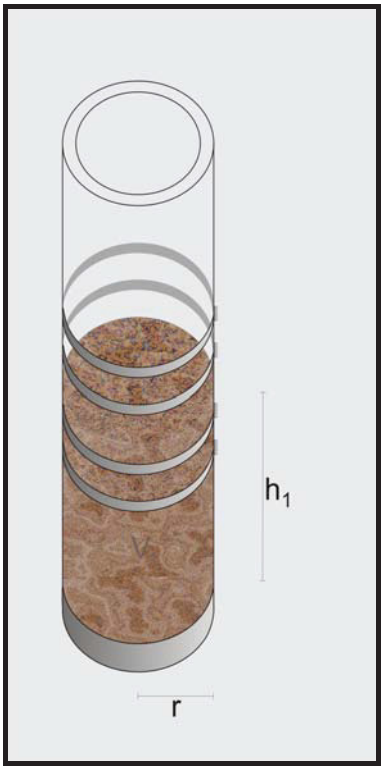

Fig. 5.4. Measurement cell

$$V = r^2 \cdot \pi \cdot h \qquad (5.13)$$

$$\rho = \frac{m}{V} \qquad (5.14)$$

$$\phi_1 = 1 - \frac{\rho}{\rho_0} \qquad (5.15)$$

V... volume of the sample material

r... radius of the sample material

h... high of the sample material

m... mass of sample

ϕ_1 ... porosity

ρ ... density of the sample

ρ_0 ... grain density of the sample

5.3.2.3. Porosity determination by using volumes

The grain density ρ_0 of the material is supposed according to the analysis of the thin sections.

For the second method, a certain amount of sample material in the cell is water-saturated. The volume of the used water for a complete water saturation is measured and after equation 5.16, the porosity can be determined.

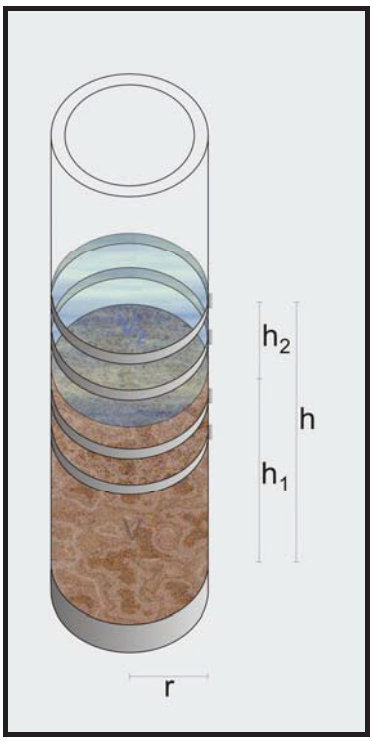

Fig. 5.5. Measurement cell

$$h_1 = h - h_2 \qquad (5.17)$$

$$V_{pore} = V_w - V_2 \qquad (5.18)$$

$$\phi_2 = \frac{V_{pore}}{V} \qquad (5.19)$$

h …high between sample bottom and waterlevel

h_1 …high between sample top and waterlevel

h_2 …high between sample bottom and sample top

V_{pore} …pore volume

V_w …volume of used water

V_2 …volume of water above the top of the sample

ϕ_2 …porosity

5.3.2.4. Measurement by using logging tools

5.3.2.4.1. Resistivity log

Porosity can also be determined by using the resistivity log. But for a usable determination, the lithology and the Archie-parameters a and m have to be known or calculated. The equation 5.20 after Archie (1942) and Dachnow (1962) derive the porosity for formations without clay content ("clean rocks"):

$$F = \frac{R_0}{R_w} = \frac{a}{\Phi^m} \qquad (5.20)$$

To get R_0 and R_w, a correction to eliminate the influence of the spacing l of the logging measurements devices and to eliminate the influence of the borehole diameter d has to be done. Dachnow (1962) found a chart where the R_0 values can be read out by input of the measured resistivity (R_m), the spacing, the R_w value and the diameter of the well.

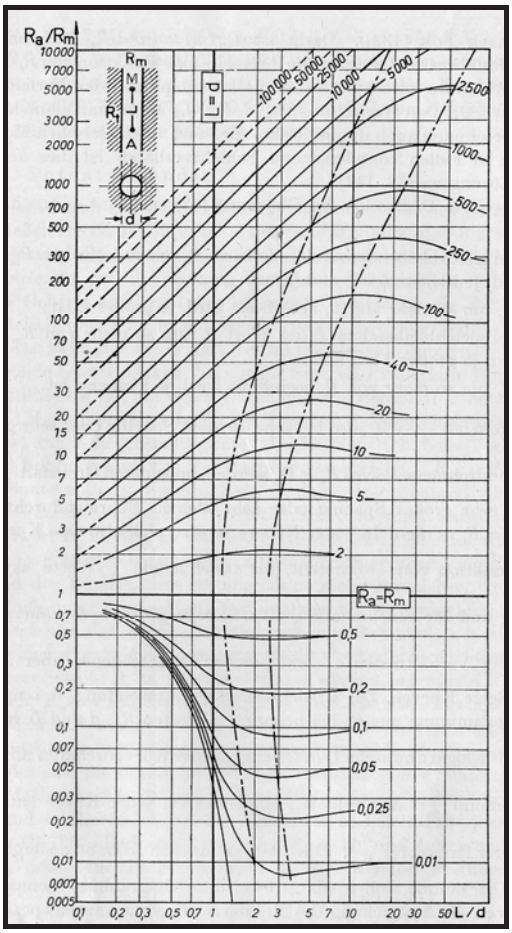

Fig. 5.6. Correction diagram of Dachnow (1962)

To accelerate the determination of R_0, a numerical solution geared to the chart of Dachnow is found.

It must also be considered that R_w values are not always measured at the same time as the R_0 values, and so, in some boreholes, the R_w values have to be calculated as well. The R_w for each temperature can be calculated with the equation after Arps (1953).

$$R_w(T_2) = R_w(T_1) \cdot \frac{T_1 + 21.5}{T_2 + 21.5} \qquad (5.21)$$

By considering the shale content, one of the various shaly sand equations must be applied (see for example Worthington, 1985) A relative simple form has the following equation for a laminated shaly sand:

$$\frac{1}{R_0} = \frac{V_{sh}}{R_{sh}} + \frac{1 - V_{sh}}{F \cdot R_w} \qquad (5.22 , Poupon, Loy \& Tixier;s. Schön, 1983)$$

$$\frac{1}{R_0} = \frac{C_W}{F} + V_{sh} \cdot C_{sh} \qquad (5.23, Simandoux, 1963)$$

R_{sh} …resistivity of shale
V_{sh} …shale volume
C_{sh} …conductivity of shale
C_0 …conductivity of watersaturated zone
C_w …conductivity of formation water

5.4. Determination of permeability

5.4.1. Introduction to permeability

In practice, permeability is mainly measured in the unit Darcy [d]. One Darcy is defined as the permeability of a material which permits a volume flow density of 1cm/s of a fluid with a viscosity of 1cp (Centi Poise) under a pressure gradient of 1atm/cm.

Converted to SI units, permeability has the dimension of an area, 1 Darcy is equivalent to 9.869×10^{-13} m² or 0.9869 µm². This conversion is usually approximated as 1 µm².

In Hydrology, the unit kf is frequently used, which has the dimension of a velocity [cm/s] after the equation 5.24.

$$u = k_f \cdot \frac{\Delta h}{l} \qquad (5.24)$$

For water with an assumed constant viscosity and density, a connection between the kf- value and Darcy results in the following:

1md~10^{-6}cm/s = 10^{-8}m/s 1m/s = 10^{5} d

For a usable determination, some important issues of permeability have to be known.

The first issue is that there are different types of permeability (Schön, 1997) which control permeability. To know the types or to know about a possible absence of a type helps finding the right kind of permeability determination. The main types are:

- Inter-granular permeability
- Intra-granular permeability
- fracture, crack and fissure permeability
- vugular permeability (Schopper, 1982)

The second issue is the influence of parameters on the permeability (Schön,1997). Because a direct measurement of permeability in boreholes is rarely made, the permeabilty can only be determined by knowing the influences of the permeability. The main influences are:

- porosity
- pore size and its distribution,
- pore shape, pore surface morphology, specific internal surface and
- arrangement of pores and pore throats (topology of the pore network).

The third issue is the knowledge of permeability tendencies. After experiencing direct measurements of different samples, permeability tendencies can be determined.

- If permeability increases,
  - Grain size increases
  - Porosity increases

- If Compaction and Cementation Porosity increases,
  - Permeability increases

5.4.2. Possibilities of permeability estimation

The permeability estimation based on logging tools can be realized by the following different techniques:

5.4.2.1. Permeability estimation from NMR

The estimation of permeability concerning NMR measurements is based on a combination of theoretical connection and experimental measurements (Ellis, D.V. and Singer, J.M., 2007). The physical basis for using NMR measurements is the dependence of permeability on the size of the pore throats of the medium. The T2 distribution of NMR measurements is related to a typical pore dimension and the pore size dimension is also weakly connected to the throat size, which is more reliable among sandstones. (Ellis, D.V. and Singer, J.M., 2007)

At present, there are two general transformations which are in widespread use to estimate the permeability. The first is called Coates-Timur-relationship and is given by:

$$k = a\phi^4\left[\frac{FFI}{BVI}\right]^2 \qquad (5.25)$$

FFI …volume of free fluid

BVI …bound volume fraction

The second, referred to as the SDR relationship:

$$k = a\phi^4 T_{2,LM}{}^2 \qquad (5.26)$$

$T_{2,LM}$ …logarithmic mean value of the measured T2 distribution

The value a is a constant and has to be adjusted to local conditions or the exponents on porosity and on the NMR parameters should be adjusted to get a better fit to known permeability from core samples or by other means.

5.4.2.2. Permeability estimation from porosity and empirical relationships

A lot of researchers have found out that there is often a good correlation between porosity and permeability in detrital rocks. The permeability can be estimated using an empirical relationship between porosity and permeability. These empirical relationships are based on the type of reservoir or even better on the type of facies, environment and diagenetic effects. To characterize the individual types, parameters like grain size, pore size mineralogy and surface conditions of the grains are gathered.

A few models from different researchers have been found to estimate the permeability.

5.4.2.2.1. Permeability model (Kozeny-Carman-relationship)

Permeability can be described after Carman, 1956; Amyx et al., 1960; Timur, 1968; Hearst and Nelson 1985 in a model.

The Kozeny-Carman-relationship is a tube-like model where a flow through a porous media is characterised by a flow through a bundle of tubes of different radii, where the flow is laminar because of a low flow-rate. Each tube defines a tortuous route from one hand of the rock to the other. The tortuosity is defined as the following equation:

$$\tau = \left(\frac{L_a}{L} \right)^2 \qquad (5.27)$$

The consideration of a flow through tubes results in the equation 5.28, 5.29 and 5.30. The different shapes of the equations depend on what volume is used to normalize the pore surface area:

$$k = \frac{\phi R_h^2}{f\tau} = \frac{\phi}{f\tau \sum_p^2} \qquad (5.28)$$

$$k = \frac{\phi^3}{f\tau \sum_r^2} \qquad (5.29)$$

$$k = \frac{\phi^3}{f\tau \sum_g^2 (1-\phi)^2} \qquad (5.30)$$

ϕ …porosity

L …sample length

L_a …tube length

R_h …hydraulic radius

f …shape factor (1.7-3)

τ …tortuosity

$\sum_p$ …ratio of pore surface area to pore volume

$\sum_r$ …ratio of pore surface area to rock volume

$\sum_g$ …ratio of pore surface area to grain volume

5.4.2.2.2. Empirical relationship based on grain size after Krumbein and Monk

The equation after Krumbein and Monk (1942) is based on sand packs of 40% and does not include porosity as a parameter, but Beard and Weyl (1973) showed that the equation 5.32 also gives acceptable results with porosities which are between 23% and 43%. The laboratory studies were made with sandstones from a common source where the grain properties did not vary much. The equation only can be used with these ideal conditions because a disproportionate amount can drastically reduce k in unconsolidated sands.

$$k(darcy) = 760 D_g^2 e^{(-1.31\sigma_D)} \qquad (5.32)$$

D_g …geometric mean diameter in millimeters

σ_D …standard deviaton of grain diameter in phi units

5.4.2.2.3. Empirical relationship based on grain size after Van Baaren

The Van Baaren's Model (1979) uses the Kozeny-Carman expression of form 5.31 and substitutes $F\phi = \tau, \sum_r = 4/d,$ and $F = \phi^{-m}$ to get k,

$$k = c_2 d^2 \phi^m \qquad (5.31)$$

c_2 is a constant and is found out by using a set of experimental measurements of ϕ and mercury injection. Finally

$$k = 10 d_{70}^2 \ \phi^m \qquad (5.32)$$

is obtained.

d_{70} …effective pore diameter at 70% water saturation [µm]

The formula 5.33 is, after van Baaren (1979), an intermediate step for permeability prediction based on petrological data. To improve the model, data from sandstones and carbonates are used to establish a relationship between ϕ and $\frac{d_{70}}{D_d}$

$$\phi = C\left(\frac{d_{70}}{D_d}\right)^{0.55} \qquad (5.33)$$

Sorting	**C**	**D_d**
Extremely well to very well sorted	0.70	2.5
Very well to well	0.77	-
Well	0.84	3.5
Well to moderately	0.87	-
Moderately	0.91	8.0
Moderately to poorly	0.95	-
Poorly	1	-

Tab. 5.1. Relation of sorting coefficient C to spread of dominant grain diameter, Dd from Van Baaren(1979)

After substitution of equation 5.33 into equation 5.32 the following equation occurs:

$$k = 10 D_d^2 \phi^{3.64+m} C^{-3.64} \qquad (5.34)$$

The equation can be used for estimation of k from observation of the consolidation rate of dominant grain diameter D_d and sorting index C.

5.4.2.2.4. Empirical relationship based on the Formation Factor

Walsh and Brace (1984) reworked the Kozeny Carman relationship and established a relationship between electrical properties and tortuosity. The Formation Factor is related to the tortuosity and the porosity (Equation 5.35), and after applying the equation in equation 5.28, the equation 5.36 is established. It can be observed that there is a dependence on k and R^2.

$$F = \frac{\left(\frac{L_a}{L}\right)^2}{\phi} = \frac{\tau}{\phi} \qquad (5.35)$$

$$k = \frac{\phi R_h^2}{fF} = \frac{1}{f\tau \sum_p^2} \qquad (5.36)$$

5.4.2.3. Permeability estimation from porosity and sieve analyse data

The Berg (1972) model links grain size shape and sorting. The Berg formula considers that the pores are situated between various packings of spheres without change in shape or direction. The influence of the smaller grains is higher than the influence of the bigger grains, which introduces a sorting term p (Equation 5.39). The sorting term p is expressed in phi units and is called the percentile deviation for accounting for the spread in grain size distribution.

The equation of Berg (Equation 5.37) demonstrates that the permeability increases rapidly with the increasing porosity. The method of Berg is useable for unconsolidated sands and especially in relatively clean quartzose consolidated rocks, and the formula is applicable for porosity values higher than 30%.

$$k(darcy) = 5.1 \times 10^{-6} \phi^{5.1} D^2 e^{-1.385p} \qquad (5.37)$$

$$k(md) = 80.8 \phi^{5.1} D(\mu m)^2 e^{-1.385p} \qquad (5.38)$$

$$p = P_{90} - P_{10} \qquad (5.39)$$

ϕ …porosity

k …permeability[d],[md]

D …grain diameter[mm],[μm]

p …sorting term in phi units

P_{90} …sorting term at 90%

P_{10} …sorting term at 10%

5.4.2.3.1. Further permeability estimation

There are a few further estimation methods which are not optimal for the investigation in the area of interest but are listed for the sake of completeness.

One further possibility of permeability estimation is the equation of Herron (1987), who uses the equation after Kozeny and Carman and establishes a new equation, which uses mineralogical abundances. The permeability can also be estimated through aid for the equation after Lebreton et al. (1977), who uses sonic measurements.

5.5. Mineral content

5.5.1. Thin sections

The extracted small pieces of consolidated sediments were saturated with blue resin and prepared to thin sections. Each thin section consists of various pieces of rocks of one sample. With aid of the thin sections, the mineral content of a part of the Hassouna Formation can be determined. Additionally, the porosity can be estimated.

6. Application of technique on the selected wells

6.1. Shale content

The shale content is determined by using the gamma-ray measurements and by calculating the shale content after the GRI, which is described in detail in chapter 5.2.1.

After plotting all available GR-Data of the two selected profiles, the most frequent value is at about 20 API units, the GR_{min} is at about 10 API units and the GR_{max} value is at about 110 API units (Figure 6.1). Concerning the histogram, the GRI is calculated and the shale content is plotted. But after a second observation of the log plots, the values of the shale content are obviously too high for the formation, which means that the GR_{min} or the GR_{max} or both values are not right. After further investigation of the well descriptions and the analysis of the available sediment probes, it is found out that there are hardly any pure shale layers in the drilled wells of the two profiles, which makes a particularly determination of the GR_{max} difficult. Only an observation of the well with the highest API values can enhance the determination of GR_{max}. Finally, the GR_{max} of well W478 is used for determination (Figure 6.2).

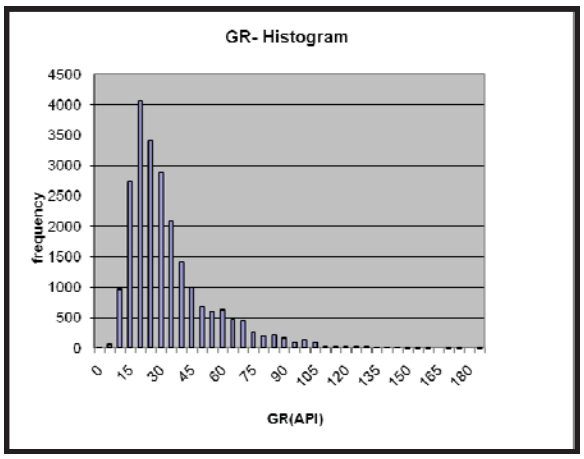

Fig. 6.1. GR- histogram of all GR-measurements

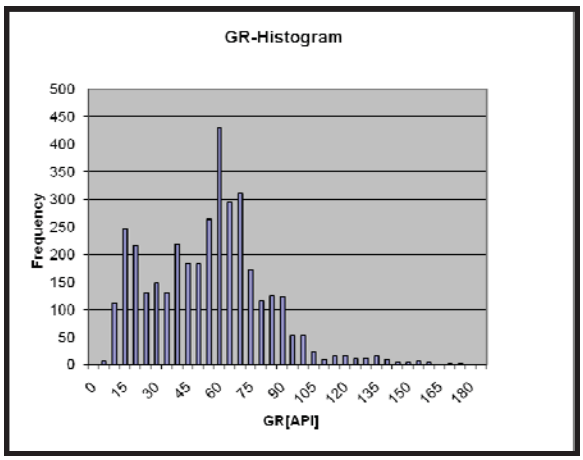

Fig. 6.2. GR- histogram of GRmeasurements of Well 47

Result of determination:

GR_{min}: 15 API

GR_{max}: 130 API

Due to the basis of the determined GR_{min} and GR_{max} values, the shale content of the wells are calculated in a logplot for each of the selected wells, which can be seen in chapter 7.1.2.

After the determination of the shale content (Chapter 5.2), after observation of the thin sections (Chapter 6.8) and after the petrophysical investigation of the samples (Chapter 6.6), it is obvious that the shale has an influence on the resistivity measurements and the shale content has to be considered in all the following calculations, determinations or estimations. All values of $R_{0,measured}$ have to be rectified by the value X. The precise equation can be observed in chapter 5.2.3.

Result of determination:

X= 0.007 S/m

The value is referred to the samples and is a median value.

6.2. Parameters for further investigation

6.2.1. Archie parameters

Parameter m can be determined by cross-plotting porosities and formation factors. The following table (Table 6.1) displays the obtained values of porosity by the measurements of chapter 5.3.2.2 and by the measurements of chapter 5.3.2.3. The displayed values of the formation factor are from the voltage measurements of the samples (Chapter 5.1.1): These values were plotted and with aid of the overlaid functions, the factor m can be read out (Figure 6.3). Functions are made for the factor m 1.4 to 2.0. For the determination, the factor m 1.8 is selected. The function of the factor m 1.8 is displayed in the red line. The blue points in figure 6.3 mark the obtained results of the sample measurements. The factors m of the samples are less, but they are measured from unconsolidated samples and so, the factor m is assumed a little higher.

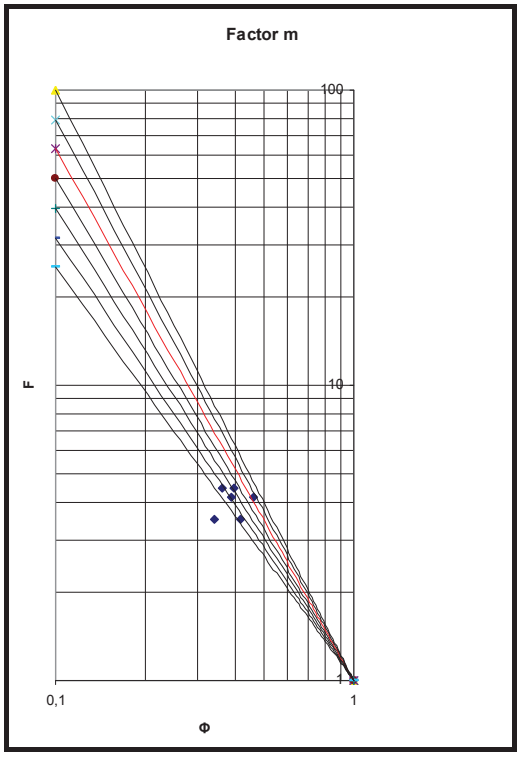

Fig. 6.3. Obtained factor m

Probe	Porosität	F
B1	0.387	4.2
	0.46	4.2
B2	0.395	4.5
	0.362	4.5
A1	0.419	3.5
	0.342	3.5

Tab. 6.1. Obtained porosities and F determined of the samples

6.3. Porosity

To determine the porosity of the formation by using logging tools, there are several possibilities, which are approached in chapter 4.2. It is only a question of availability of logging data. In the area of interest, a porosity determination is possible by using the resistivity log.

The following chart displays the procedure of the porosity determination:

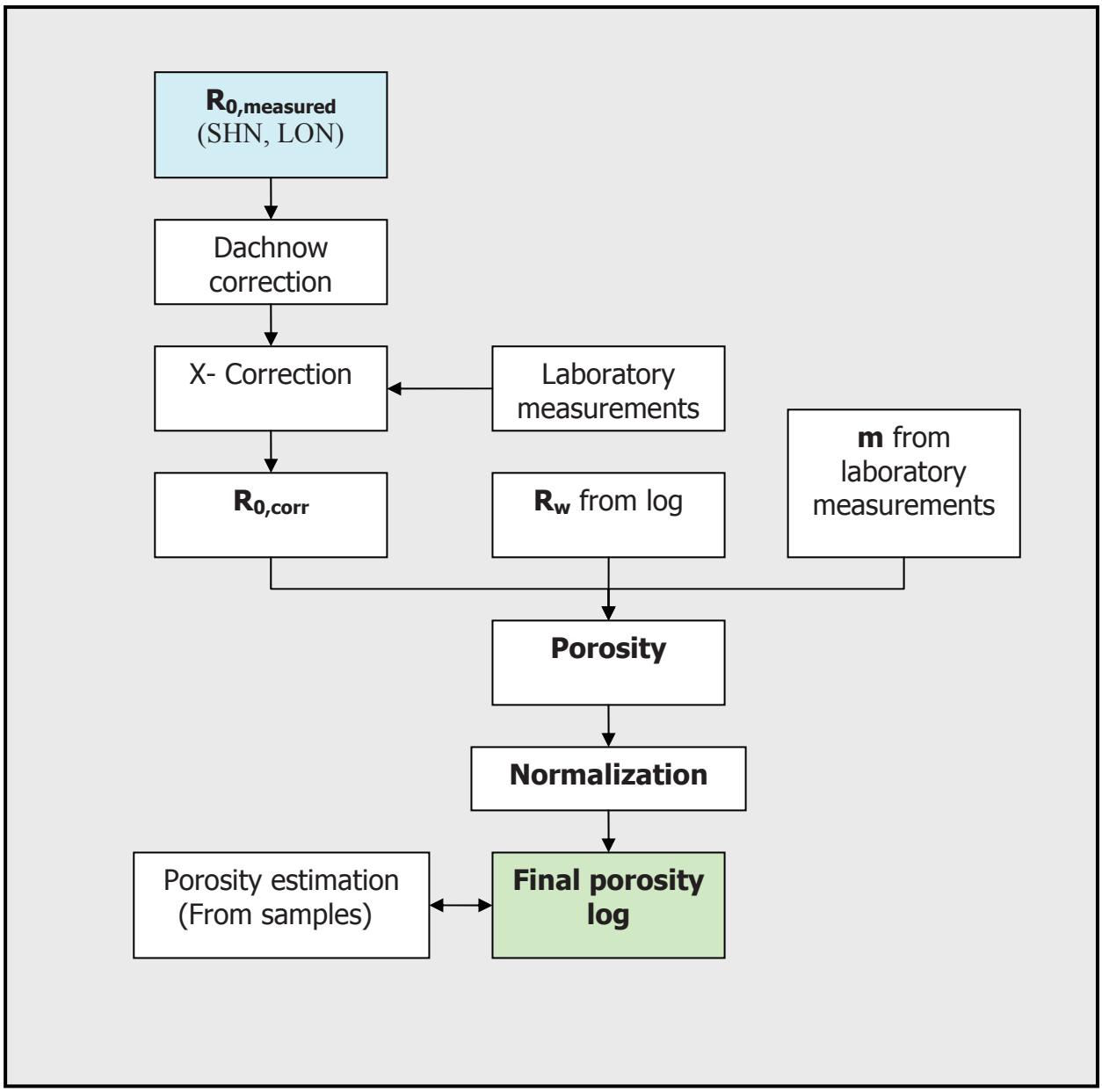

Fig. 6.4. Flowchart of porosity determination

6.3.1. R_0 corrections

6.3.1.1. Dachnow correction

The first correction of the resistivity measurements is to discharge the influence of the spacing of the logging measurements devices and the influence of the borehole diameter, which is explained in chapter 5.3.2.4.1. The influence of the borehole fluid can be neglected because there is no mud drilling fluid used.

6.3.1.2. Shale influence correction (X-correction)

Because of availability of shale, the R_0 values have to be corrected a second time. The values are rectified after the equation of chapter 5.2.3. R_0 is corrected by the value x, which is determined.

Result of determination of X: 0.007S/m

Finally, the rectified R_0 value and the R_w value can be inserted into the Archie equation. The formation factor can be determined and with the aid of the determined Archie parameters of chapter 6.2.1, the porosity is calculated and a porosity log is accrued.

6.3.2. Normalization

The following two plots display the porosity distribution of the two profiles. Because of different measurement conditions between the wells, a correction of the measured porosities has to be done. There are several possibilities of normalization (John H. Doveton, 1986). For this correction, the equations 6.41 and 6.42 are used:

$$M = \frac{\prod_{n=well}^{12} (\phi_{mean,\,n}) \cdot (l_n)}{\sum_{n=well}^{12} l_n} \qquad (6.41)$$

$$f_n = \frac{M}{\phi_{mean,\,n}} \qquad (6.42)$$

n …well number

l …length of well section

M …mean value of porosity of all wells

f_n …factor of normalization

$\phi_{mean,\,n}$ ...mean porosity of well n

The obtained mean porosity is 29.15% with a deviation of 12.79%.

All calculated porosities are multiplied with the factor f, and the corrected normalized log plot is obtained.

Additionally, the measured porosities from the samples are compared with the obtained log-based porosity values:

6.3.3. Porosity estimation from samples

6.3.3.1. Porosity estimation by using densities and volumes of rock samples

The raw density and the grain density are used for estimation of the porosity and the volume of the pore fluid and the volume of the matrix are used to estimate the porosity. It has to be noted that the porosity is determined for unconsolidated sediment samples of the areas A and B. That means that the calculated porosity is only estimation and the real porosities are supposed to be a bit lower. The porosities which are obtained can be observed in table 6.1.

6.3.3.2. Porosity estimation by using the thin sections

Because of the blue resin which saturated the pores of the probes, the porosity can be estimated by estimating the volume content of the pores by using a reflected-light polarization microscope. The precision of the estimation is +/- 5% and should only be used for comparison with the determined porosities in the chapters before. The estimations can be viewed in chapter 6.5.

6.4. Permeability

The following chart displays the procedure of the permeability determination:

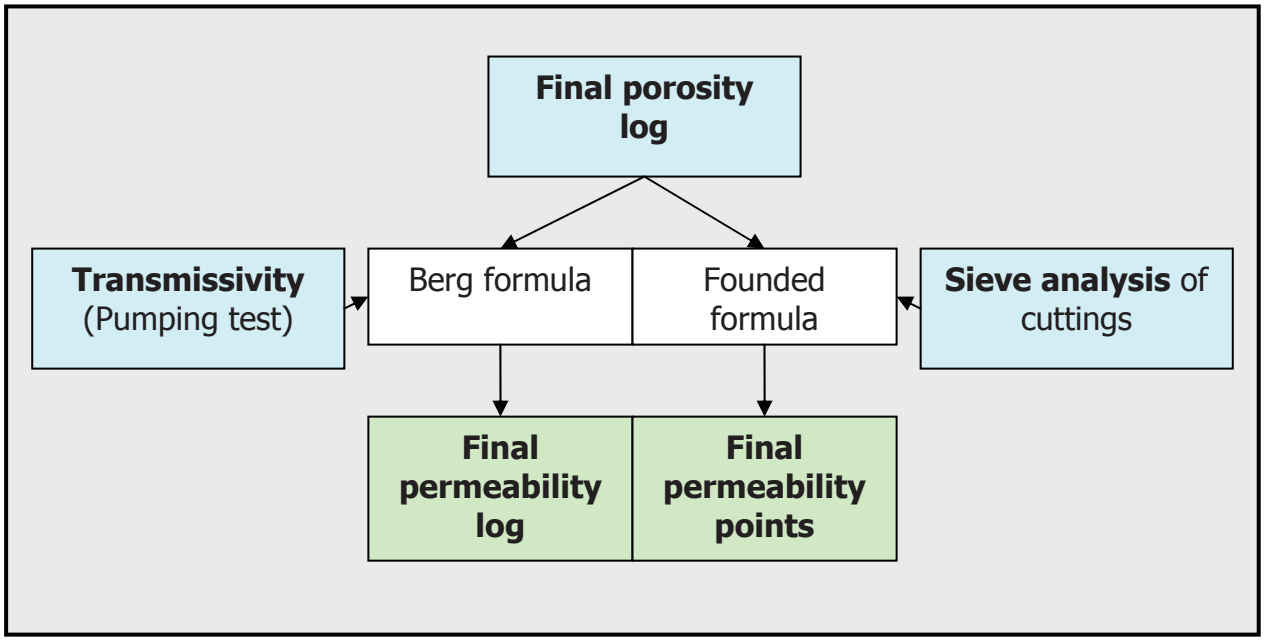

Fig. 6.5. Flowchart of permeability determination

In the course of the logging measurements of the available wells there was no logging tool which measured the permeability. Neither petrophysical measurements at cores are available to find out the permeability of the Hassouna Formation.
According to the problem it is possible anyway to estimate the permeability by using models and relationships based on porosity and different attributes. Some methods are covered in chapter 5.4. The following table displays the available measurements which can be brought up to estimate the permeability.

Attributes	**Thoroughness**	**Used parameters**
Porosity estimation:	From Resistivity log(SHN,LON) and corrected with Caliper log and R_w.	Φ(z)
Pumping test:	Single stage test from all wells	Transmissivity from single stage test.
Sieve analyse of cuttings	Every 20m depth in each well	Sieve analyse curve

Tab. 6.2. Available data for the permeability estimation

6.4.1.1. Permeability estimation by using pumping test data

For every borehole of the two profiles, a single stage testing was done and through the obtained transmissivity (Table 6.2) and knowledge of the aquifer thickness, the average permeability can be calculated. The following table 6.3 shows the transmissivity data, the aquifer thickness of the formation and the calculated average permeabilities in the unit m/s and in the unit Darcy.

Well	T[m²/s]	TOP	BOTTOM	t	kf[m/s]	d(Darcy)
W121	0.00239	273.5	500	226,5	1.05519E-05	1.055
W126	0.01730	273.5	500	226,5	7.63797E-05	7.638
W85	0.02190	273	500	227	9.64758E-05	9.648
W134	0.00185	273.5	500	226,5	8.16777E-06	0.817
W139	0.00330	273.5	500	226,5	1.45695E-05	1.457
W141	0.04850	285	500	215	0.000225581	22.558
W142	0.00389	285	530	245	1.58658E-05	1.587
W145	0.00574	273.5	500	135	4.25185E-05	4.252
W149	0.02740	285	420	135	0.000202963	20.296
W150	0.03840	285	500	215	0.000178605	17.860
W151	0.01310	284	500	216	6.06481E-05	6.065
W152	0.01150	285	500	215	5.34884E-05	5.349
W093	0.01400	329.5	500	170,5	8.21114E-05	8.211

Tab. 6.3. Calculated average permeabilities from the transmissivities of the aquifer range

6.4.1.2. Permeability estimation by using the sieve analyse curve of the cuttings

All 25 meter in the aquifer area are sieve analysis of the cuttings available, which are used to estimate the permeability. By using the Berg formula which is covered in detail in chapter 5.4.2.3., the permeability can be estimated.

6.5. Mineral content

8 Thin sections were made, four from samples of area A and four from samples of area B. Because the samples have a thickness of 0.5cm to 1 cm, one thin section consists of several different samples from the sampling points.

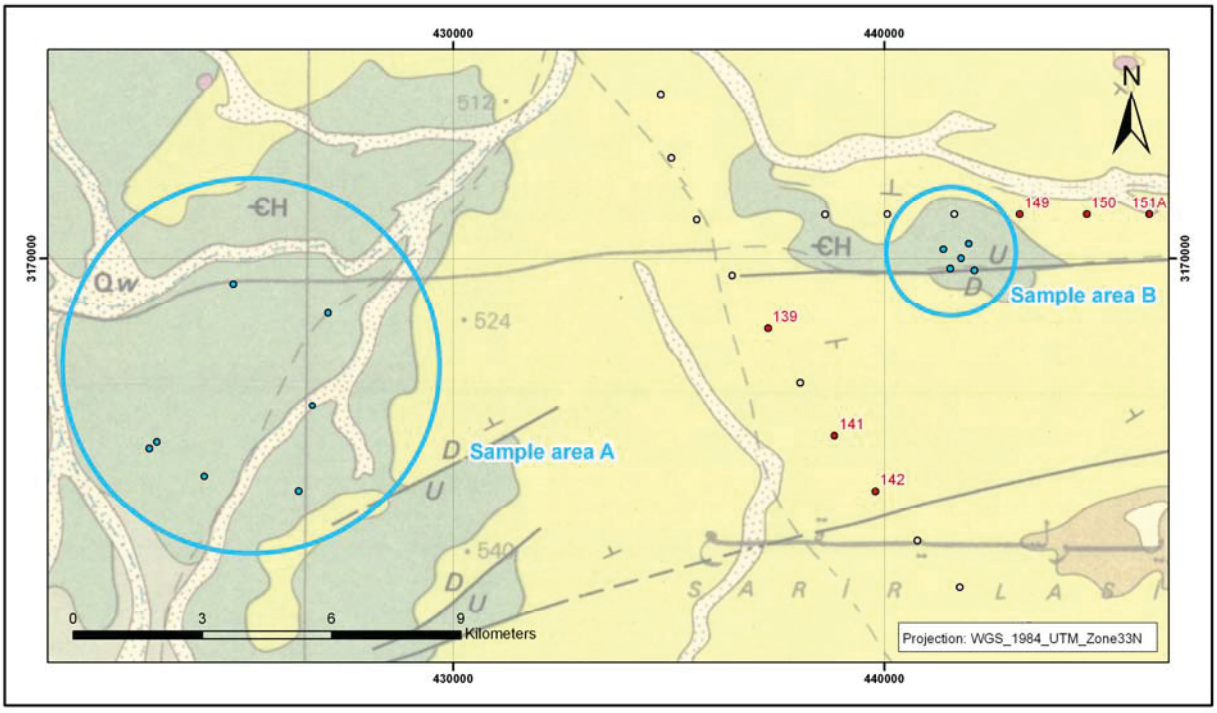

Fig. 6.6. Location of the 2 sampling areas

The samples from area A are from the bigger outcrop west of profile 1 and the thin sections of area B are from the smaller area east of profile 2. Because the samples are only taken from the surface, a general formation characterization between area A and area B is not really meaningful and not the aim. Instead, all samples of all thin sections are observed and the different characteristics of sediments which are part of the Hassouna Formation and the aquifer are explained. The thin sections are primarily made for understanding and allocating the measured and calculated porosity from the logging tools, and also to get an idea of the mineral content of the Hassouna Formation.

The general mineral content of the thin sections are more or less similar: The main component of the samples is quartz. The minor components are clay minerals, carbonates, gips, opaque minerals and limonite. The blue areas in the thin sections illustrate the free space. According to this free space, the porosity can be estimated. Although the thin sections are similar concerning the mineral content, structure, cement and matrix, the porosity distribution has a high variance. Concerning to the scale of the pictures of the thin sections, one centimetre is equivalent to 0.2 mm.

For example, figure 6.7 from location B2 describes a quartz-sandstone with angular grains, and the sandstone is hardly cemented. The grains are medium sorted and are partly grown next to each other on a flat line. But the majority of the grains are mono-crystalline. Additionally, most of the grains are coated by limonite. The porosity of this sandstone is at about 20 percent.

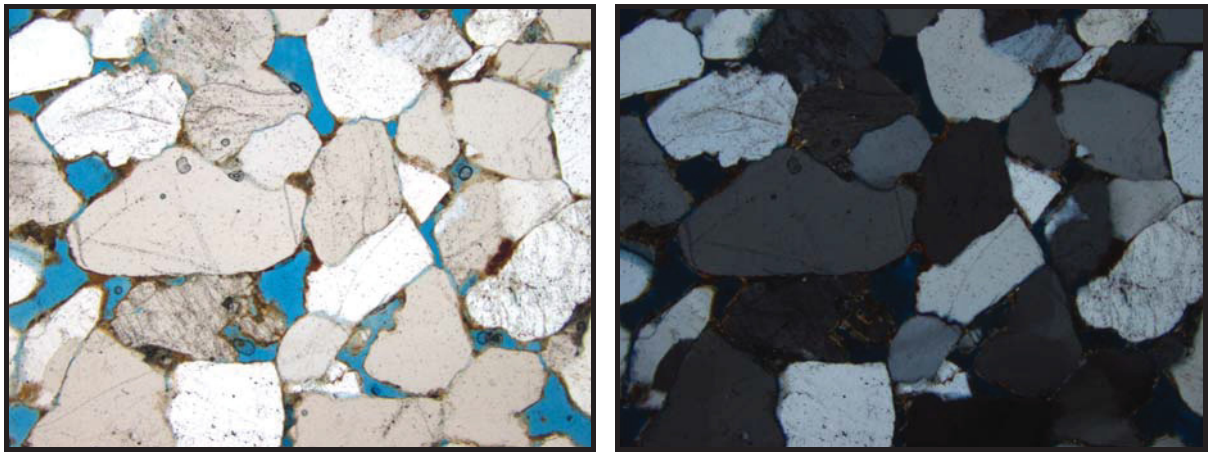

Fig. 6.7. Thin section of a quartz-sandstone (Location: B2) Right picture observed through crossed polarizer, left picture: observed through parallel polarizer, hundredfold magnification

Another example is the thin section which is displayed in figure 6.8. This section is also from location B2. A quartz-sandstone with angular grains can be observed and the grains are embedded in a matrix of clay minerals, carbonates, opaque minerals and limonites. The grains are medium sorted and the majority of the grains are mono-crystalline. The grains are cemented with the matrix, and probably the sandstone has hardly any porosity. The actual porosity probably comes from dissolution reactions after bedding. The porosity of this sandstone is at about ten percent.

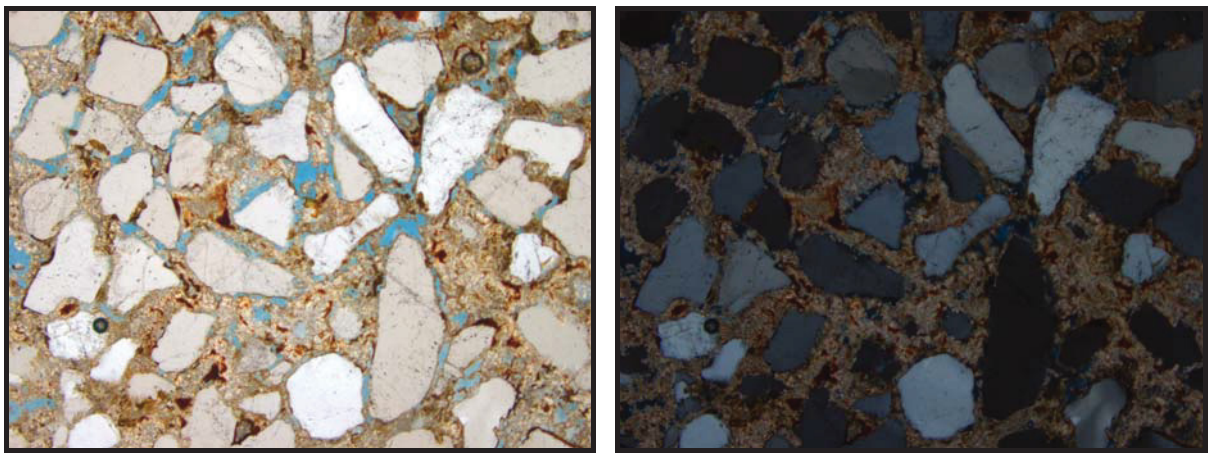

Fig. 6.8. Thin section of a quartz-sandstone (Location: B2) Right picture observed through crossed polarizer, left picture: observed through parallel polarizer., hundredfold magnification

The section of figure 6.9 displays a quartz-sandstone which is badly sorted and the grains are embedded in a probably clay and carbonate matrix. The proportion of matrix is about 30 percent. The shape of the grains is angular and the matrix is partly dissoluted. Porosity can be observed, which reaches about ten percent.

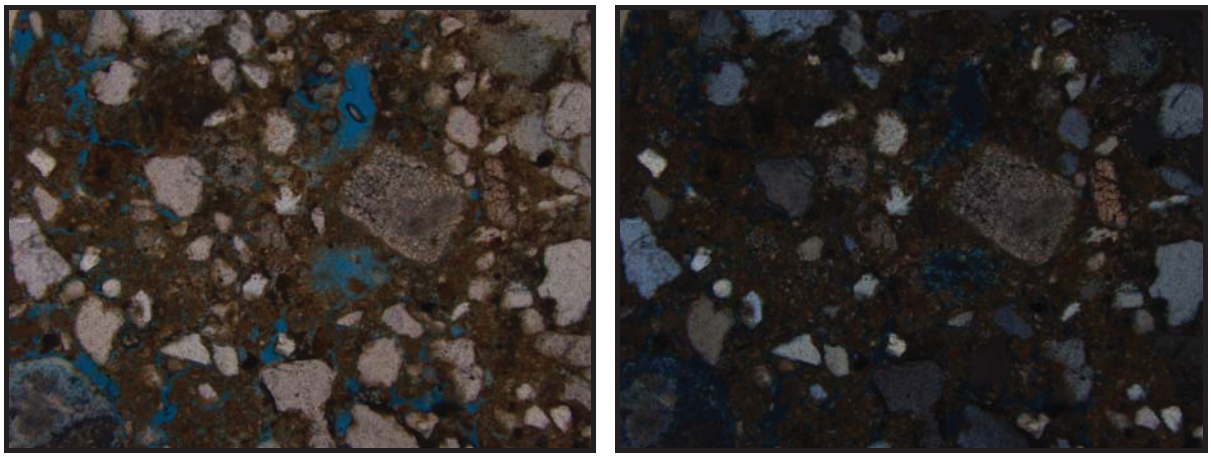

Fig. 6.9. Thin section of a quartz-sandstone (Location: B1) Right picture observed through crossed polarizer, left picture: observed through parallel polarizer, hundredfold magnification

Thin section of figure 6.10 shows that there are matrix-minerals where some quartz grains are bedded. In figure 6.10 a microfracture in the matrix can be observed. These fractures can also contribute to the general porosity.

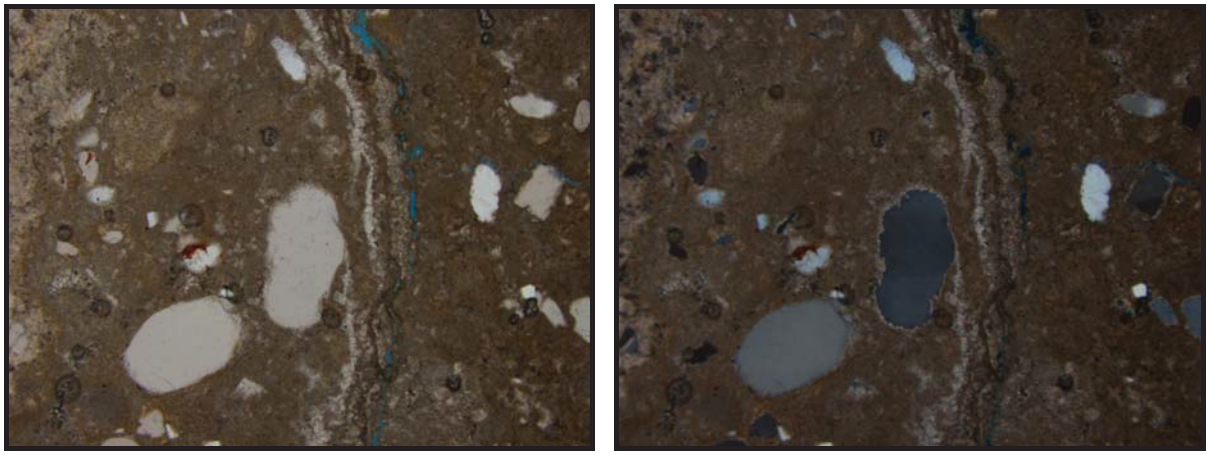

Fig. 6.10. Thin section of a quartz-sandstone (Location: B1) Right picture observed through crossed polarizer, left picture: observed through parallel polarizer, hundredfold magnification

The thin section of figure 6.11 demonstrates a quartz-sandstone which is completely cemented, and the porosity of this sandstone is close to 0.

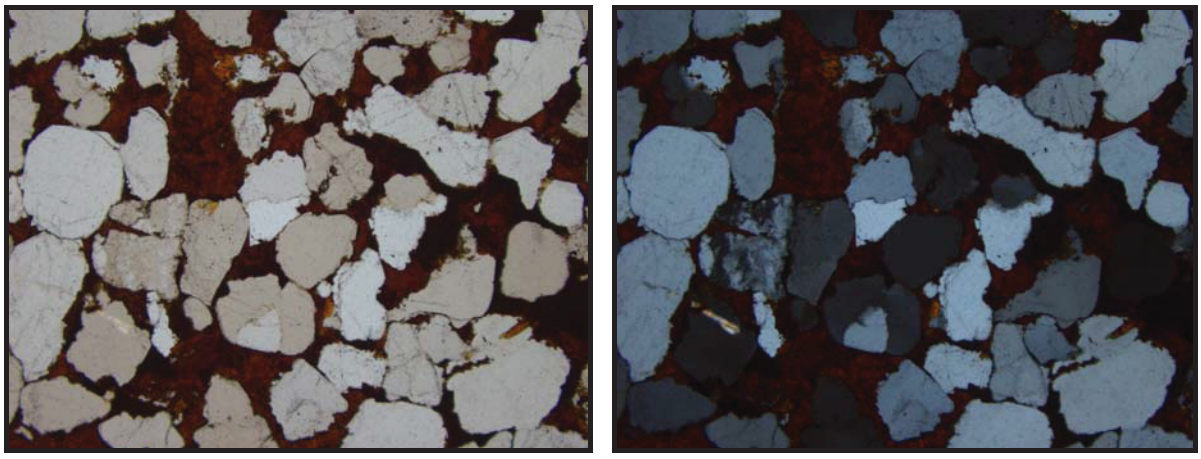

Fig. 6.11. Thin section of a quartz-sandstone (Location: B1) Right picture observed through crossed polarizer, left picture: observed through parallel polarizer, hundredfold magnification.

7. Interpretation, Conclusion, Discussion

7.1. Interpretation of logplots

The following chart displays the procedure of the log derivation:

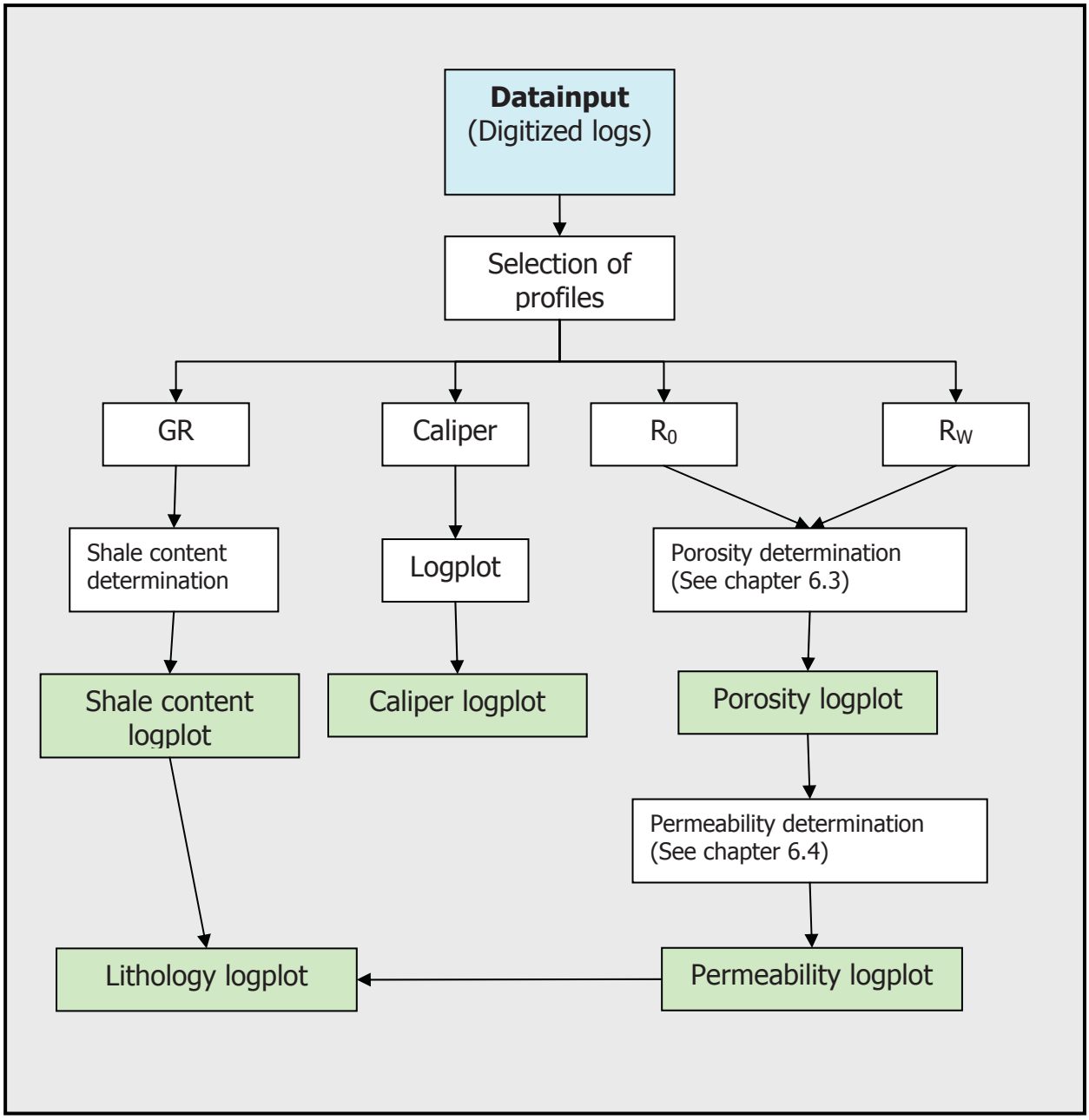

Fig. 7.1. Flowchart of logplot determination

7.1.1. Caliper- bitsize logplot

The red line on the logplot assigns the diameter of the bit size in the borehole and the black line assigns the measured caliper in the borehole. The units for the logplot are meters for depth and inches for the diameter. The diameter ranges from 0 to 50 inches. It can be observed that on the top of the logplot to 300 m, the diameter of the bit-size accords more or less with the diameter of the caliper. Between 310 m and 350 m, a great difference in the diameter can be observed, and deeper downwards, there are further zones where there is more difference between the diameters. These observations can also be made with the other wells of the selected profiles. Concerning shape and depth of the diameter, the washouts can also be interpreted, which is covered in chapter 7.3.1.

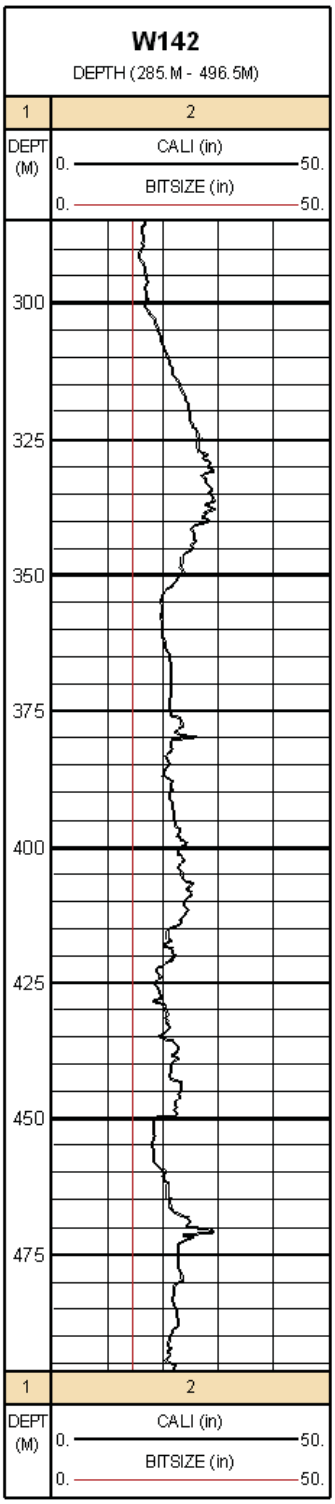

Fig. 7.2. Caliper- bitsize logplot

7.1.2. Shale content logplot

Finally, the shale content logplot was created by using the gamma-ray log and calculating the GRI, which is precisely, explained in chapter 5 and 6. The values range from 0 to 1, which means that at the value 0, there is no shale and at the value 1, there is only shale. The range can also be displayed in percent. In the logplot of well 142, a general trend of shale concentration can be observed. By analysing the logplot after the sequence-stratigraphical point of view, it is obvious that the trends follow coarsening-upward and fining-upward sequences, either at a higher level of shale content like for example between 280 and 335 or at a lower level of shale content like between 325 and 370. The highest peaks finally identify the maximum flooding surface. But it also has to be mentioned that the logplot is only based on gamma-ray measurements, which means that a few peaks can be errors, caused by a high concentration of mica or feldspars, which have a similar gamma radiation like shale. But after the petrologic observation and after the literature, the feldspars and mica concentration should not be that dominant. Because of the local width dispersion of the maximum flooding surface, the shale content logplot can be used for correlation, which is done in chapter 7.2.1.

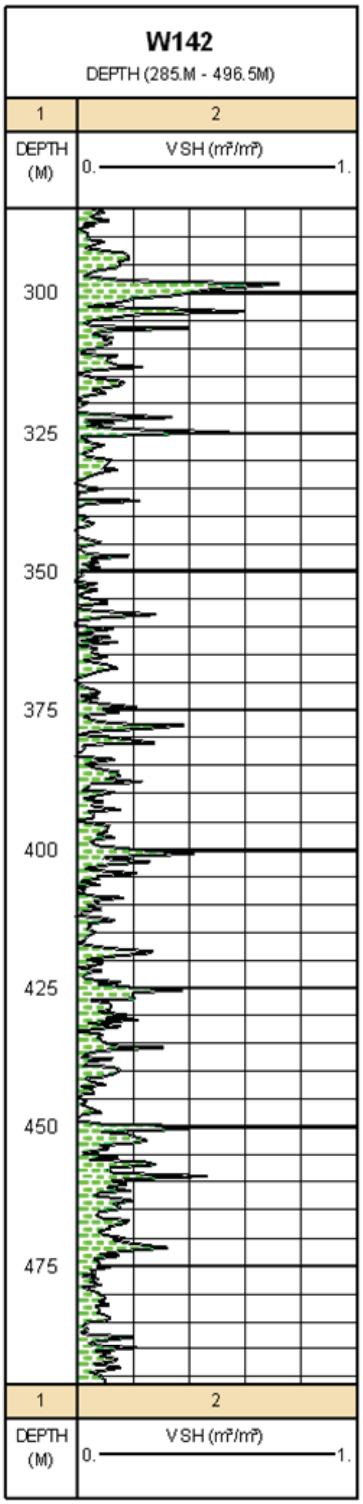

Fig. 7.3. Shale content logplot

7.1.3. Porosity logplot

The development of the porosity logplot is explained in chapter 5 and 6. The unit for the log-plot are meters for depth and for porosity, the unit is dimensionless. The values range from 0 to 0.5, which means that at the value 0, there is 0% porosity and at the value 0.5, the porosity equals 50% porosity. The porosity in the logplot is relatively constant. But generally, the logplot can be divided into two parts: the upper part of the log-plot from 300 m to 380 m where the porosity is higher than 20% and in the lower part from 380 m to 480 m where the porosity is lower than 20%. There are also two zones at 400 m and at 425 m in the lower part where the porosity declines to 15%. The interpretation of the porosity in the other wells is done similarly to this well. According to the porosity distribution, there can also be a interpretation of the porosity distribution in the profiles, which is covered in chapter 7.3.2.

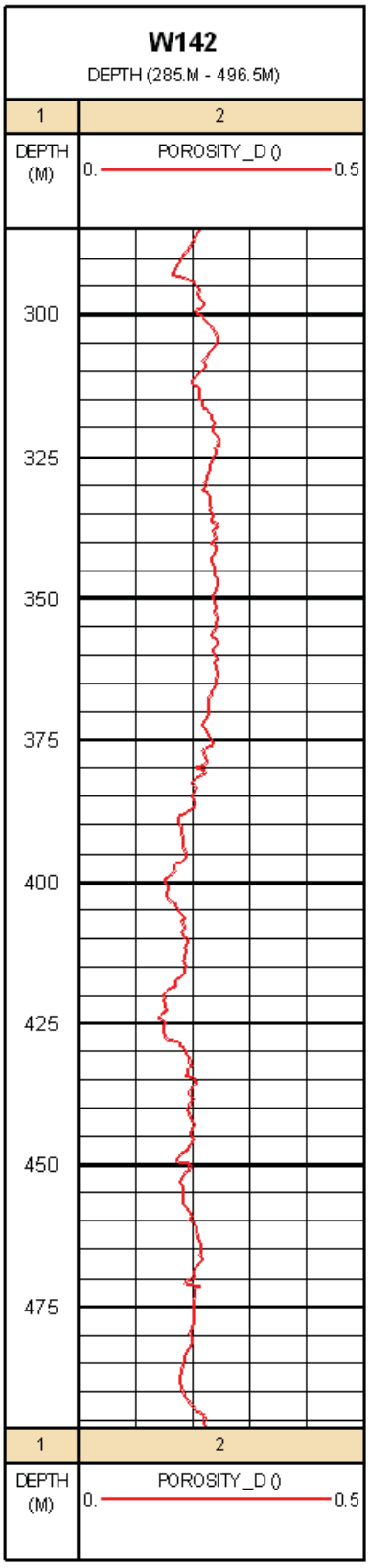

Fig. 7.4. Porosity logplot

7.1.4. Lithology logplot

The lithology logplot uses the calculated shale content log and the calculated porosity log. The appreciation for plotting both together in one logplot is to get an idea of how the formation is built up concerning pore space, (sand) grains and shale. Both logs are displayed mirror-inverted and the proportion of pore space of the formation is displayed on the right side of the logplot. The proportion of shale is displayed on the left side of the logplot. The proportion in the middle characterizes the space of the sand grains of the formation. The individual shading makes the plot more demonstrative. With the aid of the logplot, zones with little shale content and high porosities can be extracted and a selection of zones for good aquifer conditions can be interpreted. The interpretation of the aquifer can be seen in chapter 7.3 and is accomplished together with the permeability plot, which will be explained in the following chapter.

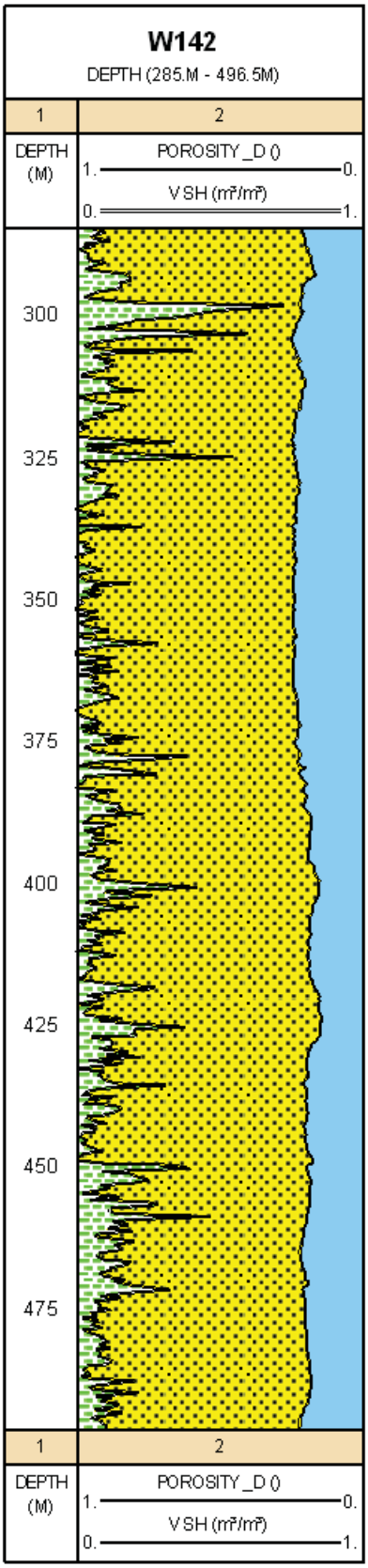

Fig. 7.5. Lithology logplot

7.1.5. Permeability logplot

The permeability logplot is based on the calculated porosity, the sieve analysis and the pumping test data, which is precisely explained in chapter 6.1. The units for the logplot are meters for depth and for permeability, the unit is Darcy. The values range from 0.01 to 100 Darcy and are displayed in a logarithmic scale. The orange line displays the permeability which is calculated based on the porosity, and the pumping test data and the black points are the calculated permeabilities aid to the sieve analysis. The permeability on basis of the sieve analysis is only determined where sieve analysis were available, and the values often differ from the calculated pumping test data permeability because the data are point measurements. Also by calculating the permeability on basis of the sieve analysis, only inter-granular porosity can be calculated. The permeability from fractures cannot be displayed. A further reason of the deviation of both measurements is the loosing of fine fraction of the cuttings in the drilling fluid. For a general overview of the permeability, the pumping test data based on permeability achieves a better result. The precise calculation workflows are explained in chapter 6.4

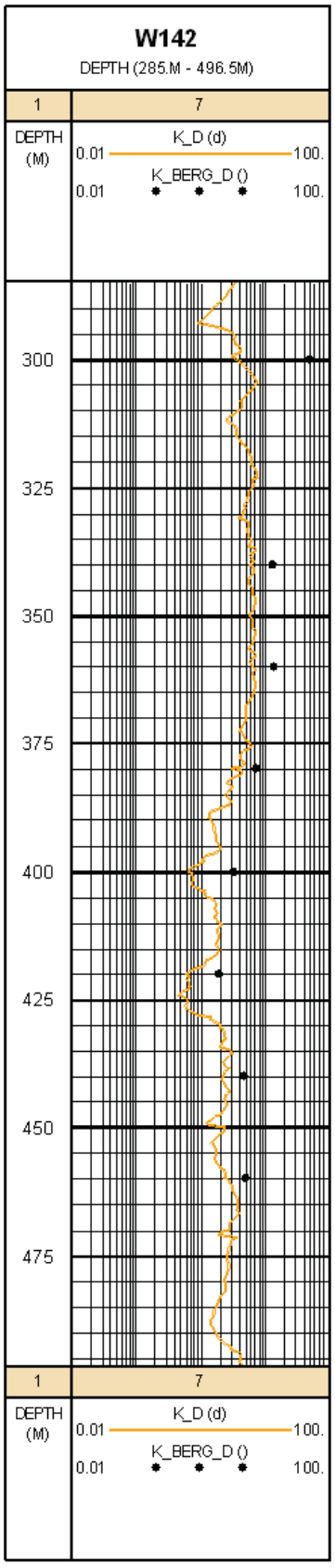

Fig. 7.6. Permeabiliy logplot

7.2. Interpretation of the profiles

The following chart displays the procedure of the interpretation of the profiles:

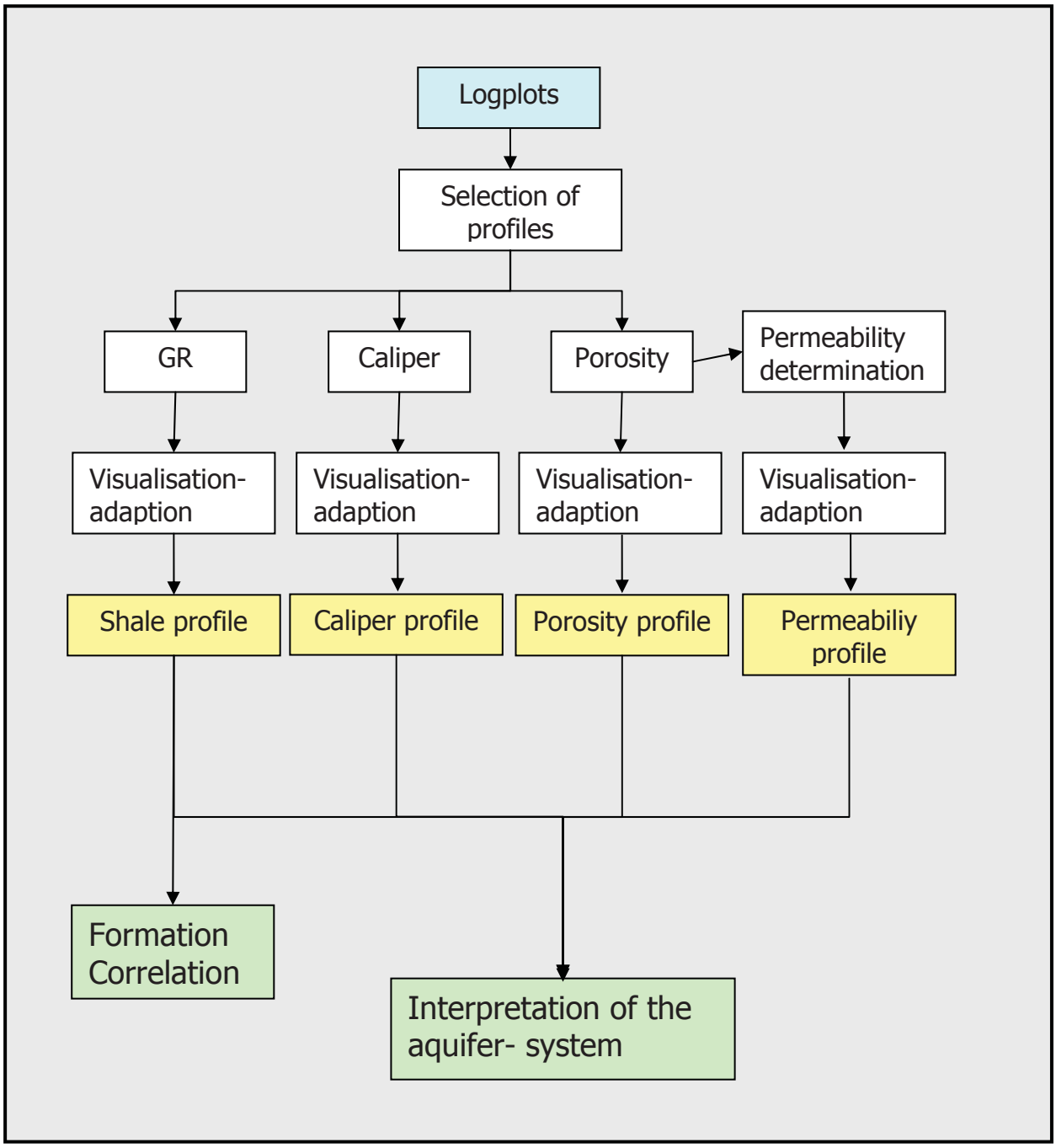

Fig. 7.7. Flowchart of Formation Correlation and Interpretation of the aquifer- system

7.2.1. Formation Correlation

Formation Correlation with the gamma logplots is done. The Formation Correlation is processed with the interpretation software Petrel 2008.

The first step enhances the visualization of the data, which can be done with assistance of the advanced tools of the program Petrel. In this step, a color-table is created and all values are assigned to the color table. The selection of colors of the color-table is done by testing different colors, color distributions and ranges to receive an optimal result for correlation.
For enhancing the correlation, the geological map after Jurak (1978) is considered. The geological map shows that there are faults between the wells 142 and 145, between the wells 139 and 134, between the wells 139 and 149 and between the wells 121 and 126.

After this adaption, the main correlation is done. Peaks, with high gamma-ray values, which mark the maximum flooding surfaces, are searched and are picked. Then, the high gamma-ray peaks are correlated with high gamma-ray peaks of the neighbor wells. The peaks are characterized as so-called well tops, which mark the top of a formation. But because some peaks cannot be clearly correlated, other sequence-stratigraphical markers like coarsening-upward and fining-upward are consulted to characterize several peaks more precisely. The names of the main well tops have numbers from 1 to 6.

There are several influences on the gamma responses which complicate the correlation. The gamma-ray responses are generally influenced by the changing caliper of the borehole. Because of different mineral content, there can also be a difference in the general gamma response.

It has to be considered that the result of the correlation is only one possibility of interpretation and assumes a similar dip of the formation as on the surface.

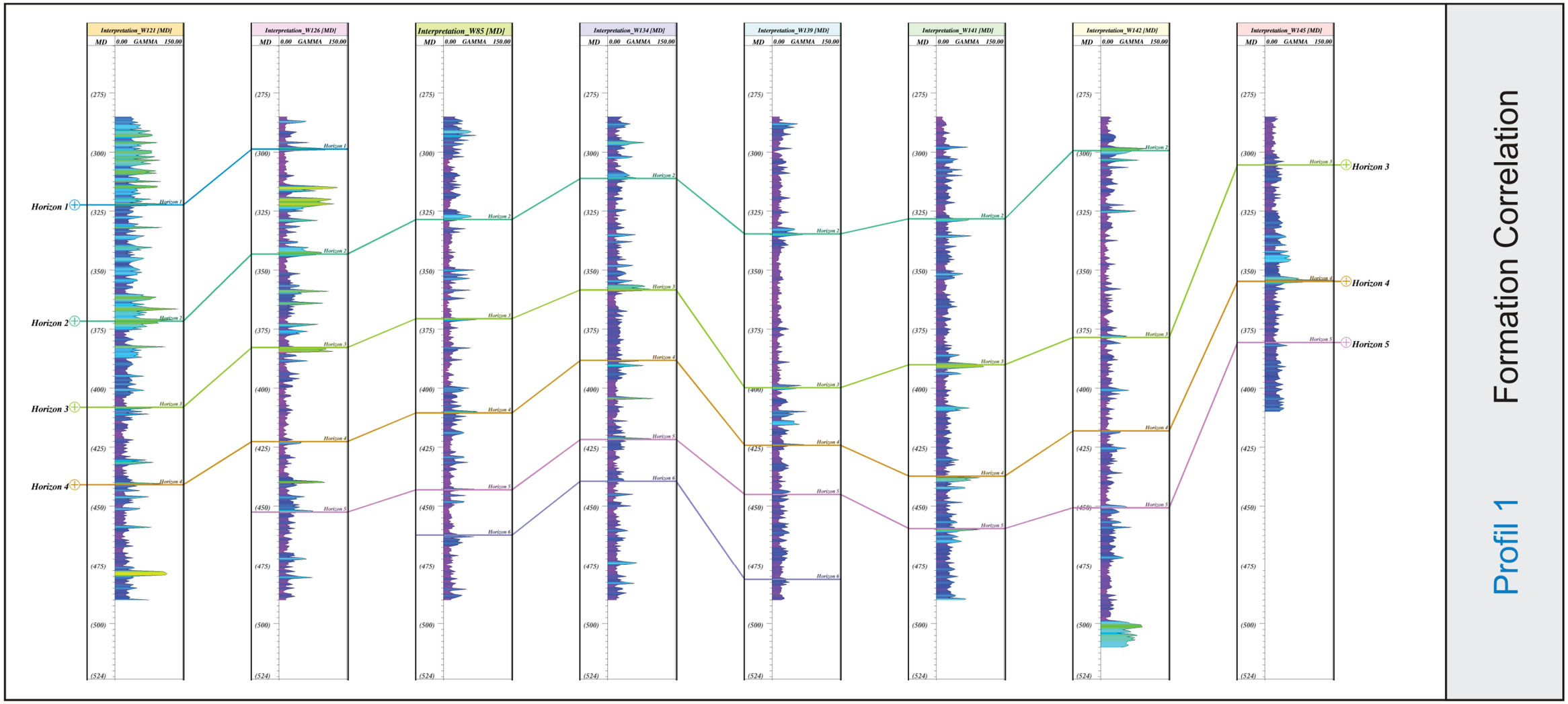

Fig. 7.8. Formation Correlation of profile 1

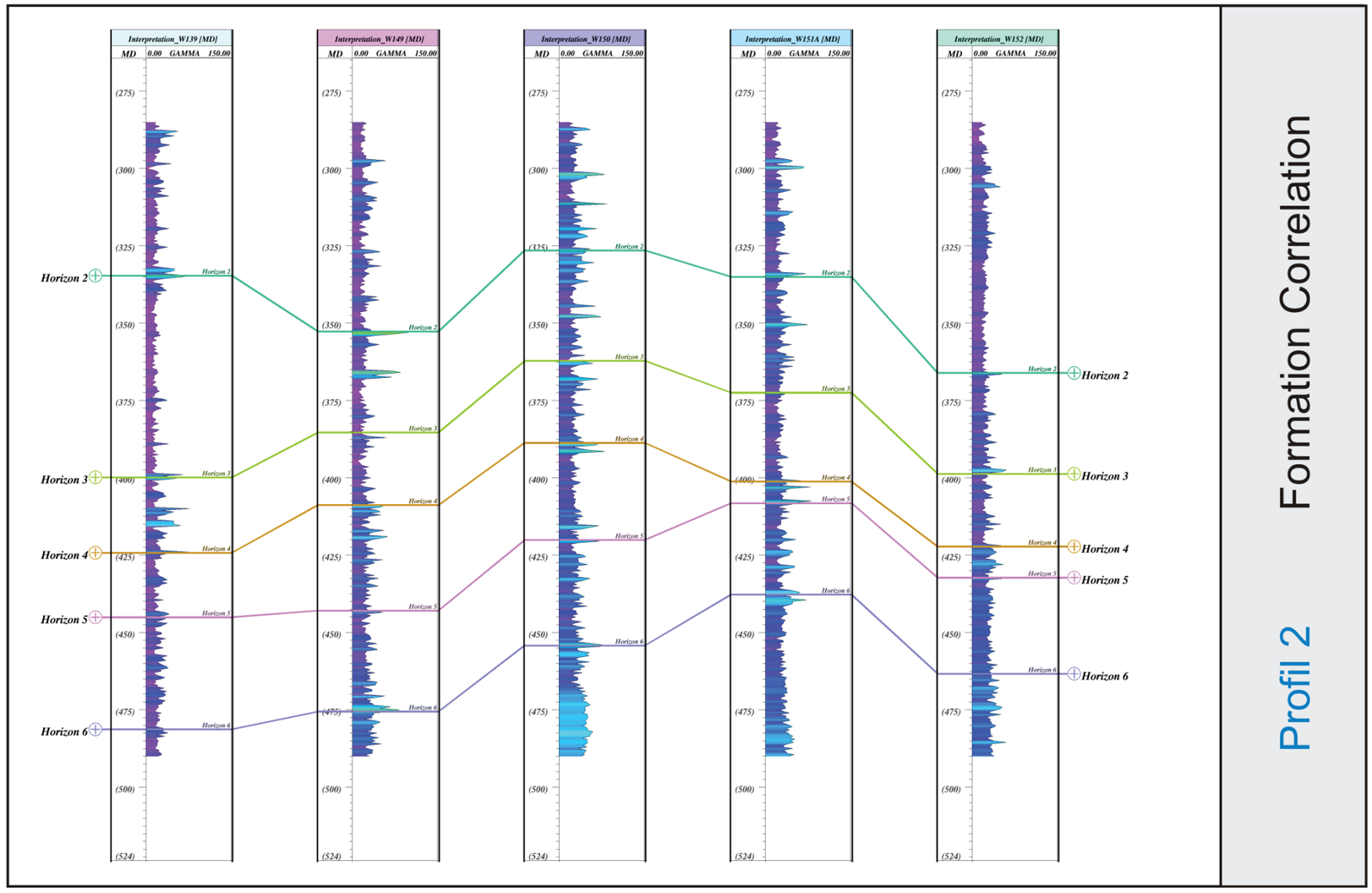

Fig. 7.9. Formation Correlation of profile 2

7.3. Interpretation of the aquifer- system

For interpretation of the aquifer system washouts, distribution of the estimated porosities and distribution of the estimated permeabilities are interpreted. Additionally, faults of the geological map after Jurak (1978) are consulted and displayed in the profiles. Furthermore, the gamma-ray logs are displayed next to the specific logs and the interpreted Formation Correlation is also displayed.

7.3.1. Washouts

For interpreting the washouts, the caliper profiles are created by displaying all caliper log-plots together side by side of the same scale and same range. The range of the caliper log is appointed from 14.75 to 40 inches. 14.75 inches is the diameter of the bit size, which means that all values which are higher than 14.75 are defined as washouts.

For visualization of the caliper log, a color table is created, which can be observed in figure 7.10. The value of the color table ranges from 14.75 to 30, which means that all values which are higher than 30 are displayed in red.

During interpretation, in figure 7.10, where both profiles are displayed, it can be observed that a huge amount of caliper values are a lot higher than the bit size. There are areas like in well 141 where the caliper values are higher than the doubled bit size. These washouts can be caused by excessive bit jet velocity, soft or unconsolidated formations, fractured zones, in-situ rock stresses, mechanical damage by BHA components, chemical attack and swelling or weakening of shale as it is in contact with fresh water. Generally speaking, washouts become more severe after a certain time (Schlumberger oil glossary, 2009). The large washout zones are situated on the south part of profile 1 and on the east part of profile 2. The large washout zones are in the upper part of the aquifer. It can also be observed that the large washout zones are high where fault systems are found in the geological map of Jurak (1978).

There are hardly any washouts in well 126 and 149, which is probably a sign that the borehole is stable. But it can also be caused by a casing in the borehole or by a non-operating probe.

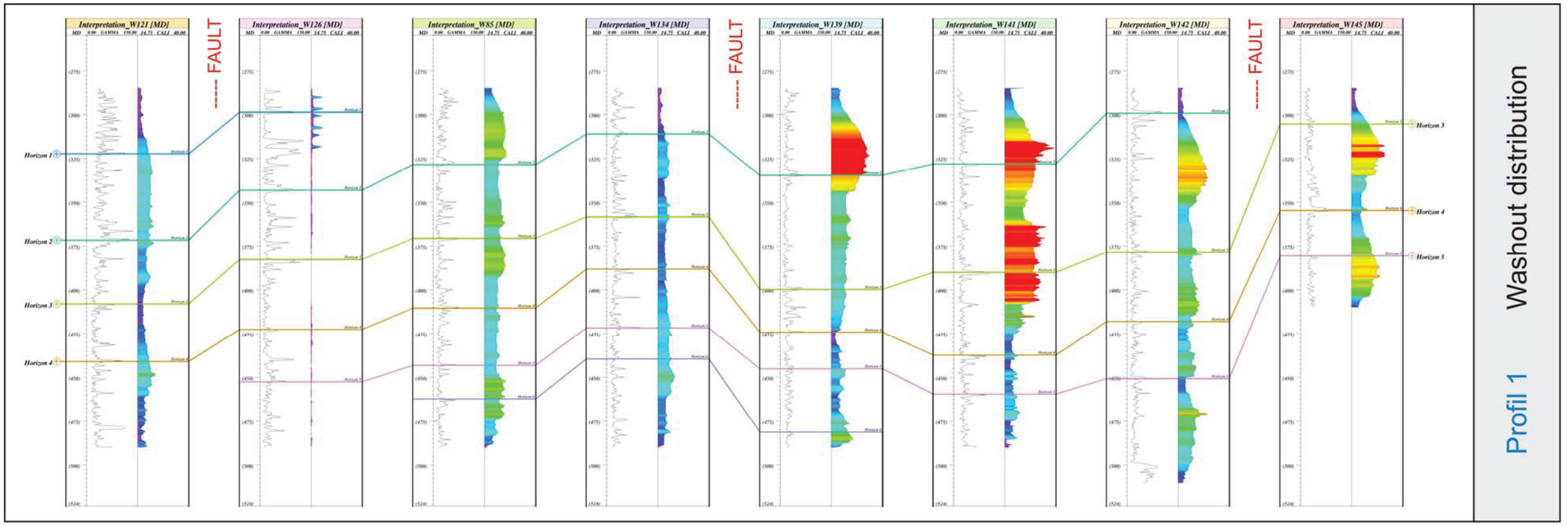

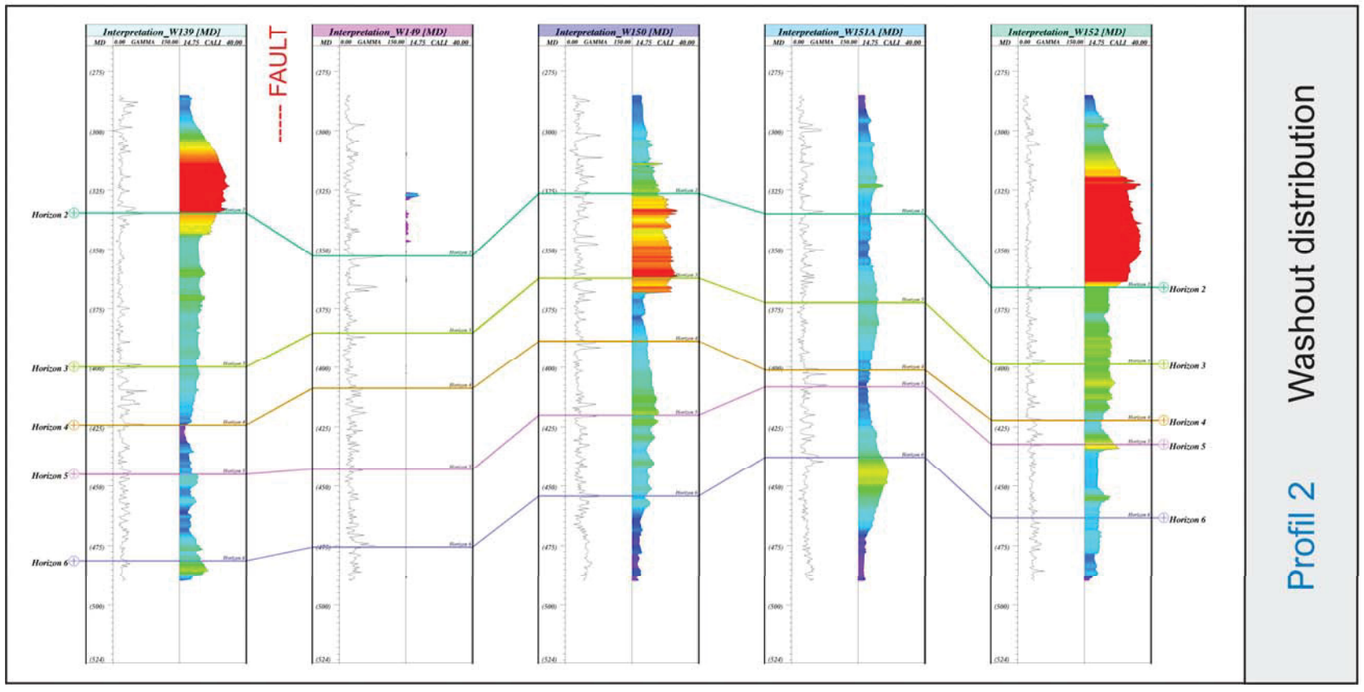

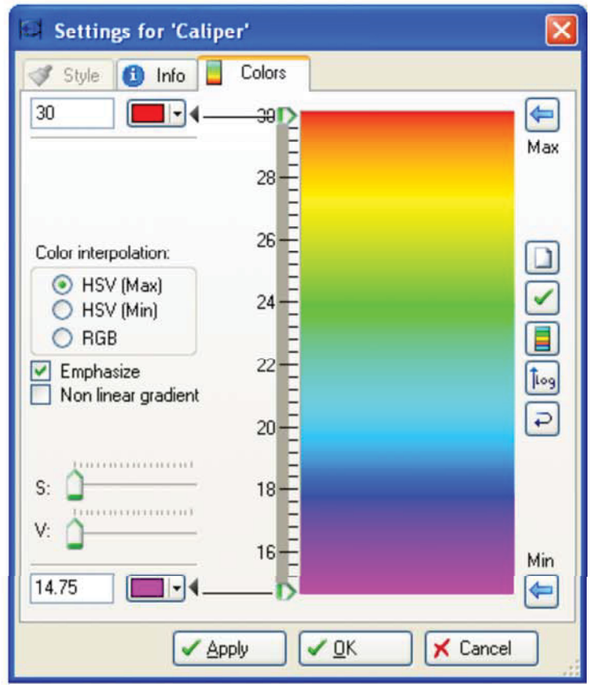

Fig. 7.10. Washout distribution of profile 1 and profile 2

7.3.2. Porosity distribution

For interpreting porosities, the porosity profiles are created by displaying all porosity log-plots together side by side with the same scale and same range. The range of the porosity log is appointed from 0 to 0.5. 0.5 means 50 percent porosity (Figure 7.11).

For visualization, a new color table is invented. The precise color table is displayed next to the profiles in figure 7.11. The color red displays all porosity values which are 20% and lower, the blue color displays all porosities which are 30% and higher and the other colors display the porosity between 20% and 35%. Due to this classification, the aquifer can be layered.

A general distribution of the porosity can be observed after the corrections and the visualization adaption. The porosity decreases with increasing depth, which is obviously because of increasing compaction of the formation. Up to a depth of 350 m to 400 m, the porosity distribution is mostly higher than 30% and under the depth of 425 m , the porosity is lower than 20%. Only well 121 and 126 show a porosity which is still 30% or more at a depth of 425 m and deeper. In profile 2, it can be observed that the porosity decreases towards the east of the profile.

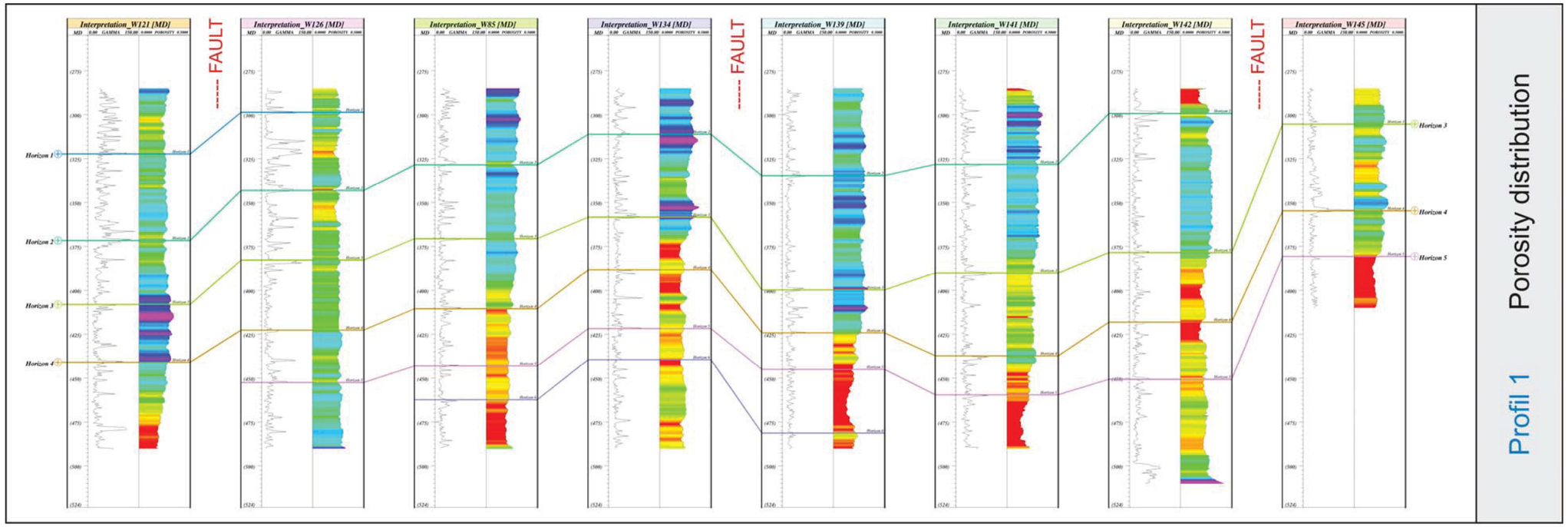

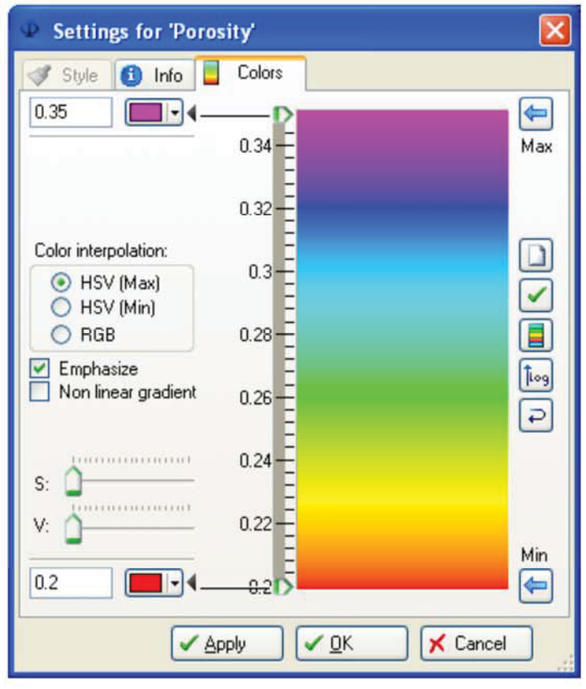

Fig. 7.11. Porosity distribution of profile 1 and profile 2

7.3.3. Permeability distribution

For interpreting permeabilities, the permeability profile is created by displaying all porosity logplots together side by side in the same scale and same range. The range of the permeability log is appointed from 0.01 to 100 Darcy. The permeability log is displayed logarithmically (Figure 7.12).

For visualization, a logarithmic color table is invented. The precise color table is displayed next to the profiles in figure 7.12.

Generally, the permeability values of profile 2 are especially in the upper parts higher. East of the fault between well 139 and 149, values are higher. Especially the wells 149 and 150 show high permeabilities like 40 and up to 60 Darcy in the upper part of the aquifer. In profile 1, well 141 shows similarly high values in the upper part of the aquifer. If the pumping tests are done correctly, a possible reason of the high values can be the occurrence of faults or fractures.

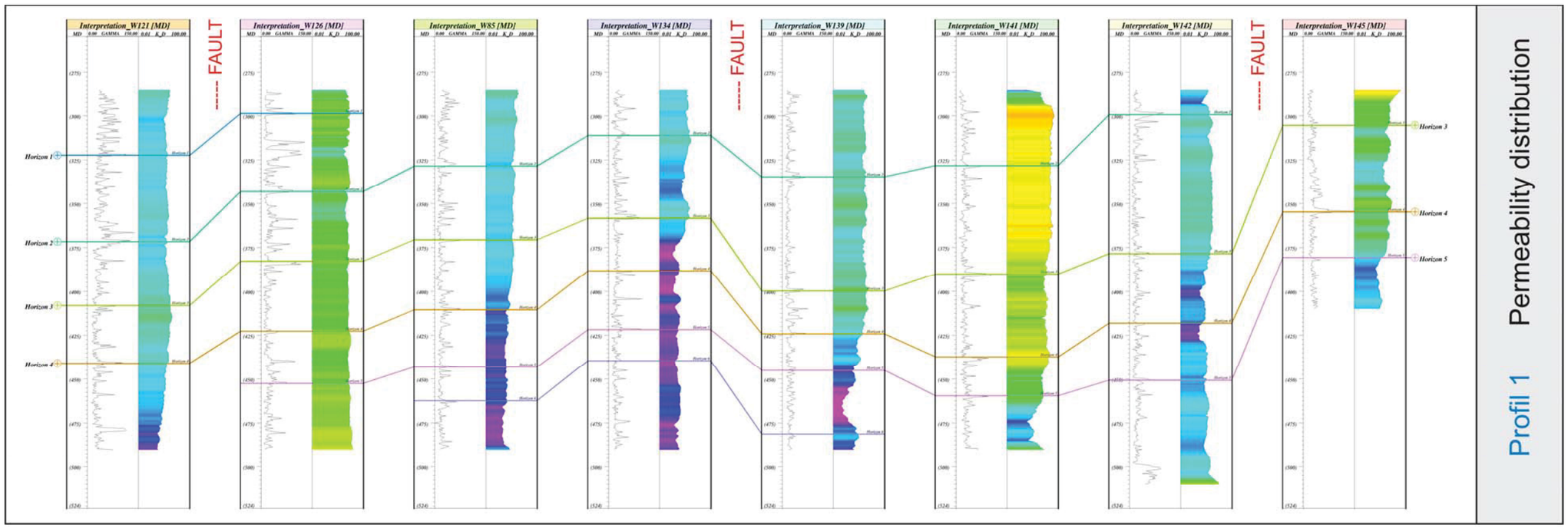

Fig. 7.12. Permeability distribution of profile 1 and profile 2

7.4. Comparison between samples and logdata

The porosity and permeability measurements are based on resistivity measurements. It cannot be distinguished between the different porosities. But thin sections of the samples demonstrate that there are different kinds of porosities. That means that the measured porosity is not only an inter-granular porosity. It is important to know the kind of porosity for steering the determination steps.

After Schopper (1982), it can be distinguished between:

1. inter-granular porosity

   Created space between grains, particles or fragments of clastic materials, loosely packed, compacted or even cemented (primary porosity).
2. inter-crystalline or intra-granular porosity

   Generated space by shrinking or contraction of grains.
3. fissure or fracture porosity

   Results from mechanical and partial chemical action on primarily massive rock (secondary porosity).
4. vugular porosity

   Void space created by organism during genesis or by chemical action. (primary or secondary porosity, mostly in carbonates)

All these kinds of porosity except for the vulgular porosity can be observed in the thin sections. The observed inter-granular and intra-granular porosity of the thin section is always lower than the estimated porosity from the logging measurements and lower than the measured porosity from the samples in the laboratory. it is obvious that a part of the porosities are from fractures and faults. By distinguishing the permeability and the porosity profiles, it can be observed, for example between well 139 and well 149, that some wells with similar porosity values have really different permeability values. This can be a indicator for fracture porosity.

7.5. Conclusion

The evaluation of the log data with respect to a reservoir characterization was difficult and limited by some critical constrictions:

- There is no relevant "porosity tool combination" (Neutron-Density or/and Sonic log),
- there are no cores for validation and calibration of log measurements. This is extremely critical in respect of the Archie-parameters and a porosity-permeability correlation.

Furthermore, because of the big washouts the data conditions were not easy to use. There was no possibility to take an in-situ inventory to control the geological situation in the area of interest.

But still, in principle, there are possibilities to get a porosity and permeability estimate from the very limited set of the available data. These possibilities were summarized and the best possible ways were selected. From the available logs, particularly the

- shale content was calculated from gamma log
- porosity was calculated from resistivity logs.

The calculation implements some specific methods like resistivity approximation (Dachnow correction) and log normalization.

Log-plots were created by executing the obtained data.

For the investigation, rock- sediment samples, pumping test data and sieve analysis of the cuttings were used. Porosity and permeability as a function of depth were obtained and were displayed in log-plots. For every well, one sheet was created where all important logplots were displayed.

Profiles were created with all important log-plots as well as with the calculated data as well as with the important raw data like the gamma-ray log plot.

Additionally, a correlation was done with the gamma-ray profiles. Furthermore, the distribution of porosity and permeability was plotted along the profiles and an interpretation of the distribution of the aquifer parameters was possible. – Gaps and interruptions of correlation agree in some cases with fracture and fault systems observed by surface investigations.

7.6. Discussion

The porosity determination based on resistivity measurement should only be used if there is no other possibility; if the shale content is high, the determination is not correct.

By using sieve analyses data and pumping test data for the permeability calculation, it was possible to verify the influence of fractures and faults.
With the available log-data, structures of the fault systems cannot be verified; therefore, important migration tracks of the aquifer cannot be detected.
For this reason, reflection seismic profiles would back up to understand the structure of the aquifer of the Hassouna Formation. Furthermore, special logging tools for fault detection like FMI®/FMS® (Schlumberger Ltd.) or Televiewer® (Schlumberger Ltd.) can help to understand the structure of the Hassouna Formation.

The bottom of the aquifer cannot be reached by the wells and therefore, the bottom boundary of the aquifer is not clearly known. For understanding the aquifer better, this information must be derived through further investigations including wells.

For a further determination, it is necessary to receive a representative collection of rock samples (core samples) to optimize the porosity calculations and also the permeability determinations.

List of literature

AMYX, J.W., BASS, D.M. and WHITING, R.L. 1960. In: Petroleum Reservoir Engineering, McGraw-Hill, Toronto, Ont.

ANKETELL, J.M. 1996. Structural history of the Sirt Basin an ist relationship to the Sabratah Basin and Cyrenaican Platform, northern Libya. First Symposium on the Sedimentary Basins of Libya. Geology of the Sirt Basin. Vol. . (eds. M.J. Salem, M.T. Busrewil, A.A. Misallati, and M.A. Sola). Elsevier, Amsterdam, 57-89.

ARCHIE, G. 1942. The electrical resistivity log as an aid in determining some reservoir characteristics, Trans. Am. Inst. Min. Metall. Pet. Eng. Inc. 146 , 54–62.

BERG, R. R. 1970. Method for determining permeability from reservoir rock.Properties. Transactions of the Gulf CoastAssociation of Geological Societies,20, 303–317.

BAAREN, J.P. van. 1979. Quick-look permeability estimates using sidewall samples and porosity logs (pp. 11). SPWLA London, Sixth European Logging Symposium, March.

BEARD, D.C. and WEYL, P.K. 1973. Influence of texture on porosity and permeability of unconsolidated sand. Am. Assoc. Petrol. Geol. Bull. 57 , 349–369.

CARMAN, P.Z. 1956. Flow of gases through porous media, Butterworths, London .

CEPEK, P. 1980. Sedimentology and facies development of the Hasawnah Formation in Libya. In: The Geology of Libya, M.J. Salem and M.T. Busrewil(Eds). Academic Press, London, II, 375-382.

CLAVIER, C., COATES, G., DUMANOIR, J. 1984. Theoretical and experimental bases for the dual water model for the interpretation of shaly sands. Soc. Petrol. Eng. J., 153–168.

CLAVIER, C., COATES, G., DUMANOIR, J. 1971. Quantitative interpretation of thermal neutron decay time logs. J.Petr. Techn., 737-755.

DACHNOW, W.N. 1962. Interpretazija rsultatow geofisitschkich issledowanii rasresow skwaschin, Gostoptech, Moskau

DESPBRANDES, R. 1985. Encyclopedia of Well Logging. Editions Technip, Paris.

DOVETON, J.H. 1986. Log analysis in subsurface geology. John Wiley and Sons, 2nd edition, New York.

ELLIS, D.V., SINGER, J.M. 2007. Well Logging for Earth Scientists (Second Edition). Springer, Dordrecht.

ESRI LTD. ArcGis 9.2. Desktop, Software.

FRICKE, S., SCHOEN, J. 1999. Praktische Bohrlochgeophysik. Enke im Thieme Verlag, Stuttgart.

GARDING, M. 1996. Introduction to Drilling. Schlumberger Educational Service.

HALLET, D. 2002. Petroleum Geology of Libya. Elsevier, Amsterdam.

HEARST, J.R. and NELSON, P.H. 1985. Well Logging for Physical Properties. McGraw-Hill book company, New York.

JURAK, L. L. 1978a. Geological map of Libya 1:250,000 sheet Jabal AI Hasawanh NH 33-14. Explanatory booklet. Industrial Research Centre, Tripoli, Libya.

KLITZSCH, E. 1971. The structural development of parts of north Africa since Cambrian time. First Symposium on the Geology of Libya(ed. C. Gray). Faculty of Science, University of Libya. Tripoli, 253-262.

LARIONOW, W.W. 1969. Radiometrija skwaschin. Nedra, Moskau

KRUMBEIN, W.C. and MONK, G.D. 1942. Permeability as a function of the size parameters of unconsolidated sand. American Institute of Mining and Metallurgical Engineering, Technical Publication No. 1492, 11.

MITICA, N. 1997. Drilling, testing and completion report of Well No.142, Line D5 North East Jabal Hassawnah Wellfield. Dong Ah Consortium, South Korea.

PIRSON, S.J. 1966. Geological well log analysis. Gulf Publishing Comp., Houston.

RIDER, M.H. 1996. The Geological Interpretation of Well Logs. John Wiley Sons, New York.

PATNODE, H.W. and WYLLIE, M.R.J., 1950. The presence of conductive solids in reservoir rocks as a factor in electric log interpretation. *Trans. AIME* 189, 47–52.

POUPON, A., LOY, M.E., TIXIER, M.P. 1954. Contribution to electrical log interpretation in shaly sands. Trans. AIME, Philadelphia, 201, 138.

SCHLUMBERGER, 1989. Log Interpretation Principles/Applications. Schlumberger Educ. Services, Houston.

SCHLUMBERGR LTD. Interactive Petrophysics 3.4, Software.

SCHLUMBERGR LTD. Petrel 2008, Software.

SCHLUTER, T. 2008. Geological Atlas of Africa 2nd edition. Springer, Berlin.

SCHOEN, J.H. 1983. Petrophysik. Ferdinand Enke, Stuttgart.

SCHOEN, J.H. 1996. Physical properties of rocks: Fundamentals and pronciples of petrophysics. Handbook of Geophysical Exploration, vol. 18, Pergamon Press, Oxford.

SIMANDOUX, P., 1963. Mesures dielectrique en milloux poreux, application a mesure des saturations en eaux, etude du comportement des massifs argileux. Rev. de l'institut Francais du Petrole, supplementary issue.

SCHOPPER, J.R. 1982. Porosität der Gesteine Vol. 1. Springer, Berlin, 184–219.

TERRAPLAN LTD. Didger 1.0.37. Software.

TIMUR, A. 1968. An investigation of Permeability, Porosity and Residual Water Saturation Relationships. SPWLA.

VINOS, 2007. Topographic map of Libya 1:1 300 000. Vinos Prints, Tripoli

WALSH, J.B. and BRACE, W.F. 1984. The effect of pressure on porosity and the transport properties of rock. J. Geophys. Res. 89 B 11, 9425–9431.

WAXMAN, M. and SMITS, L. 1968. Electrical conductivity in oil bearing shaly sands. Soc. Petrol. Eng. J. 243, 107–122.

WORTHINGTON, P. F. 1985. The evolution of shaly-sand concepts in reservoir evaluation. The Log Analyst, 26, no. 1, 23-40.

List of websites

http://www.lib.utexas.edu/maps/libya.html

http://www.glossary.oilfield.slb.com/

http://www.geologging.com/english/products/probes/probes.htm

List of figures

List of tables

Appendix- Logplots

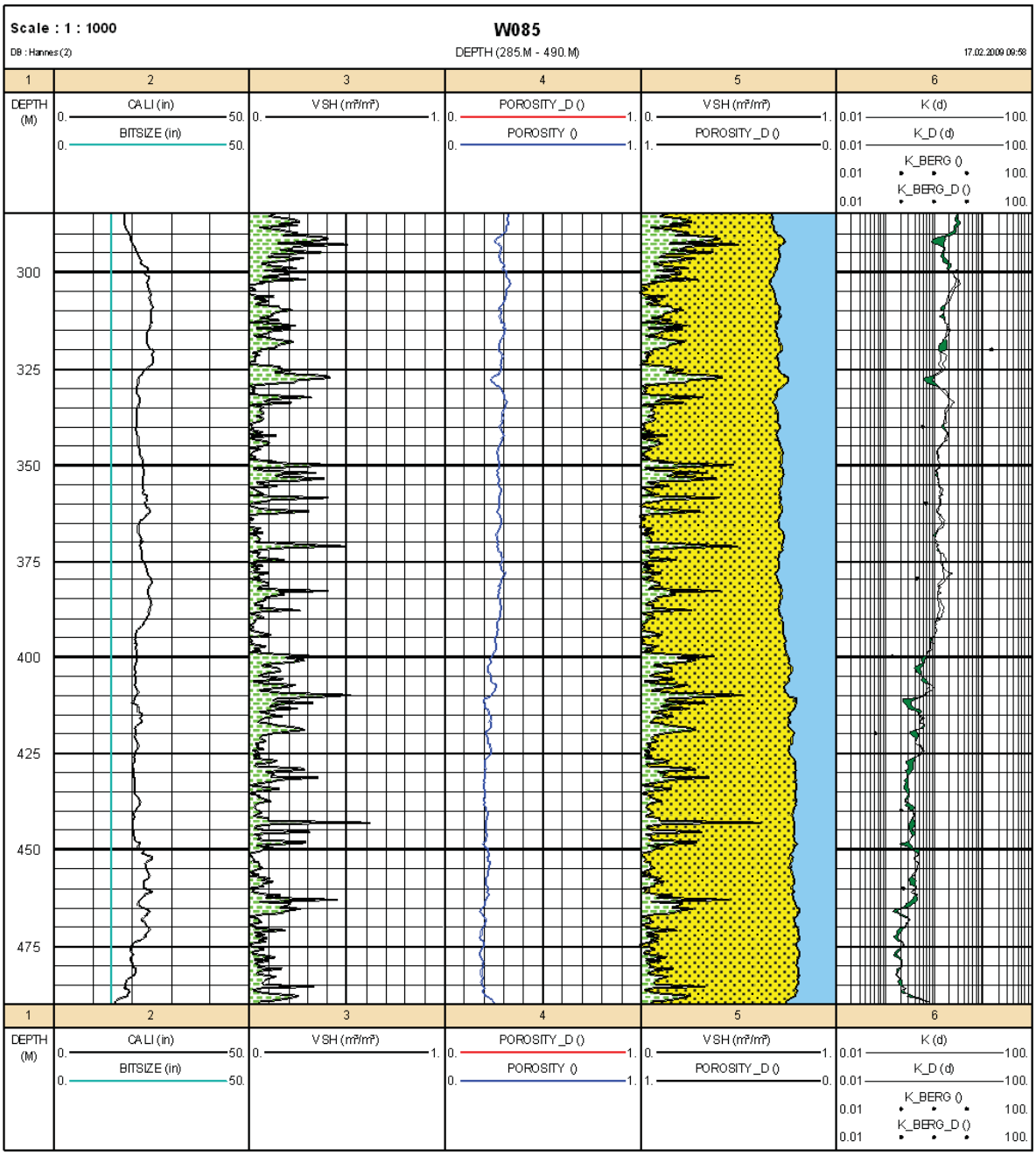

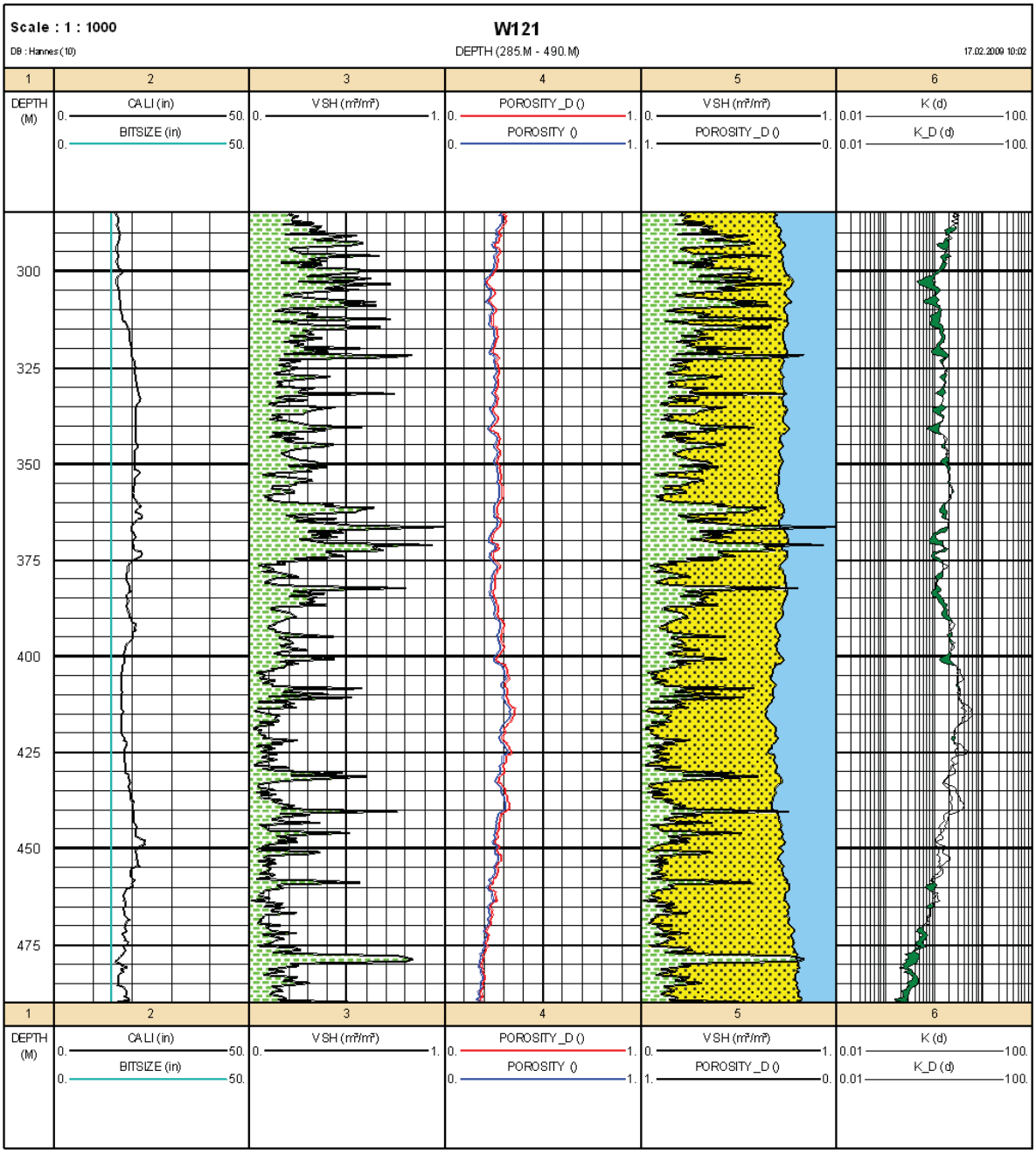
Scale : 1 : 1000
W121
DB : Hannes (10)
DEPTH (285.M - 490.M)
17.02.2009 10:02
1
2
3
4
5
6
DEPTH (M)
CALI (in)
0.
50.
BITSIZE (in)
0.
50.
VSH (m³/m³)
0.
1.
POROSITY_D ()
0.
1.
POROSITY ()
0.
1.
VSH (m³/m³)
0.
1.
POROSITY_D ()
1.
0.
K (d)
0.01
100.
K_D (d)
0.01
100.
300
325
350
375
400
425
450
475

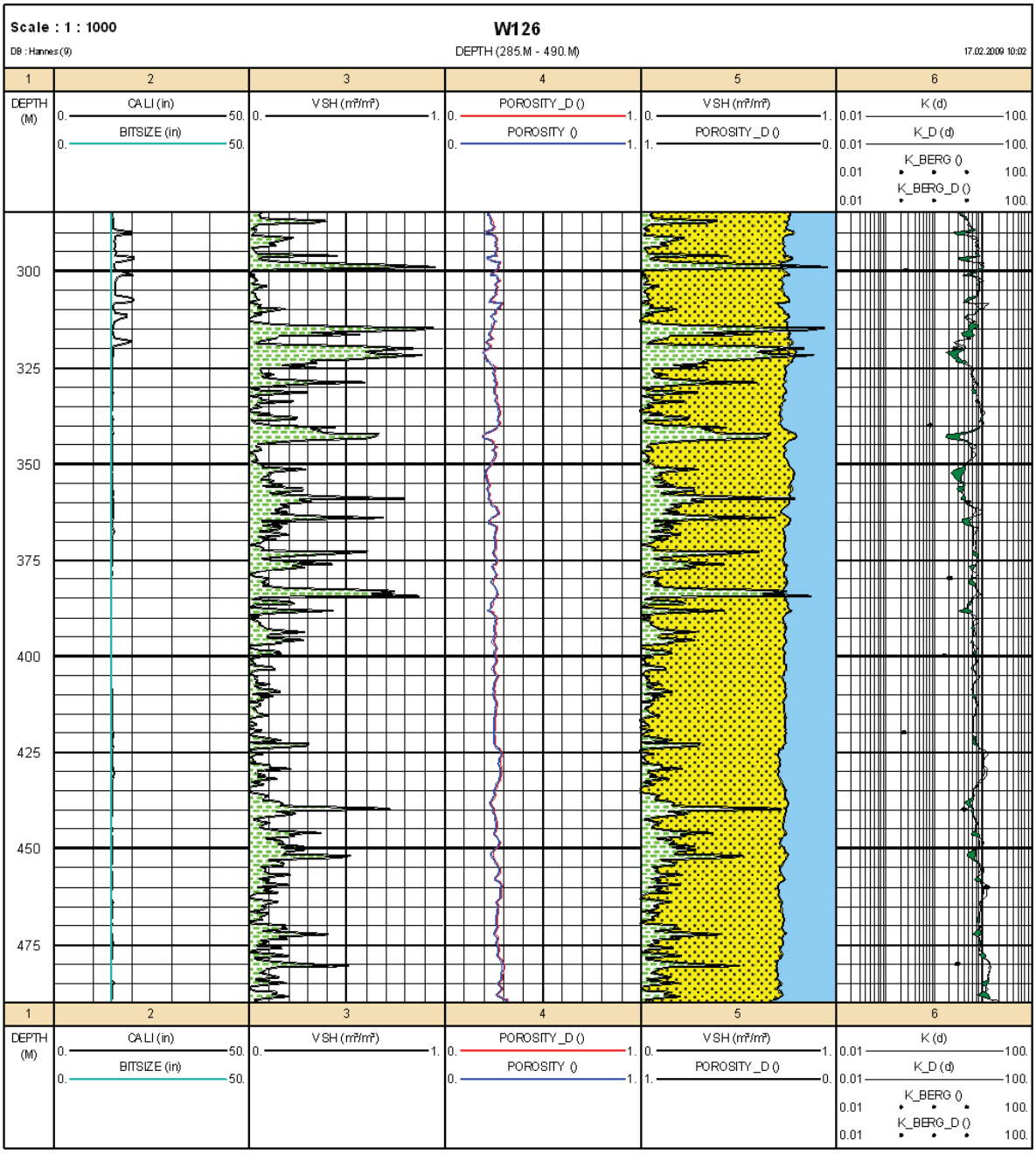
Scale : 1 : 1000
W126
DB : Hannes (9)
DEPTH (285.M - 490.M)
17.02.2009 10:02
1
2
3
4
5
6
DEPTH (M)
CALI (in)
0.
50.
BITSIZE (in)
0.
50.
VSH (m³/m³)
0.
1.
POROSITY_D ()
0.
1.
POROSITY ()
0.
1.
VSH (m³/m³)
0.
1.
POROSITY_D ()
1.
0.
K (d)
0.01
100.
K_D (d)
0.01
100.
K_BERG ()
0.01
100.
K_BERG_D ()
0.01
100.
300
325
350
375
400
425
450
475

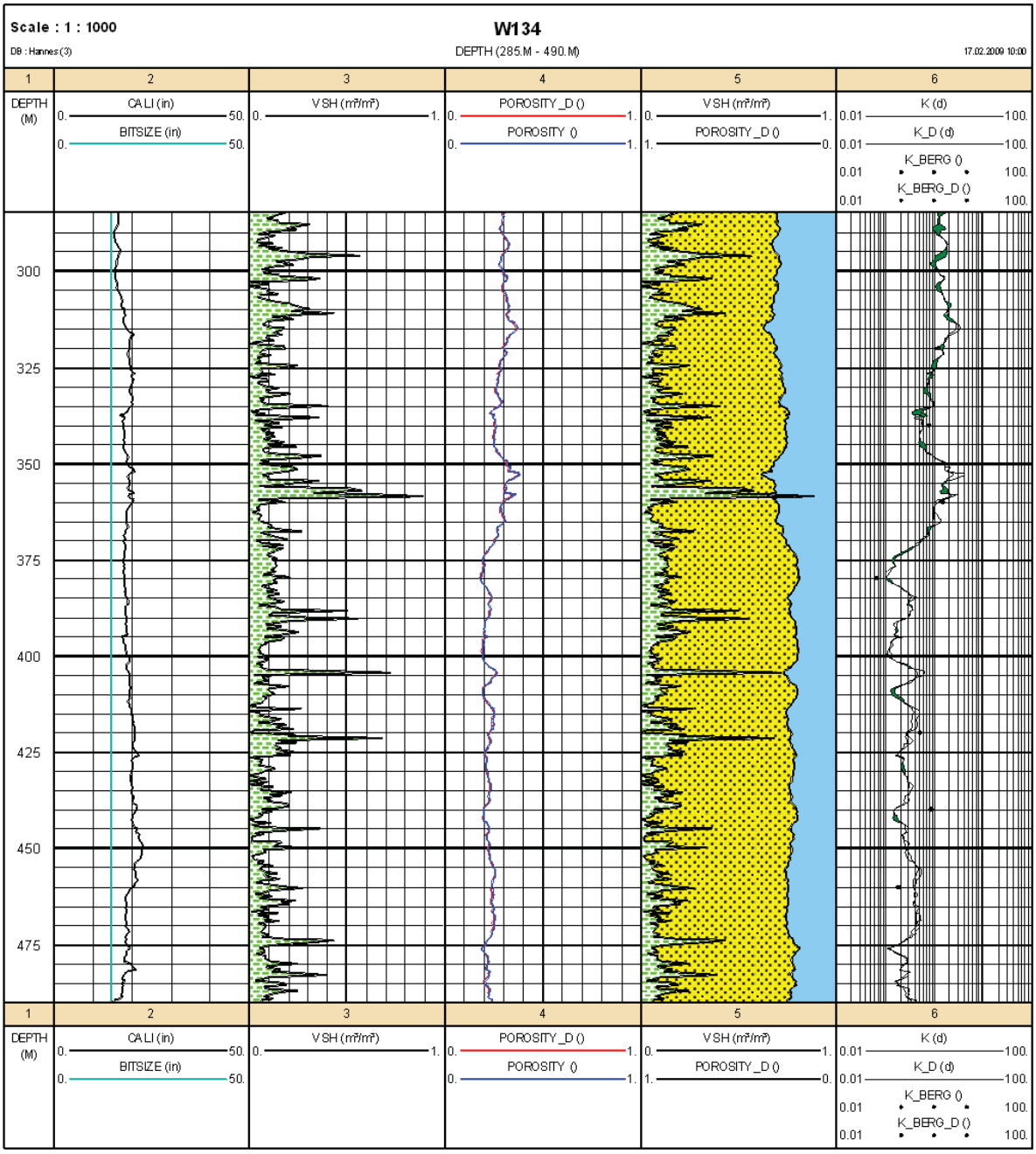
Scale : 1 : 1000
W134
DB : Hannes (3)
DEPTH (285.M - 490.M)
17.02.2009 10:00
1
2
3
4
5
6
DEPTH (M)
CALI (in)
0.
50.
BITSIZE (in)
0.
50.
VSH (m³/m³)
0.
1.
POROSITY_D ()
0.
1.
POROSITY ()
0.
1.
VSH (m³/m³)
0.
1.
POROSITY_D ()
1.
0.
K (d)
0.01
100.
K_D (d)
0.01
100.
K_BERG ()
0.01
100.
K_BERG_D ()
0.01
100.
300
325
350
375
400
425
450
475

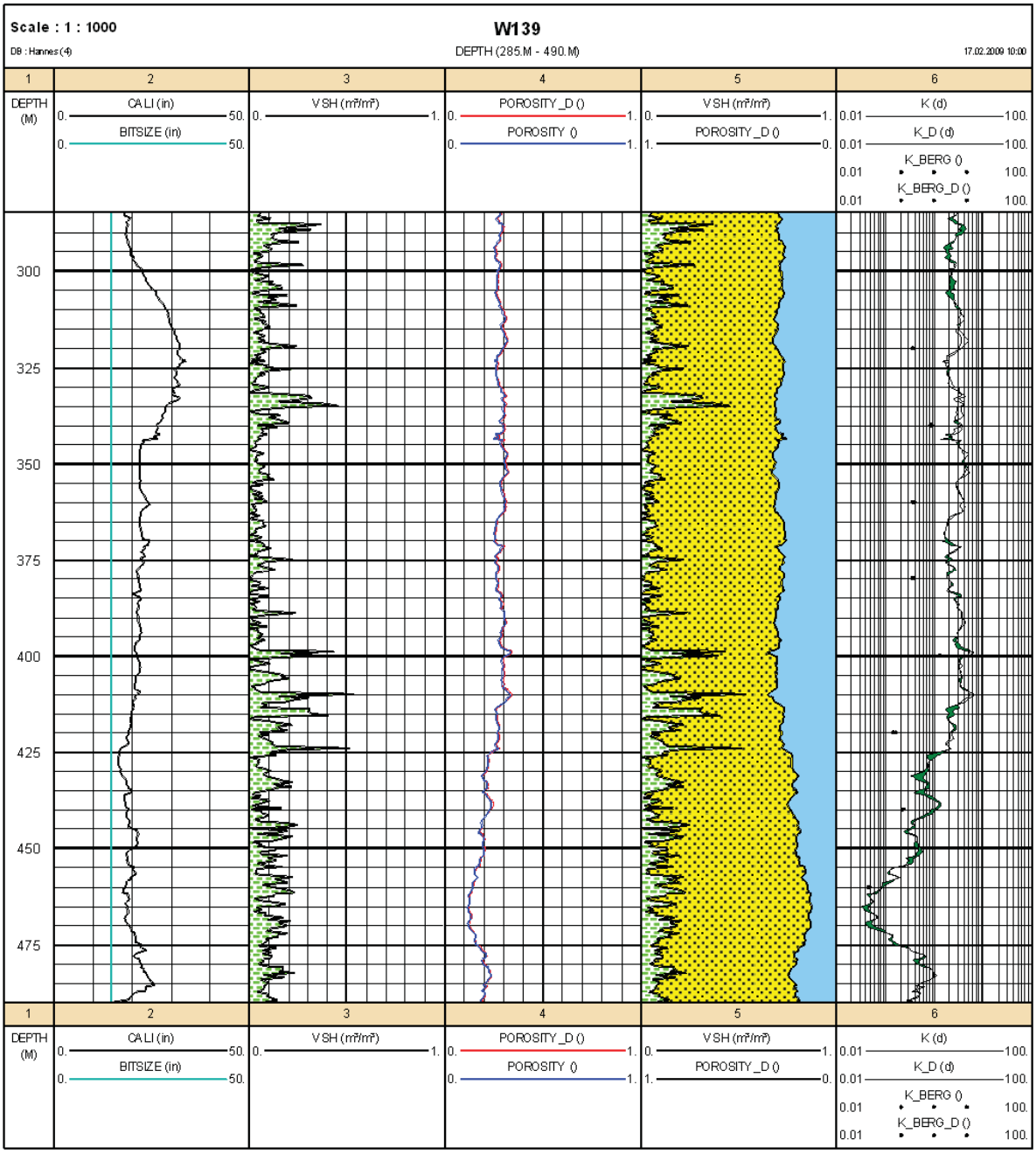
Scale : 1 : 1000
W139
DB : Hannes (4)
DEPTH (285.M - 490.M)
17.02.2009 10:00
1
2
3
4
5
6
DEPTH (M)
CALI (in)
0.
50.
BITSIZE (in)
0.
50.
VSH (m³/m³)
0.
1.
POROSITY_D ()
0.
1.
POROSITY ()
0.
1.
VSH (m³/m³)
0.
1.
POROSITY_D ()
1.
0.
K (d)
0.01
100.
K_D (d)
0.01
100.
K_BERG ()
0.01
100.
K_BERG_D ()
0.01
100.
300
325
350
375
400
425
450
475

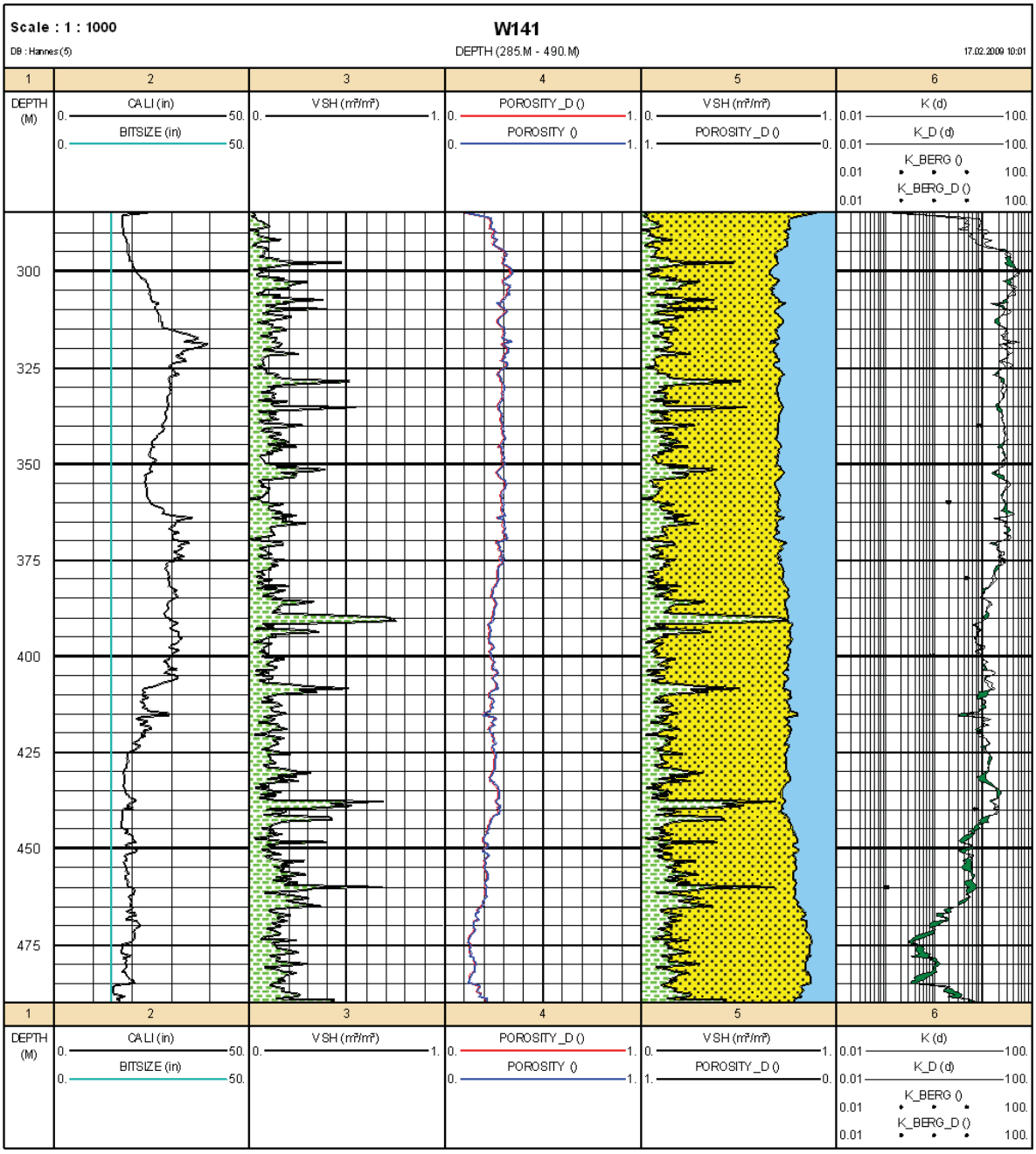
Scale : 1 : 1000
W141
DB : Hannes (5)
DEPTH (285.M - 490.M)
17.02.2009 10:01
1
2
3
4
5
6
DEPTH (M)
CALI (in)
0.
50.
BITSIZE (in)
0.
50.
VSH (m³/m³)
0.
1.
POROSITY_D ()
0.
1.
POROSITY ()
0.
1.
VSH (m³/m³)
0.
1.
POROSITY_D ()
1.
0.
K (d)
0.01
100.
K_D (d)
0.01
100.
K_BERG ()
0.01
100.
K_BERG_D ()
0.01
100.
300
325
350
375
400
425
450
475

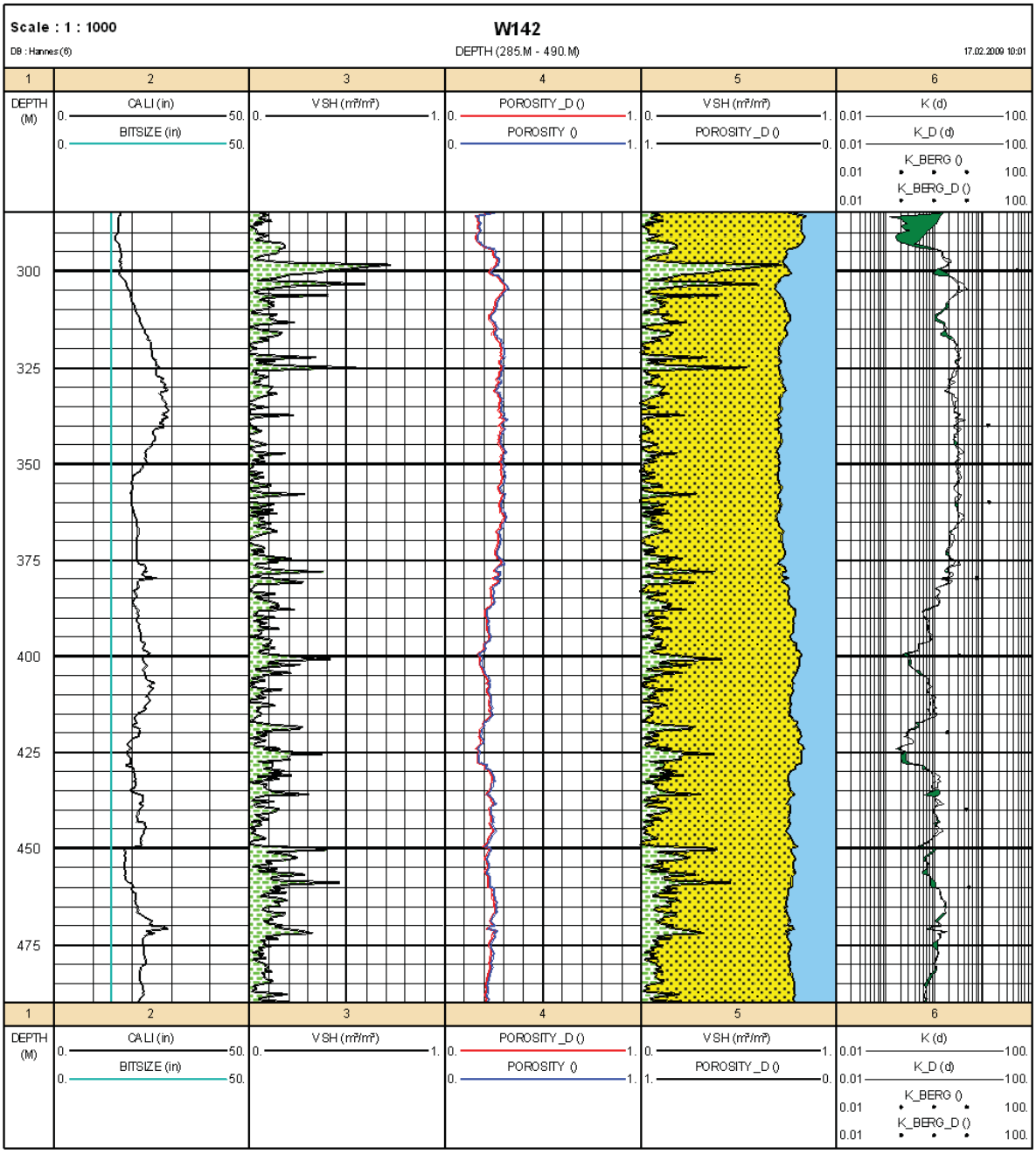
Scale : 1 : 1000
W142
DB : Hannes (6)
DEPTH (285.M - 490.M)
17.02.2009 10:01
1
2
3
4
5
6
DEPTH (M)
CALI (in)
0.
50.
BITSIZE (in)
0.
50.
VSH (m³/m³)
0.
1.
POROSITY_D ()
0.
1.
POROSITY ()
0.
1.
VSH (m³/m³)
0.
1.
POROSITY_D ()
1.
0.
K (d)
0.01
100.
K_D (d)
0.01
100.
K_BERG ()
0.01
100.
K_BERG_D ()
0.01
100.
300
325
350
375
400
425
450
475

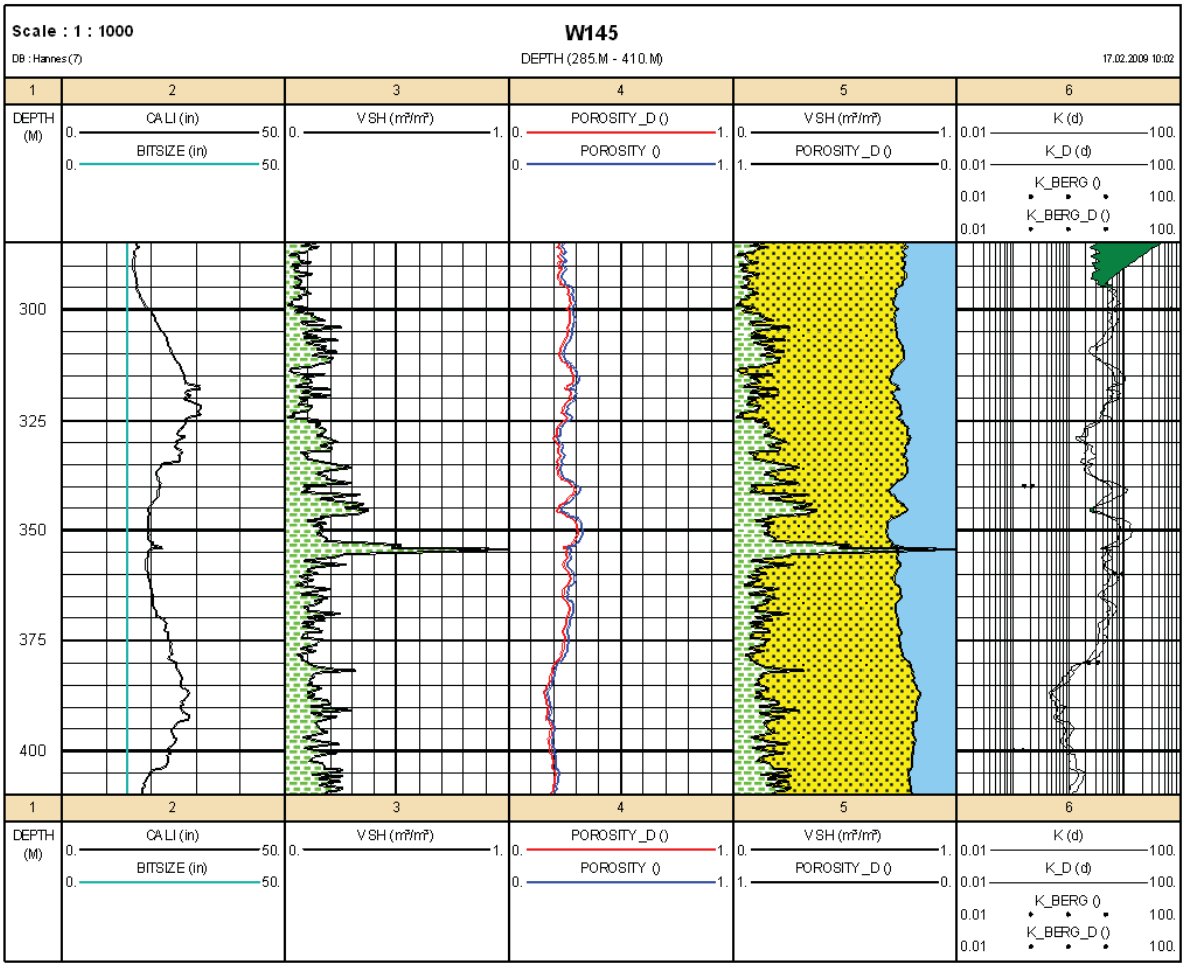
Scale : 1 : 1000
W145
DB : Hannes (7)
DEPTH (285.M - 410.M)
17.02.2009 10:02
1
2
3
4
5
6
DEPTH (M)
CALI (in)
0.
50.
BITSIZE (in)
0.
50.
VSH (m³/m³)
0.
1.
POROSITY_D ()
0.
1.
POROSITY ()
0.
1.
VSH (m³/m³)
0.
1.
POROSITY_D ()
1.
0.
K (d)
0.01
100.
K_D (d)
0.01
100.
K_BERG ()
0.01
100.
K_BERG_D ()
0.01
100.
300
325
350
375
400

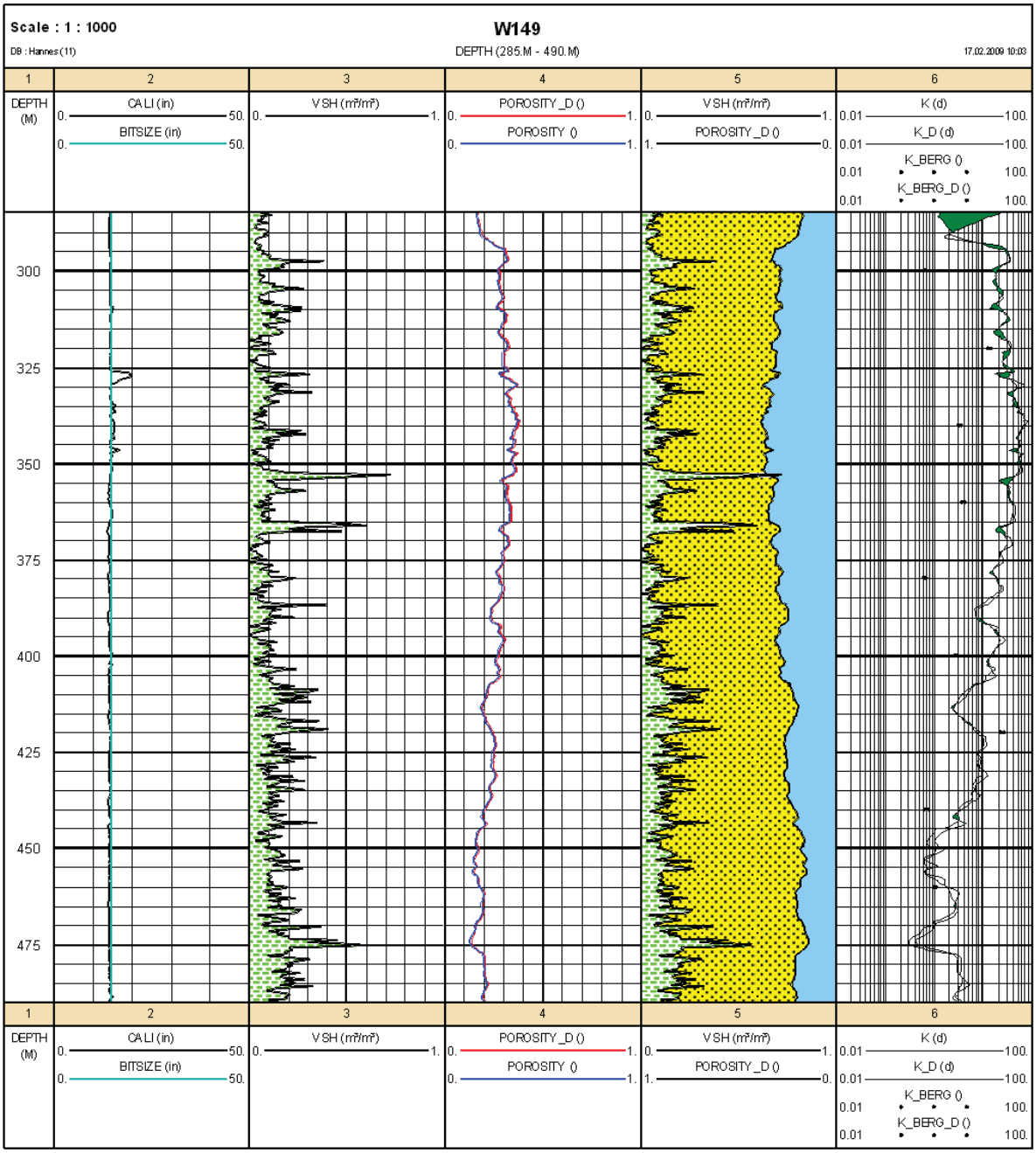
Scale : 1 : 1000
W149
DB : Hannes (11)
DEPTH (285.M - 490.M)
17.02.2009 10:03
1
2
3
4
5
6
DEPTH (M)
CALI (in)
0.
50.
BITSIZE (in)
0.
50.
VSH (m³/m³)
0.
1.
POROSITY_D ()
0.
1.
POROSITY ()
0.
1.
VSH (m³/m³)
0.
1.
POROSITY_D ()
1.
0.
K (d)
0.01
100.
K_D (d)
0.01
100.
K_BERG ()
0.01
100.
K_BERG_D ()
0.01
100.
300
325
350
375
400
425
450
475
1
2
3
4
5
6
DEPTH (M)
CALI (in)
0.
50.
BITSIZE (in)
0.
50.
VSH (m³/m³)
0.
1.
POROSITY_D ()
0.
1.
POROSITY ()
0.
1.
VSH (m³/m³)
0.
1.
POROSITY_D ()
1.
0.
K (d)
0.01
100.
K_D (d)
0.01
100.
K_BERG ()
0.01
100.
K_BERG_D ()
0.01
100.

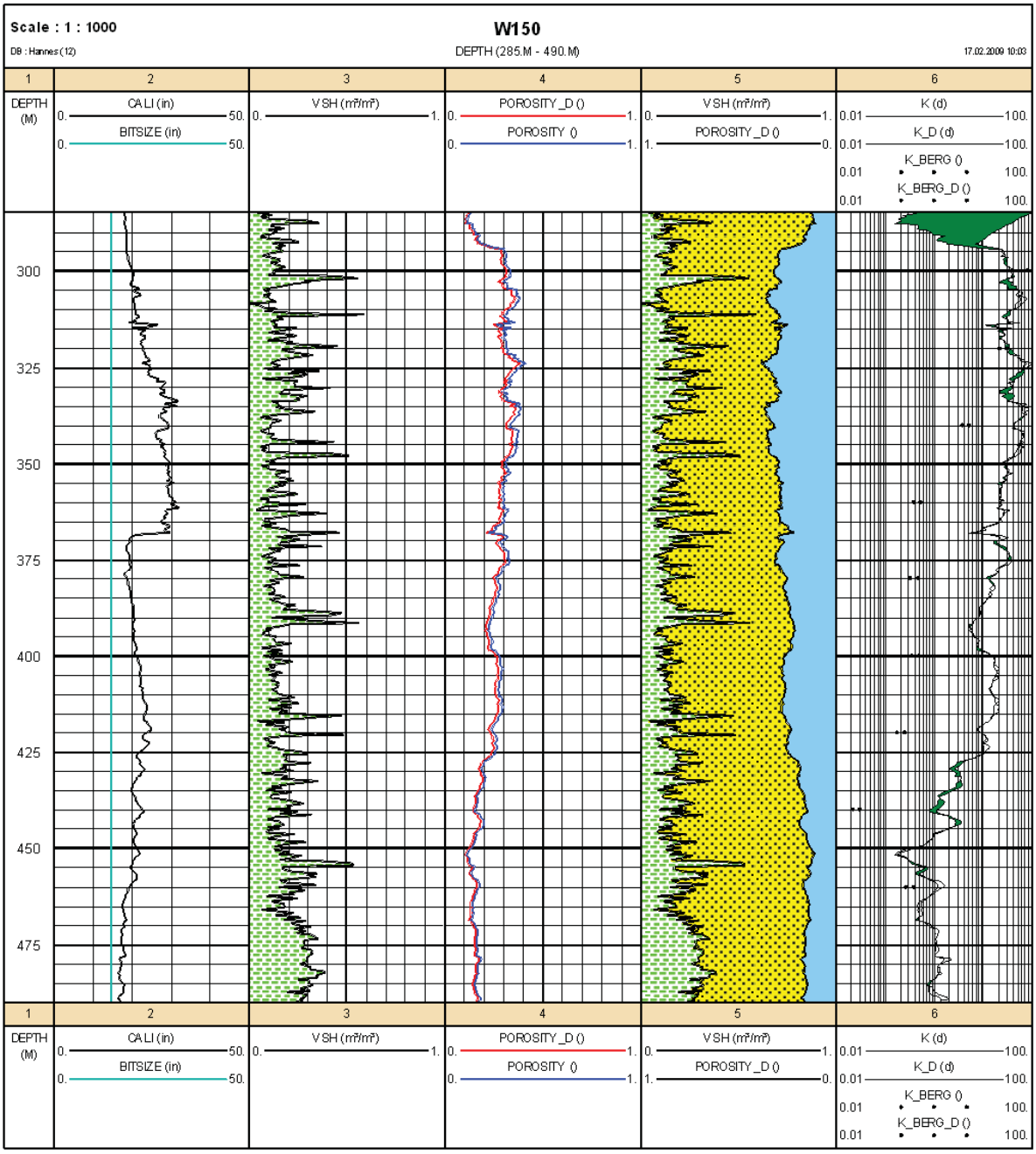
Scale : 1 : 1000
W150
DB : Hannes (12)
DEPTH (285.M - 490.M)
17.02.2009 10:03
1
2
3
4
5
6
DEPTH (M)
CALI (in)
0.
50.
BITSIZE (in)
0.
50.
VSH (m³/m³)
0.
1.
POROSITY_D ()
0.
1.
POROSITY ()
0.
1.
VSH (m³/m³)
0.
1.
POROSITY_D ()
1.
0.
K (d)
0.01
100.
K_D (d)
0.01
100.
K_BERG ()
0.01
100.
K_BERG_D ()
0.01
100.
300
325
350
375
400
425
450
475

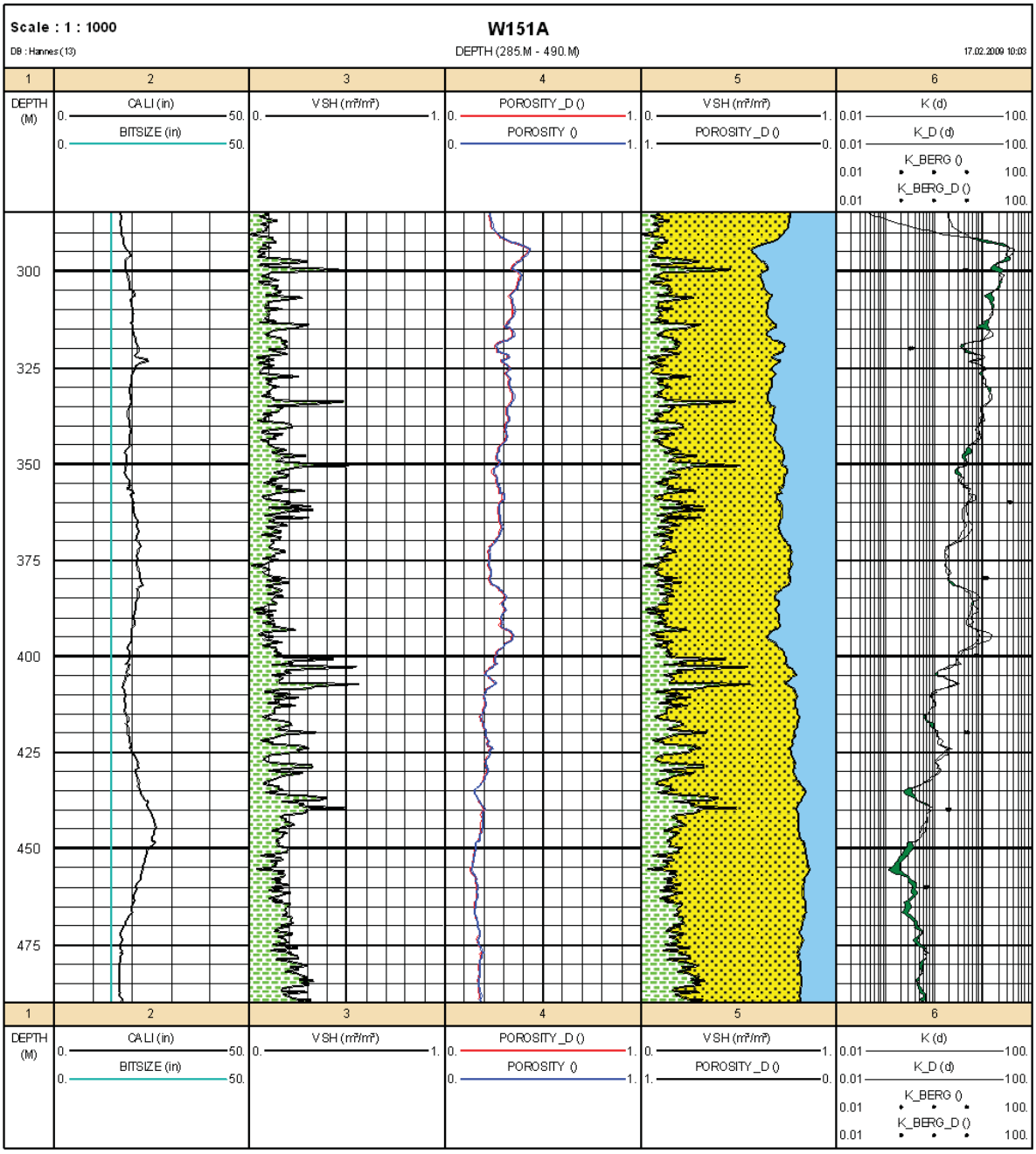
Scale : 1 : 1000
W151A
DB : Hannes (13)
DEPTH (285.M - 490.M)
17.02.2009 10:03
1
2
3
4
5
6
DEPTH (M)
CALI (in)
0.
50.
BITSIZE (in)
0.
50.
VSH (m³/m³)
0.
1.
POROSITY_D ()
0.
1.
POROSITY ()
0.
1.
VSH (m³/m³)
0.
1.
POROSITY_D ()
1.
0.
K (d)
0.01
100.
K_D (d)
0.01
100.
K_BERG ()
0.01
100.
K_BERG_D ()
0.01
100.
300
325
350
375
400
425
450
475
1
2
3
4
5
6
DEPTH (M)
CALI (in)
0.
50.
BITSIZE (in)
0.
50.
VSH (m³/m³)
0.
1.
POROSITY_D ()
0.
1.
POROSITY ()
0.
1.
VSH (m³/m³)
0.
1.
POROSITY_D ()
1.
0.
K (d)
0.01
100.
K_D (d)
0.01
100.
K_BERG ()
0.01
100.
K_BERG_D ()
0.01
100.

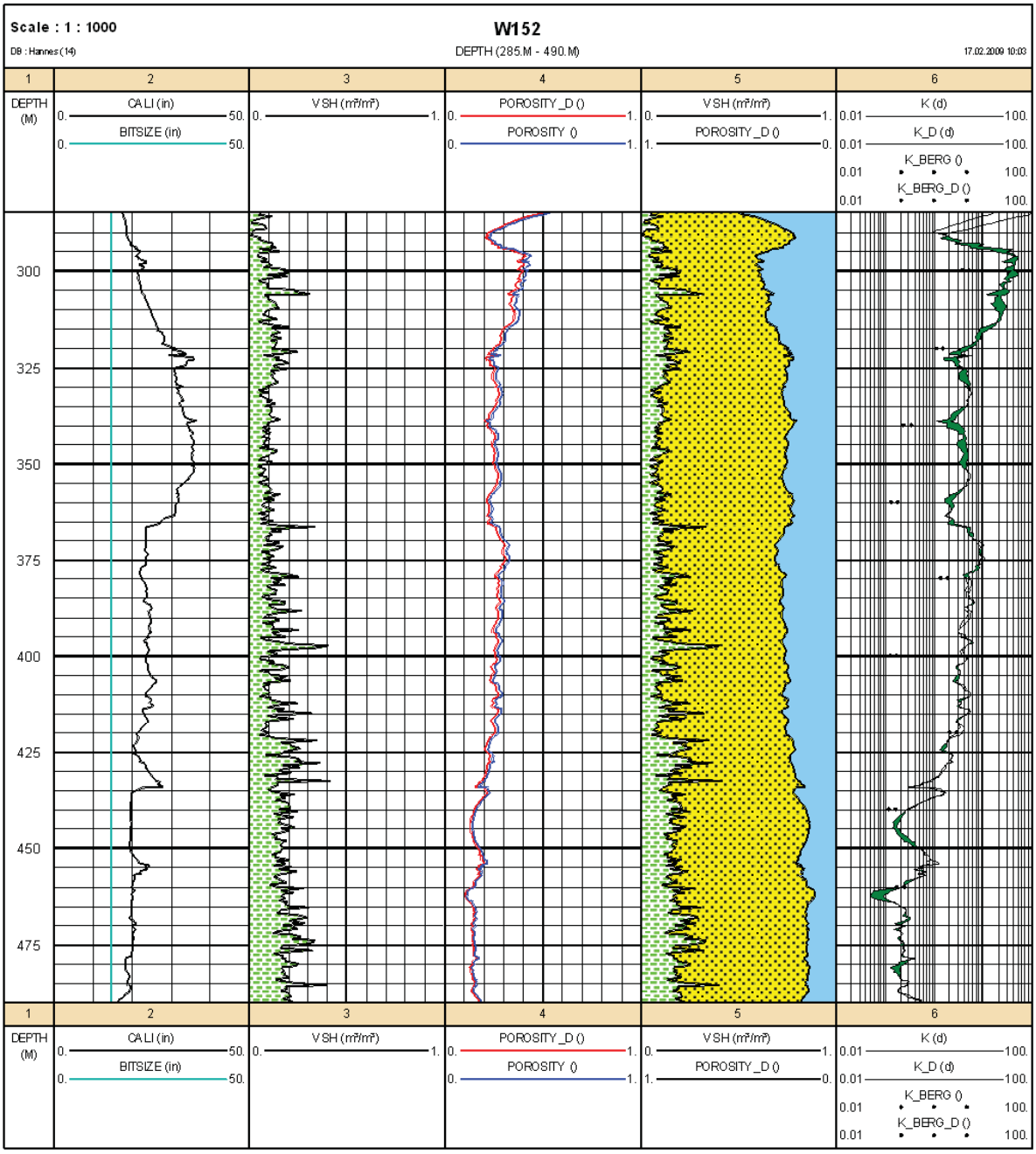
Scale : 1 : 1000
W152
DB : Hannes (14)
DEPTH (285.M - 490.M)
17.02.2009 10:03
1
2
3
4
5
6
DEPTH (M)
CALI (in)
0.
50.
BITSIZE (in)
0.
50.
VSH (m³/m³)
0.
1.
POROSITY_D ()
0.
1.
POROSITY ()
0.
1.
VSH (m³/m³)
0.
1.
POROSITY_D ()
1.
0.
K (d)
0.01
100.
K_D (d)
0.01
100.
K_BERG ()
0.01
100.
K_BERG_D ()
0.01
100.
300
325
350
375
400
425
450
475